Department of Meteorology

Representing black carbon snow darkening in the JULES land surface model

A thesis submitted for the degree of Doctor of Philiosophy

Helen Rose Johnson

May 2024

Declaration

I confirm that this is my own work and the use of all material from other sources has been properly and fully acknowledged.

Helen Rose Johnson

Abstract

Snow darkening contaminants, such as black carbon (BC), can significantly shorten the duration of seasonal snow cover. This can have wide ranging impacts on downstream water availability, and hence on regional hydrology and meteorology. Despite the potential impacts, this effect is often disregarded in short and seasonal term weather forecasting. This thesis aims to improve the representation of snow albedo and melt within the Joint UK Land Environment Simulator, ('JULES'), a commonly used component of weather and climate simulations across all timescales, by introducing a means of calculating BC concentration in snow.

Site based tests show that the modified JULES is capable of replicating the observed concentration of BC in snow assuming that accurate BC deposition rates are prescribed and appropriate values are selected for the top snow layer thickness and the BC scavenging efficiency. At the test site in Japan, including BC reduced the snow duration by 15 days, bringing the date of final snow clearance much closer to observations.

Though the results in Japan show substantial benefit from introducing BC to the modelled snow, globally the results are more mixed. Using a satellite albedo product to verify model performance across the Northern Hemisphere, it is found that in vegetated areas JULES already underpredicts snow albedo. Consequently, adding BC does not improve albedo prediction in these areas. Areas without much vegetation however, such as the Canadian Shield region, show considerable improvement when BC is introduced to JULES.

The addition of BC to snow in JULES is shown to impact the surface energy balance and water cycles leading to a shift in evaporation and surface runoff to earlier in the year. This is especially true in the High Mountain Asia region and has the potential to affect predictions of drought, flooding and monsoon behaviour, highlighting the importance of accurate snow albedo prediction.

Acknowledgements

Over the course of this PhD I have been fortunate to be able to rely on the support and encouragement of many individuals. I am extremely grateful to my supervisors, Prof. Tristan Quaife, Dr. Martin Best and Prof. Richard Essery, for sharing their wisdom with me and mentoring me through this journey. Their invaluable advice and encouragement have been instrumental in the completion of this thesis.

I would like to thank Prof. Michaela Hegglin, who chaired my monitoring committee, Prof. Martin King, my external examiner and Prof. Keith Shine who served both on my monitoring committee and as one of my examiners — these individuals provided fresh perspectives on my work and their insightful comments and suggestions have greatly improved the quality of this thesis.

Thanks also go to Dr. Adrian Lock and Dr. John Edwards for many thoughtful discussions and to my fellow members of APP for being excellent company and a good source of cake. I'd like to recognise the assistance of Dr. Ben Johnson who took time to guide me in setting up a CLASSIC UM simulation and humoured me when I decided that the simulation needed to be performed with a 365 day calendar rather than the 'standard' 360 days! I would also like to extend my thanks to Prof. Teruo Aoki and Dr. Masashi Niwano for kindly providing observations of snow at Sapporo and supporting me to make best use of them.

Every PhD has its challenges, and for me, my health was one of them. During that time I relied heavily on my family and friends, I am eternally grateful for their unwavering support. In particular, special thanks go to Anke for visiting me every fortnight when I was too ill to leave the house — you kept me sane. And to my partner Chris, thanks for believing in me, even when I was struggling to believe in myself.

Contents

Chapter 1

Introduction

1.1 Why snow matters

Snow is precipitation that forms in freezing atmospheric conditions. As with rain drops, a snow flake will typically form when water vapour condenses around a nucleation particle but the exact structure of the snow flake depends on conditions such as air temperature and supersaturation when it is forming (*Hallett and Mason*, 1958). Unlike rain water that flows off land straight away, snow can sit for weeks or months on the land surface acting as a store of water for eventual release during the spring melt season. In many regions, the local ecology depends on this cycle of winter snow cover followed by a spring surge in water availability. Many populations, especially those in arid parts of the world, depend on snowmelt from mountains upstream to supply water for agriculture, industry and domestic needs.

In the summer of 2022 there was a severe drought in Europe that was exacerbated by a long term trend in declining summer river flow in alpine catchments that has been found not to be caused by a lack of precipitation but rather a shift to more precipitation falling as rain rather than snow and therefore peak river flow shifting to earlier in the year (*Montanari et al.* (2023), *Zampieri et al.* (2015)). The river flow on the Po River in Italy that year was so low that saline intrusions rendered the water unsuitable for agriculture up to 40km inland (*Tarolli et al.*, 2023), meaning many crops were devastated as they could not be irrigated. In France, nuclear power production had to be scaled back due to a lack of water available for cooling. And on the Rhine River in Germany, water levels dropped so low that it became difficult for ships to navigate the river. This event serves as a reminder of how dependent Western Europe is on meltwater from snow in the Alps and the importance of snowpacks for providing water storage in order to maintain water supplies throughout the summer months.

As well as the quantity of annual snowmelt being crucial for maintaining water supply, the timing of snowmelt can also have huge impacts on downstream populations. For example, in Alberta,

in June 2013, a rain on snow event led to rapid snowmelt triggering widespread flooding which resulted in four fatalities, thousands of people made homeless and damages that made it one of the most expensive natural disasters in Canadian history (*Liu et al.*, 2016).

Snowmelt timing can also have various ecological implications, with earlier snowmelts being of increasing concern under a warming climate. *Westerling et al.* (2006) argued that earlier snowmelt in the Western United States since the mid 1980s has led to increasing frequency and duration of wildfires along with an extended wildfire season. Impacts of earlier snowmelt on plant populations are complex and may vary depending on factors such as elevation (*Francon et al.*, 2020) but various studies have found that earlier snow melt can lead to reduced plant growth [*Campbell* (2019), *Potter* (2020)] and some have found evidence of reduced flowering and seed production (*Campbell*, 2019) leading to concerns for population sustainability under a warmer climate.

The impacts of timing of snowmelt are not limited to local effects. For example, it has long been noted that late snow melts in the Himalayan region can lead to weakening or failure of the Indian summer monsoon rains (*Blanford*, 1884). It was hypothesised that this effect contributed to the drought that led to the Great Famine of 1876 in India. Conversely, earlier snowmelt could lead to heavier monsoon rains and potential flood events.

1.2 Predicting snowmelt

Given the capability of snow to impact the availability of water and food, the potential to influence the success of harvests or the likelihood of natural disasters such as floods, landslides, wildfires and droughts, humans have been interested in predicting the timing of snowfall and melt for a very long time, at least as early as the ancient Greeks and Babylonians. Early efforts to predict the weather and seasons were based on astronomical calculations (*Lawrence-Mathers*, 2021) though observations of environmental phenomena such as the movements of animals likely also contributed to predictions - the practice of observing animal movements in order to prepare for the autumn freeze up and the spring thaw is still used by Inuit communities to this day (*Bates*, 2007). The advent of the printing press allowed for predictions to be publicised more widely in almanacs some of which still produce weather forecasts using these methods, e.g. The Farmers' Almanac (*Bartles*, 2023). However, these days most people rely on forecasts produced using modern numerical weather prediction (NWP) methods - i.e. physically based computer simulations constrained by meteorological observations.

Snow forecasting capabilities have lagged behind other aspects of weather forecasting for a number of reasons. Maintaining observation networks in remote snowy locations can be very challenging so limited datasets are available to drive and validate weather models. Snowfall and snow cover can vary considerably on very localised scales due to surface features such as

topography and vegetation cover and weather models have struggled to represent this fine scale heterogeneity. Limited understanding of complex snow physical processes, such as changes to snow crystal size and shape with temperature and age, has delayed development of snow models in the past.

As NWP models evolved, an increased understanding of the potential for snow cover to impact wider atmospheric circulation motivated a focus on improving snow related aspects of NWP models. A series of model intercomparison projects sought to identify weaknesses in snow modelling as well as the most important aspects of a snow model to prioritise (*Slater et al.*, 2001; *Bowling et al.*, 2003; *Etchevers et al.*, 2004; *Rutter et al.*, 2009; *Krinner et al.*, 2018) and in 2017, the 'Year of Polar Prediction' was launched as a multi-national effort to enhance observation of polar regions and progress modelling capabilities.

The PILPS project compared 21 land surface models to better understand sensitivities to different 'parametrizations' within the models - these are the mathematical formulations that describe the physical processes within a model gridbox. Phase 2d of the PILPS project (*Slater et al.*, 2001) considered 18 year simulations at a single grassland site in Russia and found that differences in snow accumulations between models were largely controlled by the rate of mid-season melt. Snow albedo and snow covered fraction were identified as two components of the models that worked in combination to control the amount of energy absorbed by the snowpack (and hence the rate of melt). Evaporation/sublimation processes and wind blown snow processes were identified as areas requiring further research as it was not clear the extent to which they contributed to the differences in accumulation.

Phase 2e of PILPS (*Bowling et al.*, 2003) had more of a focus on predicting runoff but the location in the Scandinavian Arctic meant snow was a major factor in this. The lack of incoming radiation for much of the winter meant albedo was not deemed to have as much control on the snow accumulation and so differences in accumulation were instead attributed to differences in the amount of sublimation from the snow pack. Again, the authors considered that blowing snow may be an important unrepresented process that required further investigation but also highlighted vegetation canopy interactions as an area for investigation as it was thought that canopy snow interception may impact the amount of winter evaporation.

Both these studies were limited to single locations or confined areas. The SnowMIP project expanded on this work and considered snow models of varying purpose and complexity at a range of sites. In the first phase of that study, *Etchevers et al.* (2004) highlighted the importance of accurately representing the snow albedo (i.e. the ratio of incoming radiation that is reflected vs. absorbed) in order to predict impacts of snow on the wider energy balance of the land surface system. As snow has one of the highest albedos of any land surface, it has the potential to significantly impact the earth's energy balance. They found that more complex albedo parametrizations were not always required but that albedo parametrizations that incorporated a representation of snow type or snow grain properties, including changes with aging, generally

performed best. They also highlighted that at some sites, model performance was limited by the fact that none of the snow schemes studied included a representation of the impacts of snow impurities on albedo.

The second phase of the SnowMIP project (*Rutter et al.*, 2009) focused on differences in performance of snow models at forested sites compared to open sites. It was found that models predicted snow water equivalent, 'SWE', and snow depth more consistently at open sites, suggesting that forest-snow interactions did complicate model performance but it was also found that model performance was more sensitive to melt and refreezing processes during warm periods than to parametrization of forest canopy interception and unloading.

All of these studies considered standalone land surface simulations so there were no differences between models in the amount of snowfall or radiation received at the surface. Therefore, all differences in model results were determined by treatment of snow on the ground. Taken together, these studies show that the timing of eventual snow clearance is dependent on the rates of snow accumulation and melt throughout the entire snow season. These processes are predominantly governed by the amount of energy absorbed by the snowpack (controlled via the snow albedo and snow cover fraction) and lost via sublimation and refreezing. Factors influencing the distribution of snow, e.g. wind blown effects or canopy interception, can also play a role in the accumulation but will have limited influence on melt patterns.

Ultimately these model intercomparison projects were unsuccessful in identifying any one set of parametrizations that performed best in all situations and it was clear that additional complexity did not necessarily improve simulations. The comparison of different model representations of snow processes was complicated by the fact that models often relied on several poorly constrained parameter values. It was not clear whether differences in model performance were due to differences in their formulations of snow processes or due to choices of parameter values within those formulations.

Essery et al. (2013) adopted a different approach to investigate the importance of detailed representations of different snow processes. They developed a snow scheme with interchangeable options for seven processes that are commonly included in snow models. Three options were included for each process - a detailed physical representation of the process, a simpler empirical representation and a very basic representation e.g. a constant value. These options were all taken from commonly adopted parametrizations within other snow models. An ensemble of simulations was then performed that included every possible combination of these options but did not vary the parameter values used. Whilst there was no one set of parametrizations that performed best in all winters for all the four variables that were used for validation, there were some combinations that consistently performed well. It was found that snow compaction, snow albedo and retention of melt water within the snowpack were the processes that most benefitted from a more complex representation. The importance of providing physical parametrization of the latter two of these has since been confirmed by another multi-physics ensemble study at a

different site by *Günther et al.* (2019).

Whilst clearly not the only snow process of importance, there is consensus within the literature that albedo is a key component of snow models that must be well represented in order to accurately predict snow accumulation and melt.

1.3 Factors that affect snow albedo

There are many factors that affect the albedo of snow and a physically based snow albedo parametrization will need to incorporate these. The size of the snow grains is a key element with larger snow grains having lower albedos. Every time light passes through an air-ice interface it can be reflected or refracted. A snowpackwith a given SWE made up of smaller snow grains has more of these interfaces so the light will change direction more frequently. In larger snow grains, the light interacts with fewer of these interfaces and therefore is more likely to be transmitted through the snow and eventually absorbed either by the snow itself or the underlying surface. The impact of snow grain size on the spectral albedo of pure snow is illustrated by the blue lines in figure 1.1a.

The initial shape and size of a snow grain depends on the temperature and supersaturation conditions of the cloud when it formed (*Hallett and Mason*, 1958). Snow grains may be formed of individual snow crystals or clusters of crystals. Snow grains may be exposed to warming conditions or repeated melt-freeze cycles as they fall, which cause the grain size to increase as more water vapour deposits onto the snow crystal. Collisions between snow grains as they fall, or are blown by the wind, can cause clusters to break up and grains to form simpler rounded shapes (*Walden et al.*, 2003) leading to snow grains with fewer facets and thus reduced albedo.

Once the snow is on the ground, the snow grains continue to evolve, a process referred to as snow metamorphism. Air pores between the snow grains allow water vapour to move within the snowpack, subliming off some snow grains and depositing onto others. Vapour motion can be driven by vapour density gradients and temperature gradients within the snowpack as well as by wind which acts to ventilate the snowpack (*Cabanes et al.*, 2003). Over time, the snow grains reconfigure to simpler, rounder, shapes with lower surface area to mass ratios (i.e. larger radii). The rate of change is slow under cold temperature conditions but accelerates if the temperature of the snow pack increases. These processes are described by *Sommerfeld and LaChapelle* (1970).

If liquid water infiltrates the snowpack, either from melting snow or from rain, then the snow albedo will darken further. Curiously, it has been noted that the albedo does not then alter again if the water refreezes within the snow, at least not in the case of old snow (*O'Brien and Munis*, 1975). It has been suggested by *Wiscombe and Warren* (1980) that this is because water and ice have very similar refractive indices and so when liquid water surrounds a snow

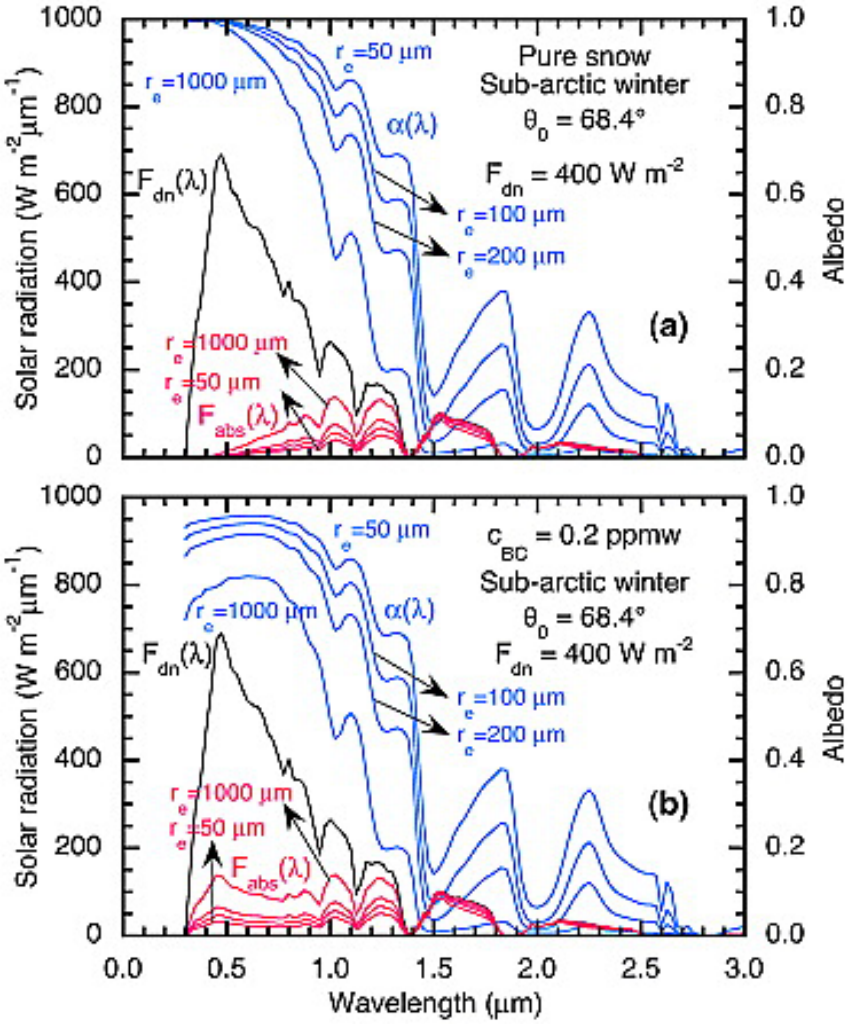

Figure 1.1: Spectral variations in snow albedo ($\alpha(\lambda)$, blue) for a range of different effective snow grain sizes (r_e) for a) pure snow and b) snow contaminated with BC, modelled using a radiative transfer model. Also shown are the quantity of incoming solar radiation received at the snow surface ($F_{dn}(\lambda)$, black) and the amount of radiation absorbed by the snow ($F_{abs}(\lambda)$, red). [Reproduced from *Aoki et al.* (2011) Fig. 10, with permission of the publisher - John Wiley and Sons, copyright 2011 by the American Geophysical Union.]

grain the aggregate structure acts as a larger snow grain. A lab based experiment by *Brun* (1989) claimed to demonstrate that the presence of liquid in the snow pack caused the snow grains to grow (with increasing growth rates for increasing snowpack saturations). It's not clear whether the grains themselves grew in this experiment as the wet snow samples were re-frozen before being studied but regardless of liquid/solid composition, it's clear from their photos that over time more water/ice amasses around the snow grains.

The angle of incidence of radiation with the surface affects how much is reflected or absorbed by the snowpack. If the sun is close to the horizon (i.e. a large solar zenith angle) then the path that the light takes through the snowpack is shallower. This shallower path means that more of

the interactions between photons and snow grains occur close to the surface of the snowpack. Scattering events closer to the snow surface are more likely to result in the photon escaping the snowpack as the likelihood of the photon being absorbed by another snow grain before it exits the snowpack is less than if it was scattered deeper within the snowpack and had a longer path to the surface (*Warren*, 1982). This means that, for direct incoming radiation, larger solar zenith angles result in more light being reflected and less absorbed by the snowpack and so a higher snow albedo.

The depth of the snowpack is also important for albedo as radiation can penetrate some distance into the snowpack. This means that the underlying surface beneath the snowpack is not fully obscured until the snow is several centimetres thick. The exact snow depth at which the surface albedo will be completely free from influence of the underlying surface depends on a number of factors - different wavelengths of radiation will penetrate to different depths, due to being scattered at different rates, and the size of the snow grains affects this scattering. As such, snow age, temperature, grain shape and wetness all play a roll in determining how far radiation will penetrate. Several studies have attempted to quantify the depth of snow cover required to completely obscure the underlying surface, for example, *Baker et al.* (1991) found that a bare soil surface (i.e. free from protruding vegetation) is completely obscured once snow reaches a depth of 5cm. However, a report by the US Army Corps of Engineers (*of Engineers*, 1956) suggested that, for high density snow, radiation could penetrate up to one foot ($\sim$30cm).

Finally, an important process that can affect the albedo of snow but which is often not represented in meteorological models is contamination with light absorbing impurities. The relevance of this factor for snow modelling was highlighted by *Warren and Wiscombe* (1980) when it was found that their modelled snow albedos were overpredicted but only in visible wavelengths. Eventually they concluded that the snow samples they were using for validation must have been contaminated with soot (having first ruled out several types of dust as possible contaminants).

There are many different light absorbing snow contaminants but most come in the form of aerosol particles that are lofted from elsewhere and then deposited onto the snow. These particles can be emitted from natural sources, such as ash from volcanic eruptions or soot from forest fires, or they can be emitted by anthropogenic activities such as black carbon (BC) being emitted from fossil fuel combustion. There are also non-aerosol snow contaminants, for example red algae that has been found to form in snow (*Ganey et al.*, 2017), in general these are less common but aerosol snow contaminants can act as fertilisers to fuel algal blooms during periods of melt.

Any substance that darkens the snow will affect the radiative balance of the snowpack. Lower albedos lead to more radiation absorption, this can be seen by comparing the red lines in figures 1.1 a and b which show radiative absorption in clean and contaminated snow respectively. In turn, this increase in absorption leads to increases in snow temperatureswhich can create a feedback cycle due to accelerated thermal metamorphism further darkening the snow. Contaminants will have a greater absorptive impact in aged snow as the larger snow grains will allow

radiation to penetrate deeper into the snowpack and interact with more of the contaminating substance.

Different locations are exposed to different quantities and types of snow contaminants. In many places, the most abundant snow contaminant by mass is dust, which has larger particle sizes than other common contaminants. However, dust absorbs less radiation than BC (*Warren and Wiscombe*, 1980) so in many cases BC is the dominant impurity in terms of radiative impacts on snow. Indeed, *Gleason et al.* (2022) found that whilst dust was the more abundant contaminant by mass at many sites in the U.S. Rocky Mountains, there was only one site out of 51 where dust dominated the radiative forcing over BC. *Doherty et al.* (2014) took snow samples from 67 sites across North America and found that whilst in some locations, such as the Pacific Northwest, almost all the light absorption from snow contaminants was due to BC, in other locations, such as the Northern U.S. Plains, 50-100% of absorption was due to dust made up of soil particles (which are commonly disturbed by agricultural practices making them more easily lofted by wind). A modelling study by *Yasunari et al.* (2015) attempted to quantify the relative contributions of BC, organic carbon (OC), and dust to Northern Hemisphere radiative absorption by snow contaminants. They found that BC was responsible for most of the absorption in East Asia, Western Europe and the United States, whilst dust caused most of the absorption in central Asia. OC contributed relatively little to the overall absorption by snow contaminants with a maximum contribution of 19% in Southeastern Siberia and Western Canada.

Overall, dust and BC are the most relevant snow contaminants for snow albedo calculations globally. This thesis focuses on the impacts of BC on snow albedo as a starting point for improving snow albedo modelling. The focus on BC is in order to build upon the work of others, in particular *Marshall* (1989), in quantifying the radiative impact of BC in snow. However, it is acknowledged that the longer term goal should be to incorporate the impact of a range of snow contaminants that includes both BC and dust into snow modelling efforts.

1.4 Black carbon as a snow contaminant

Black carbon is a dark coloured carbonaceous particle produced through incomplete combustion of carbon based fuels. The term is often used interchangeably with ‘soot’ although strictly speaking BC is a component of soot along with various organic compounds. The other term that is sometimes used to refer to BC is ‘elemental carbon’, this term refers more specifically to refactory carbon particles that withstand heating to an extremely high temperature. The exact temperature used in this definition varies depending on different measurement protocols (*Kuchiki et al.*, 2015) but defining BC in this way provides a useful distinction between BC and less strongly absorbing carbon particles which are referred to as ‘organic carbon’ and pyrolyse at lower temperatures.

BC particles are the most light absorbing of any recorded snow contaminant. Typical particle sizes are between 120 and 200nm at the time of emission (*Bond et al.*, 2013), though this depends on the efficiency of combustion and *Schwarz et al.* (2008) found that particles emitted in urban areas tended to be smaller than those emitted from biomass burning. Over time, the particles develop coatings as other chemicals in the atmosphere condense onto the BC particles, this causes the overall size of the particle to grow. By the time BC particles are deposited onto snow they have sizes of the order of 220nm and it is has been suggested that there is an element of size selection in the deposition processes favouring deposition of larger particles (*Schwarz et al.*, 2013). Freshly emitted BC has a mass absorption cross section of $7.5\mathrm{m}^2\,\mathrm{g}^{-1}$ at wavelengths of 550nm but this can increase as the particle ages because coatings can enhance absorption (*Bond and Bergstrom*, 2006).

BC emissions come from a huge range of sources including wild fires and deliberate agricultural burning; domestic cooking and heating; petrol, diesel and biofuel powered transport such as cars, shipping and aviation; industrial processes such as burning coal for steel production, and many many more.

The quantity of BC emissions has increased greatly since pre-industrial times, both as a direct result of increases in anthropogenic emissions and also as an indirect result of increased wild fires due to global warming. In the BC emissions inventory compiled by *Lamarque et al.* (2010) for the Fifth Climate Model Intercomparison Program ('CMIP5'), the global anthropogenic BC emissions were shown to increase over the entire timespan of the dataset from 1Tg/year in 1850 to 5Tg/year in 2000. Biomass burning emissions on the other hand did not start increasing until 1950 after which they increased sharply until 1990.

Once emitted, BC particles remain suspended in the atmosphere for several days although the atmospheric residence time does vary seasonally as well as regionally (*Lund et al.*, 2018). In that time the particles can be advected far from their source location before being deposited back to the surface. As a result, even the most remote snowpacks on Earth are exposed to BC deposition. For example, *Keegan et al.* (2014) examined BC particles in Greenland firn cores and concluded, based on the coexisting contaminants, that the BC originated from boreal forest fire sources. Using back trajectory modelling techniques they established that the BC had likely originated from forest fires in either North America or Far Eastern Russia.

Deposition of BC onto snow can occur through a number of mechanisms broadly broken into wet deposition and dry deposition. Wet deposition is when BC is deposited with precipitation, either due to the BC particle acting as a cloud condensation nuclei for the precipitation to form around or via collision or scavenging by falling precipitation as was observed at Sapporo by *Magono et al.* (1979). Dry deposition can occur due to eventual gravitational settling of the particles out of the atmosphere and by wind or turbulence driven collision with the surface. Another possible mechanism for dry deposition is a process known as 'wind pumping' where wind blows air through the interstitial spaces between snow grains and the snowpack acts to filter aerosols

from the air. Through this process, aerosols can be deposited not only onto the snow surface but also throughout the upper layers of the snowpack. This process has not been observed for BC particles specifically but has been observed for generic particulate pollutants by *Harder et al.* (1996) and is thought to occur with BC as well.

The deposition mechanism is relevant when BC is deposited onto snow as in the case of wet deposition, the amount of BC deposited is limited by the amount of snowfall whereas in the case of dry deposition, the BC is deposited on top of the snow and can continue to collect there until the next snowfall event. Dry deposition can thus lead to much higher concentrations of BC in the surface snow and so has a larger impact on albedo. The other reason why deposition mechanism affects snow albedo is because it affects the position of the BC particles relative to the snow grain. During wet deposition, the BC particles become 'internally mixed' (i.e. they form an integral part of the snow grains) whereas dry deposition can lead to an 'external mixture' of BC particles between the snow grains. Modelling studies have suggested that BC mixed internally within the snow grain can be $\sim$1.8–2.1 times more absorbing than externally mixed BC (*Flanner et al.*, 2012).

Very few studies have attempted to measure the ratio of wet to dry deposition, *Sinha et al.* (2017) compared BC concentrations in falling snow (collected in a windsock and a box) to concentrations in lying snow on Svalbard and concluded that the contribution of dry deposition was smaller than the uncertainties of their measurements. *Emerson et al.* (2018) compared BC concentrations in rain samples collected at the Southern Great Plains site in Oklahoma, with dry deposition samples collected by pumping air through a tube that led to a single particle soot photometer to measure the number and mass of BC particles. They reported that dry deposition contributed only 6% $\pm$4% to total BC deposition. Relative contributions of different deposition mechanisms are likely to vary both regionally and seasonally and it's not clear if wet deposition rates should be expected to be the same for rain and snow but both these studies suggest that wet deposition is by far the dominant deposition mechanism for BC.

By collating ice core records, *Kang et al.* (2020) was able to identify historical trends in concentrations of BC in snow. These trends are shown in figure 1 of that paper, reproduced in figure 1.2 here. In almost all cases the concentrations of BC have increased since the start of the records (usually between 1750 and 1850) but in some regions BC concentrations were found to have already peaked and now be decreasing. In Svalbard, Greenland, the Canadian Arctic and the Alps, the BC concentrations have reduced substantially over the latter part of the 20th century likely due to the introduction of air quality legislations in Europe and North America leading to a reduction in emissions from coal burning. BC concentrations in Arctic snow are now on par with pre-industrial levels. In the Tibetan Plateau and Himalayas regions the increases in BC concentrations accelerated later, around 1950, and the concentrations are still increasing.

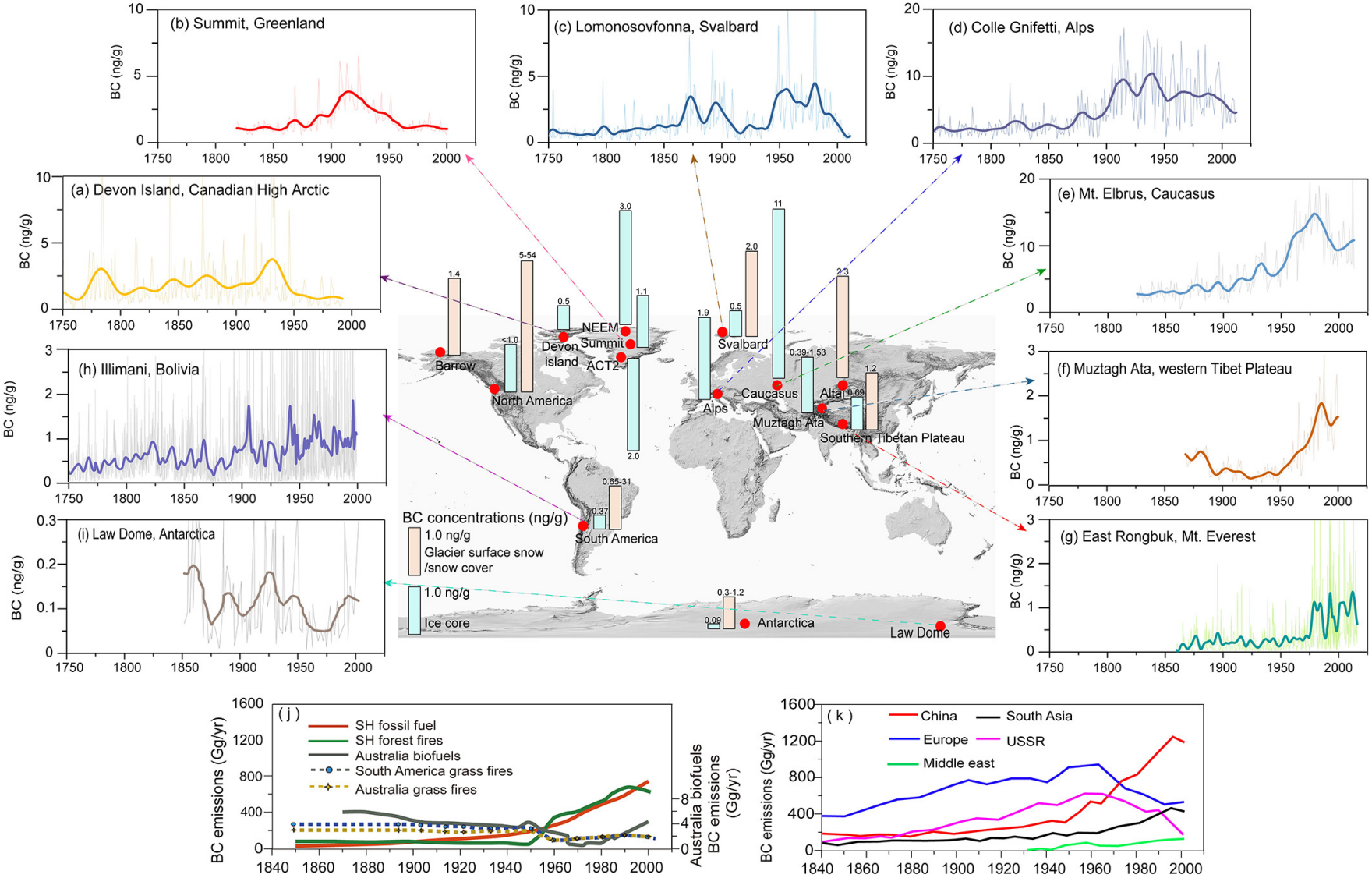

Figure 1.2: Historical records of BC concentrations from ice cores (a-i), history of BC emissions for southern hemisphere (j) and norther hemisphere (k), and spatial distributions of average BC concentrations in snow (firn) on the glacier surface and in snow cover (centre). [Reproduced from *Kang et al.* (2020) Fig. 1, distributed under a Creative Commons CC-BY license]

1.5 Efforts to model the effects of BC on snow

Although *Warren and Wiscombe* (1980) incorporated the optical effects of BC particles into their physically based snow model and highlighted its importance in accurate albedo prediction, it wasn't until 24 years later that *Hansen and Nazarenko* (2004) first predicted the contribution that BC makes to climate change. They investigated the impact of altering snow and ice albedos in climate simulations and found that BC on snow and ice has a climate forcing twice as effective as CO2 in the atmosphere. Since then, several groups have made efforts to incorporate the darkening effects of snow contaminants into climate models.

Jacobson (2004) produced the first climate model that contained physical representations of BC aerosol transport, deposition onto snow and impact on albedo. This was a coarse resolution climate simulation with a relatively simple single layer representation of the snowpack. They estimated that the global near surface temperature change due to including BC darkening of snow and ice in their model was +0.06K, this is less the +0.17K figure suggested by *Hansen and Nazarenko* (2004) but still sufficient to highlight that deposition of particulate air pollution onto snow has important impacts on the climate. Both *Jacobson* (2004) and *Hansen and Nazarenko* (2004) argue that policies to reduce air pollution would help curb global warming.

Flanner et al. (2007) developed a more detailed model of BC behaviour in snow and its radiative impacts for their Snow, Ice and Aerosol Radiative model ('SNICAR'). Unlike Jacobson's model, this one represented processes such as snow metamorphism and meltwater scavenging of BC particles. *Flanner et al.* (2007) coupled SNICAR to the CAM3 global climate model to explore the impacts of BC snow darkening on the climate, noting warming trends somewhere between the previous two studies (+0.1-0.15K). This was the first study to assess seasonal impacts of BC in snow as well as annual, the authors identified a trend of BC causing snow melt to shift earlier in the year and a very strong seasonality to the radiative forcing impacts of the change.

A later study (*Flanner et al.*, 2009) expanded the SNICAR model to include the effects of dust as well as BC on snow. Dust was found to act predominantly over north-central Asia whereas BC was active across most of the Norther Hemisphere snow; cumulatively the two contaminants had three times greater surface forcing effect over Eurasia than North America. Unlike previous studies, which only looked at 'present day' BC deposition rates (at the time the studies were performed), this study examined how the changes in aerosol deposition rates between 1979 and 2000 had affected spring time trends in surface temperature and snow cover fraction. Including BC and dust in snow led to accelerated warming and reductions in springtime snow cover over this period, bringing temperature trends more in line with those seen in observations and reanalysis products. This result reinforced the importance of including aerosol snow darkening effects in predictions of changing climate patterns.

Namazi et al. (2015) also explored the impacts of changing BC deposition rates over time between the 1950s and 2000s. Using a parametrization of BC in snow developed for the Canadian

Atmospheric Global Climate Model (CanAM4.2), they compared a simulation with a 1950s climatology of deposition rates to one with time evolving deposition rates. This is different to *Flanner et al.* (2009) who compared no aerosol snow darkening to a time evolving deposition scenario. *Namazi et al.* (2015) noted significant warming ($\sim$ 1K) over the Himalayas during this time period but most other regions did not see statistically significant changes in surface temperature or snow covered fraction due to changes in BC deposition rates. The difference between this result and that of *Flanner et al.* (2009) is likely due to the different experimental design and suggests that much of the warming and snow loss in the earlier study was due to the baseline aerosol deposition rates in 1979 rather than the changes in deposition rates over the course of the simulation. The inclusion of dust by *Flanner et al.* (2009) will also have contributed to stronger radiative forcings in that study.

Many of these early efforts to model the effects of BC in snow were validated against a small number of site based observations of BC concentration in snow. However, *Jacobson* (2004), and later *Qian et al.* (2015), point out that there was usually a mismatch between the years for which BC emissions inventories were available and years for which snow sample observations were available. Moreover, the site based observations often represented a single snapshot in time, which made validation of time-evolution of BC concentration impossible. *Aoki et al.* (2011) overcame this challenge by collecting detailed snow pit measurements twice a week throughout two entire winters at Sapporo, Japan, and used these data along with surface meteorological and radiation measurements to carefully evaluate their Physically Based Snow Albedo Model ('PBSAM') which was later incorporated into the global climate model 'MRI-CGCM3' (*Yukimoto et al.*, 2012) and the regional climate model 'NHM-SMAP' (*Niwano et al.*, 2018).

This dataset has since been used to evaluate the GOddard SnoW Impurity Module (GOSWIM) that was developed by *Yasunari et al.* (2014) for use in version 5 of the NASA Goddard Earth Observing System Model (GEOS-5). Other sites have since been used to evaluate other models (e.g. *Skeie et al.* (2011), *Meinander et al.* (2013), *Niwano et al.* (2014), *Tuzet et al.* (2020)) but the list of sites where an entire year's worth of data is available remains very small and few models have been validated against multiple sites in different meteorological conditions and climatic regions which raises questions as to the applicability of these models worldwide.

There are also questions about how representative single site based observations are of the wide area that a climate model gridbox attemps to represent. Heterogeneity in features such as orography and vegetation cover across a gridbox can lead to large variations in the amount of snow cover and the timing of melt so a measurement at a single location is unlikely to be representative of the average snow conditions across an entire gridbox.

An alternative approach to validate coarse resolution models is to use satellite products or reanalysis products. Both of these have limitations in regards to the amount of processing used to construct the product - one must be mindful that this method of validation can be more akin to comparing one model to another rather than a model to direct observations. However, both

types of product represent larger footprints than site based observations so may give a better representation of the area that a climate model gridbox is attempting to simulate. Satellite products of snow impurity concentrations are only just starting to become available and have various limitations such as difficulty being used over vegetated terrain (*Painter et al.* (2012), *Bair et al.* (2021)) so most research groups have instead relied on more mature products to validate other aspects of model performance. For example, *Yasunari et al.* (2015) used a MODIS snow covered fraction product to assess SWE values modelled with GOSWIM. They found that including the snow darkening effects of BC, dust and OC improved modelled spring time snow extent but that modelled snow extents were still greater than seen in the satellite product.

Some researchers have turned to regional climate models in order to be able to resolve more of the landscape heterogeneity. *Sarangi et al.* (2019) compared simulations with SNICAR coupled to the WRF-HR regional climate model at two different resolutions over High Mountain Asia. Evaluating these simulations against the recently developed MODIS MODSCAG products of snow covered fraction and snow grain size and MODDRFS 'dust' in snow, they found that the higher resolution simulation was able to better represent the duration of snow cover and improved representation of deposition processes led to more realistic distributions of impurities in snow.

Despite many different representations being developed for a range of models, all seven earth system models included in the most recent Coupled Model Intercomparison Project ('CMIP6') that represent BC in snow have done so using SNICAR within either the CLM4 or CLM5 land surface model (*Chen et al.*, 2022). SNICAR has continued to be developed (*Flanner et al.* (2021) and references therein). It has now been coupled to various global and regional climate models (e.g. WRF (*Oaida et al.*, 2015), SNOWPACK (*Skiles and Painter*, 2019), RegCM4.6 (*Usha et al.*, 2022), E3SM (*Hao et al.*, 2023)).

All of the models discussed so far were developed for climate modelling purposes but many of them have shown that BC (and other light absorbing impurities) in snow can have impacts on seasonal timescales. For instance, *Yasunari et al.* (2015) found that including snow darkening aerosol in GEOS-5 led to increased precipitation and reduced evaporation in spring time. These results were further explored by *Lau et al.* (2018) and *Sang et al.* (2019). *Lau et al.* (2018) described a 'wet-first-dry-later' patten induced by aerosol in the snow with earlier melting leading to drier summers. *Sang et al.* (2019) found that the East Asian monsoon rains start earlier and are strengthened by the inclusion of aerosol snow darkening effects.

These results raise the question of whether BC should be included in shorter term forecasting as well as long time climate prediction. *Tuzet et al.* (2017) developed a scheme to represent light absorbing impurities within the detailed snowpack model - 'Crocus'. This scheme allows for a user specified set of aerosol species to be represented, BC and dust were the species used in this study. In the simulations presented in this study, Crocus is coupled to a climate model but Crocus is also designed for use in short term avalanche prediction and so the authors suggest

this development could be used to explore the impacts of snow impurities on avalanche risks. As such this study represents one of the first moves towards considering aerosol snow darkening effects in shorter term forecasting.

The detailed representation of snow metamorphism processes within Crocus allowed *Tuzet et al.* (2017) to investigate the contribution of indirect feedbacks on snow metamorphism to the overall radiative impacts of snow contaminants. They found that 15% of the snow darkening at the Alpine site studied was due to feedbacks on snow metamorphism and so simpler snow models that do not account for this process may underestimate the radiative impacts of snow contaminants. However, in a later study using the same model at a different Alpine site (*Tuzet et al.*, 2020) they found that feedbacks on metamorphism had a negligible impact so uncertainty remains regarding the importance of this process and it is suggested that its impact may vary depending on meteorological conditions and the timing of deposition. Another detailed snowpack model that is used for avalanche forecasting, 'SNOWPACK', has been coupled to SNICAR in order to account for aerosol induced snow darkening (*Skiles and Painter*, 2019). When this model was applied at a site in Colorado, the indirect affect of dust on radiative forcing was found to be 20% of the overall dust related snow darkening.

1.6 Motivation for this work

BC and other snow contaminants clearly have potential to impact snow accumulation and melt across all timescales by reducing the albedo of the snow surface and yet only recently has this process begun to be considered for anything other than long term climate prediction. The Met Office Unified Model, 'UM', is unique in its design to be used for both weather and climate prediction across a wide range of timescales and spatial resolutions. However, this model does not yet have the capability to predict the concentration of light absorbing impurities in snow and so cannot adjust snow albedos accordingly. This ultimately represents a weakness in its representation of snow physics given the importance of this process. This thesis will attempt to address this limitation by introducing a new representation of BC concentration in snow within the JULES land surface model that is used in the UM so that existing snow darkening routines can be utilised.

Whilst snow physical processes are complex, the most detailed model representations don't always yield the best results and are not always suitable for shorter term forecasting. Any representation within JULES must be computationally efficient and must fit in with the existing model architecture. For example, it will not be possible to maintain a detailed history of the position of BC particles within the snowpack because that would require a large increase in the number of snow layers modelled and an associated increase in the number of variables stored in memory. Instead of striving to produce the most detailed model possible, this work will examine whether a relatively simple representation, designed around the existing snow scheme in JULES, is suffi-

cient to predict the snow darkening associated with BC and thus improve modelled snow albedo and melt on seasonal timescales.

The research questions to be addressed in this work are as follows:

1. Can a simple representation of BC evolution within the JULES snowpack simulate the real world near surface BC concentration?
2. Does incorporating BC snow darkening into JULES simulations improve predictions of snow albedo and seasonal snowmelt timing?
3. What are the subsequent radiative and hydrological impacts within JULES of including BC snow darkening?

Before introducing any changes to JULES, chapter 2 provides detail on the existing structure of the snow and snow albedo schemes within JULES, as well as demonstrating the model's performance at a test site in Japan. This chapter also discusses how BC deposition fields that are used throughout the thesis have been generated. Chapter 3 describes the proposed changes to JULES that will calculate the concentration of BC in snow and tests the new scheme using site based observations. In chapter 4, the wider implications of introducing BC on snow to JULES are explored. Impacts on snow accumulation and duration are assessed as well as onward impacts to the surface energy balance and water cycle. Regions that see the greatest impacts are identified and the river catchments that are most affected are highlighted. A satellite albedo product is used in chapter 5 to assess the performance of the updated JULES model at predicting snow albedo across the Northern Hemisphere. Unlike many assessments of land surface albedo performance, this analysis focuses specifically on the snow covered period at each gridbox in order to assess snow albedo performance specifically. As such it is possible to identify strengths and weaknesses in JULES's ability to predict snow albedo and snow cover duration and recommendations are made for further areas of development to the JULES snow scheme.

Chapter 2

Models, methods and data used

2.1 Introduction

The work in this thesis centres around using the Joint UK Land Environment Simulator (JULES) to predict the albedo of snow and its subsequent impacts on snow melt. This chapter introduces technical aspects of the JULES model that are relevant to the work undertaken in this thesis along with a description of the site data that is used for testing the response of JULES to black carbon (BC) on snow in this and subsequent chapters. Other datasets used later in the thesis will be introduced in their relevant chapters.

Having introduced the existing snow and snow albedo schemes within JULES, a demonstration will be given of how these schemes perform when BC is prescribed directly. However, it is generally more convenient to prescribe BC deposition rather than concentration as BC deposition can be readily obtained using a general circulation model (GCM) that includes a chemistry and aerosol scheme. A description is given of how this method is used to generate BC deposition values that will be used later in this thesis along with discussion of the accuracy of these values.

2.2 Joint UK Land Environment Simulator (JULES)

The Joint UK Land Environment Simulator is a community model that was developed for use as the land surface component of the Met Office Unified Model for weather and climate prediction (UM) but is also capable of running as a standalone land surface model, for research or testing purposes, when provided with atmospheric driving data. For the JULES simulations in this thesis, the driving variables supplied are: short wave and long wave downward radiation, rainfall and snowfall, near surface air temperature, pressure, specific humidity and wind speed.

JULES can run at a single point location or over a gridded domain but in either case it runs as a

one dimensional model at each gridbox that does not depend on horizonal boundary conditions or communication with neighbouring gridboxes. The surface type of each gridbox is typically expressed as a combination of nine surface tiles – broadleaf trees, needleleaf trees, C3 and C4 grasses, shrubs, urban, inland water, bare soil and ice. A detailed description of the JULES model is given by *Best et al.* (2011) and *Clark et al.* (2011).

JULES contains many optional components that can be switched on and off depending on computational resource constraints or the purpose of the simulation. New features are continually being added so there are some options available now that were not available at the start of this research project. The combination of settings used for a given simulation is referred to as the 'configuration' of the model. Most of the work in this thesis is based around the 'OS36 UKV' configuration that was introduced for operational weather forecasting in the UK in August 2015. However, a few snow specific changes have been made in order to incorporate the multi-layer snow scheme which was in the late stages of development and was expected to have considerable impact on JULES's capabilities for modelling snow so was deemed relevant to this research. The multilayer snow scheme began being used in operational weather forecasting in OS41 in September 2018. A full list of settings used for work in this thesis can be found in appendix A and any simulations shown that use settings other than that will be made clear in the text.

2.2.1 Brief overview of the snow scheme within JULES

Snow properties within JULES are calculated separately for each surface tile. In recent years the scheme has been upgraded to incorporate multiple snow layers although the original zero layer scheme is retained for cases of thin snow. Whilst the user can specify any maximum number of snow layers it is typically used with three layers and the thickness of layers is determined by user specified values. A snow layer may grow to twice its specified thickness before a new layer is added, up to the maximum number of layers and any excess snow depth beyond this is added to the bottom snow layer. Each snow layer has properties of temperature, grain size, density, and frozen and liquid water content. The number and thicknesses of layers, along with the various properties stored on layers are recalculated every timestep. This is more affordable, in terms of memory resource, than schemes such as CROCUS (*Brun et al.*, 1989) that includes many snow layers in order to allow snow with different properties, such as grain size, to be kept separate. Snowfall is added to the top of the snowpack and melt and sublimation are calculated each timestep. Meltwater can move down through snow layers and either re-freeze lower down in the snowpack or leave the bottom of the pack as runoff.

There are two methods available within JULES for calculating the rate of growth of snow grains over time which is important for accurate albedo predictions. The first method is based on work by *Marshall* (1989) and attempts to account for both equitemperature (ET) and temperature gra-

dient (TG) metamorphism by assuming a constant rate of growth for grains smaller than $150.0\,\mu m$ and assuming a temperature dependence for larger grains. Whilst this method performs well in many conditions it has been found to cause grains to grow too rapidly at cold temperatures occasionally leading to overly dark albedos (*Walters et al.*, 2019). The second is based on the quasi-equitemperature parametrization described by *Taillandier et al.* (2007), this method is expected to be suitable for snowpacks with low temperature gradients with the threshold between ET and TG metamorphism sitting somewhere between 9 and $20^{\circ}C\,m^{-1}$. The snow scheme also allows for changes in density of snow layers over time due to mechanical compaction caused by the weight of snow above as well as (optionally) equal temperature metamorphism.

There is an optional canopy snow scheme that allows a fraction of snowfall to be intercepted by the vegetation canopy and sit there for a while before eventually either melting or falling through to the main snowpack on the ground. This scheme enables the vegetation canopy to be partially obscured by snow on top of the canopy whereas if the scheme is not used then the surface albedo is based on the snow cover on the ground and the fraction of exposed vegetation. The canopy snow scheme is mainly used for needle leaf trees but could be applied to any vegetation tile. However, even when this scheme is in use, the main properties of snow layers (temperature, grain size, density, and frozen and liquid water content) are only calculated for the snow on the ground beneath the canopy and it is these values that are used for calculations elsewhere. The impacts on albedo from the canopy snow scheme are from the changes to the amount of exposed vegetation.

2.2.2 Brief overview of the snow albedo schemes within JULES

There are two main schemes within JULES for determining the albedo of snow. A third, simpler, method exists that combines user specified snow albedo values with an adjustment for the leaf area index but this method is rarely used anymore so will not be discussed further here. Of the two more commonly used snow albedo schemes in JULES, the first is based on a simplification of the parametrization proposed by *Marshall* (1989). It calculates the diffuse visible and near infrared albedos of clean snow as

$$\alpha_{vis} = 0.98 - 0.002 \cdot \left(r^{\frac{1}{2}} - r_0^{\frac{1}{2}} \right) \tag{2.1}$$

$$\alpha_{nir} = 0.7 - 0.09 \cdot \ln\left(\frac{r}{r_0} \right) \tag{2.2}$$

where r is the snow grain radius in the surface snow layer and r_0 is the grain radius of freshly fallen snow. These equations are illustrated in figure 2.1. For direct albedos, the same equations are used but the snow grain size is adjusted according to the cosine of the solar zenith angle,

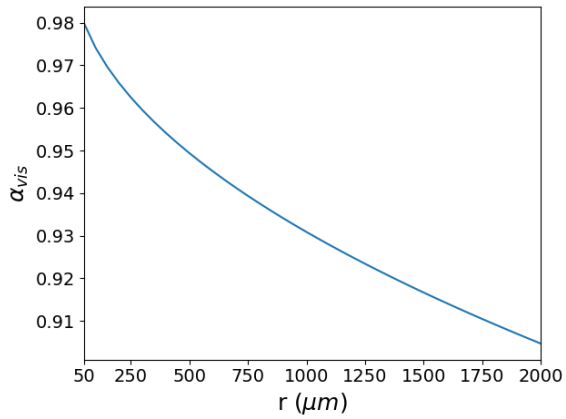

(a) Diffuse snow albedo in the visible waveband

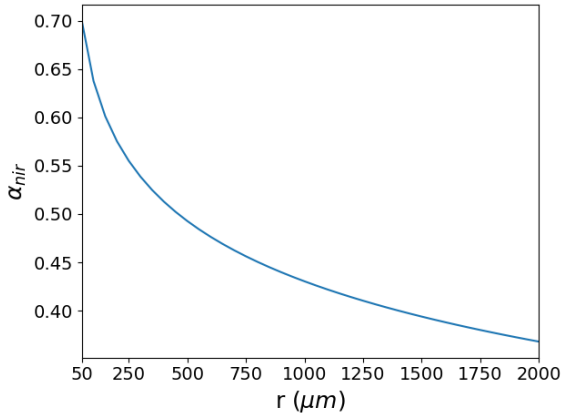

(b) Diffuse snow albedo in the near infrared waveband

Figure 2.1: Dependence of diffuse snow albedo on snow grain size according to equations a) 2.1 and b) 2.2.

μ_0, to give an effective snow grain radius of

$$r_{eff} = [1 + 0.77 \cdot (\mu_0 - 0.65)]^2 r. \tag{2.3}$$

The resulting dependence of direct albedos on the solar zenith angle given by these equations is illstrated in figure 2.2.

The snow albedos are then adjusted to account for the presence of soot in the snow. The adjustments for visible and near infrared albedos follow the same form but use different constants, there are two different forms for the soot adjustment depending on whether the soot mass frac-

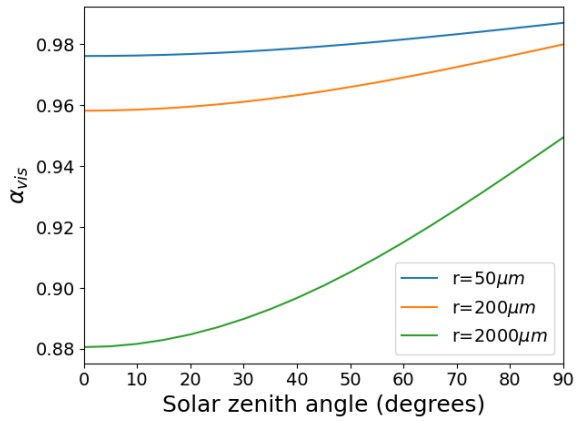

(a) Direct snow albedo in the visible waveband

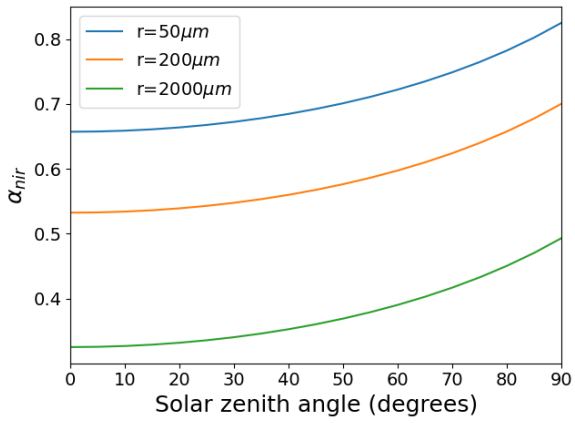

(b) Direct snow albedo in the near infrared waveband

Figure 2.2: Dependence of direct snow albedo on solar zenith angle for three different values of snow grain radius, r. Calculated by combining equation 2.3 with equations 2.1 and 2.2.

tion, s, is above or below a threshold, $S2$. $S2$ is related to the snow grain size and is expressed differently for visible and near infrared radiation: $S2_{vis} = 0.00017r^{-1}$ and $S2_{nir} = 0.004r^{-1}$. For low soot mass fractions, $s < S2$, the albedo adjustments are:

$$\alpha = \alpha_{clean} - 0.5 \cdot \left(\alpha_{clean} - \frac{AL}{2}\right)\left(\frac{s}{S2}\right)^{kl}. \tag{2.4}$$

The values of kl are 0.6 and 0.7 for visible and near infrared equations respectively. Note that for soot concentrations of $s = 0$, this equation simply returns the clean snow albedo that was calculated previously. Soot mass fractions higher than the thresholds above give:

$$\alpha = \frac{AL}{2} + 0.5 \cdot \frac{\left(\alpha_{clean} - \frac{AL}{2}\right)}{\left(\frac{s}{S2}\right)^{kh}}. \tag{2.5}$$

The values of kh are 0.46 and 0.6 for visible and near infrared equations respectively. AL represents a minimum possible snow albedo value and regardless of the soot content, the values of $\frac{AL}{2}$ used in equations 2.4 and 2.5 are 0.07 for visible radiation and 0.06 for near infrared. In all cases, no distinction is made for visible or diffuse radiation. Whilst these equations to adjust snow albedo for the presence of soot have existed in JULES for many years, until now there has not been any infrastructure within JULES to prescribe or calculate the concentration of soot so the value has always defaulted to zero.

Having calculated the snow albedos, the overall albedo of the surface tile is then given as a combination of snow covered and snow free albedos with the snow covered fraction being given as

$$f_{snow} = \frac{d}{d + 10z_0} \tag{2.6}$$

where d is the snow depth and z_0 is the roughness length of momentum (which here is a fraction of canopy height).

More recently, the two-stream embedded snow albedo scheme has been introduced. This scheme was designed for use with the multi-layer snow scheme and the canopy snow scheme. It began being used for operational weather forecasting at the Met Office in September 2018 (mid-way through work on this PhD). This scheme uses scattering properties of snow grains and BC particles based on assuming spherical geometry of grains and applying Mie Theory calculations. The equation used for the single scattering albedo of snow is

$$\omega_0 = \left[1 + C_1 + C_2 \cdot ln(D_e) + C_3(ln(D_e))^2 + B_2.s\frac{D_e}{D_{ec}}\right]^{-1}, \tag{2.7}$$

the optical depth of the snow layer is

$$\tau = \frac{3M_s}{\rho_{ice}D_e} \tag{2.8}$$

and the asymmetry parameter that characterises the directionality of scattering is

$$g = G_1 + G_2 ln(D_e). \tag{2.9}$$

These properties are calculated separately for visible and near infrared radiation bands and the values depend on the mass of snow, M_s, the density of ice , ρ_{ice}, the effective diameter of the snow grains, D_e, and BC particles, D_{ec}, and the mass mixing ratio of BC, s. C_1, C_2, C_3, G_1 and G_2 are constants that were determined by fitting curves to results of Mie calculations *Edwards* (2014)[unpublished]. B_2 is a combination of several other constants, averaged across frequencies. The effective diameter of BC particles used is $0.248\,\mu\text{m}$, based on *Schwarz et al.* (2008) and *Schwarz et al.* (2013). Again however, although the ability to account for BC exists in these calculations, it is never used as the concentration of BC has always been set to zero when running JULES.

The scheme then adopts the Practical Improved Flux Method (PIFM) that was described by *Zdunkowski et al.* (1980) for calculating radiative fluxes of direct and diffuse radiation through clouds and uses it instead to determine the transmission and reflectance of radiation through a layer of snow based on the previously calculated snow scattering properties. These transmission and reflectance values are then used to generate an albedo value for the snow surface.

In the case of vegetated tiles, an effective leaf area index, L_e is calculated for exposed vegetation above the snow as

$$L_e = L\left(1 - \frac{d}{h}\right)^n \tag{2.10}$$

where L is the snow-free leaf area index, d is the snow depth, h is the canopy height of the vegetation and n is a parameter for expressing the distribution of leaves throughout the canopy. In recent configurations, the value of n has been set to 1.0. L_e is then used to calculate the calculate the albedo of the exposed vegetation with snow underneath, this step uses the vegetation albedo scheme (again based on two-stream equations) but here uses the previously calculated snow albedo for the underlying surface rather than a bare soil albedo as would be used in snow-free conditions. Finally, if the canopy snow scheme is being used then a separate snow albedo is calculated for snow on top of the canopy. To account for uneven distribution of snow in the canopy, a 'clumping factor', C, is applied with canopy snow said to occupy $1/C$ of the canopy such that the overall albedo seen above the canopy is

$$\alpha = \left(\frac{1}{C}\right)\alpha_{snow\_c} + \left(1 - \frac{1}{C}\right)\alpha_{snow\_g+veg} \tag{2.11}$$

where α_{snow_c} is the albedo of the snow on top of the vegetation canopy and α_{snow_g+veg} is the combined albedo of the snow on the ground and the exposed vegetation above it.

Whichever snow albedo scheme is used, the net shortwave radiation on each tile is calculated based on sum of the direct and diffuse visible and near-infrared radiation and associated albe-

dos. In standalone JULES, only a total shortwave incoming radiation field is provided in the driving data so this is divided into the four radiation streams according to user specified fractions defined via the 'wght_alb' parameter. The equation used is

$$SW_{net} = \left(1.0 - \sum_{n=1}^{4} (wght\_alb[n]\alpha[n])\right) SW_{down}. \tag{2.12}$$

Here, n represents the four different radiation streams, $\alpha[n]$ is the albedo corresponding to each. The sum of the weighted albedos is used to determine the amount of incoming radiation, SW_{down}, that is reflected by the surface and this is subtracted from the incoming radiation to give an overall net radiation, SW_{net}, absorbed by the surface. Typically, the fractions used are 0.5 for the two diffuse streams and 0.0 for the two direct streams - i.e. an even split between visible and near infrared radiation but all radiation assumed to be diffuse and none direct. This default has been used in the JULES simulations in this thesis. In JULES, visible radiation refers to that with wavelengths less than 700nm and larger wavelengths than that are treated as near infrared (*Edwards et al.*, 2018). The spectrum is divided at this wavelength because there are significant changes in albedo behaviour (and also atmospheric absorption behaviour) at approximately this point but it also happens to be roughly the mid-point in terms of the amount of solar radiation received at the Earth's surface. Table 148 in *List* (1949) indicates that the 50/50 split between visible and near infrared wavebands is appropriate for radiation received under clear sky conditions when the sun is directly overhead but may become less appropriate under cloudy conditions or large solar zenith angles when the fractions of radiation received are closer to 0.4 in the visible waveband and 0.6 in the near infrared. However, standalone JULES does not have a mechanism for altering the wght_alb parameter over the course of a simulation and so the even partitioning was maintained for these simulations.

The assumption that all radiation is diffuse is unlikely to be accurate and may lead to some errors in diurnal patterns of the amount of radiation reflected vs. absorbed at the surface due to the lack of zenith angle dependence of albedo but without cloud cover information it is difficult to know how else to partition the incoming radiation. Based on the data in figures 2.1 and 2.2 the largest differences between direct and diffuse albedos would be 0.044 for the visible waveband and 0.12 for the near infrared waveband, these represent the maximum possible errors from incorrectly partitioning the radiation between direct and diffuse. Note that the impact is much smaller in the visible waveband which is of more relevance in this thesis as the snow albedo in the near infrared waveband is much less affected by the addition of black carbon.

2.3 Description of site based data used in this thesis

Whenever testing the prediction capabilities of a land surface model it is necessary to have accurate atmospheric driving data to force the model with as well as other appropriate observations to validate the model output against. To test the model in the broadest range of settings it is common to use global gridded re-analysis products to provide the driving data and satellite products for the validation data. However, both re-analysis driving data and satellite products require further modelling steps to generate so whilst this approach is useful, and will be applied in chapter 5, to isolate JULES model performance from any other modelling processes in our validation it is best to use direct meteorological observations collected from ground observation stations. To drive JULES, regular observations are required of short wave and long wave downward radiation, precipitation, near surface air temperature, pressure, specific humidity and wind speed. For the work in this thesis, regular observations of snow depth, albedo and concentration of black carbon in snow are also required for validation purposes. The latter is particularly labour intensive to observe so is only collected regularly at a small handful of sites. One site at which all the relevant driving and validation observations are regularly collected is the Institute of Low Temperature Science at Hokkaido University campus in the city of Sapporo, Japan (43.082°N, 141.342°E). Data from this site will be used for validating JULES performance and testing model changes throughout this thesis.

The location of this site on the Sea of Japan means it experiences heavy snowfalls due to the 'Japan Sea polar air mass convergence zone' (JPCZ) – a convergence of warm moist surface air, supplied by the Tsushima warm current in the Sea of Japan, with the cold dry polar air mass from Siberia, driven by the Asian Winter Monsoon. This phenomenon has recently been observed in shipboard observations by *Tachibana et al.* (2022). The Asian Winter Monsoon also supplies aerosol from Siberia and North-East China (*Yamamoto et al.*, 2011) with further aerosol contribution likely coming from the local urban environment. As such, it is likely that this site is strongly affected by BC-snow-albedo interactions.

The meteorological observation field at Hokkaido University is a short grass surface with clay soils within an urban area. Snow pit measurements have been collected at this site twice weekly for winters from 2007 to 2013. Meteorological data is also available year round but is only quality controlled during the winter months, during the summer months it is therefore better to use reanalysis data. A 60 minute forcing data set for JULES that uses Sapporo observations in winter and re-analysis data in summer (June–October) was compiled for ESM-SnowMIP (*Krinner et al.*, 2018) and is available online (*Menard et al.*, 2019). The observations at Sapporo have previously been used for validating the Snow Metamorphism and Albedo Process (SMAP) model and are described by *Niwano et al.* (2012).

Broadband albedo values are determined as a ratio of measurements of upward to downward shortwave ($\lambda = 0.305 - 2.8\mu\text{m}$) radiation flux, obtained using pyranometers. Details of the

specific instrument setup used are provided by *Aoki et al.* (2011).

The mass concentration of BC in the snow was determined using the following method: Samples of snow were collected from snow pits for the top 2cm and top 10cm of snow. To determine the total mass of snow contaminants present, the snow samples were melted and then passed through a filter. The difference in the weight of the filter before and after this process indicates the total weight of snow contaminants. The filter was then examined using a thermal optical reflectance method to measure concentrations of organic and elemental carbon (OC and EC). For the purposes of this thesis EC and BC are assumed to be equivalent. Any remaining weight of impurities that had not been attributed to OC or EC were assumed to be dust. Observations of EC concentration in snow were multiplied by a factor of 1.45 to account for undercatch of the quartz fibre filter as a coagulant hadn't been used in the filtering of samples collected prior to 2013. The need for this multiplication factor is discussed, along with other details of the methods used for assessing mass concentrations of impurities in the snow samples, by *Kuchiki et al.* (2015).

2.4 Impact of prescribing snow black carbon concentration in JULES

It is possible to use the observed values of BC concentration in snow at Sapporo to test the existing infrastructure within JULES for altering the albedo of snow in the presence of BC. Whilst there is no in-built infrastructure within JULES to read in BC concentration data, it is relatively straightforward to add this. To do so, I took a branch from JULES vn5.2 and added extra code to open a file containing BC concentration values for snow at Sapporo at the start of the simulation and then on each timestep read the value from the next line in the file. This value is then converted from ppm to kg/kg and passed to the soot_conc field in albsnow_jls_mod.F90 (the Marshall snow albedo scheme) for use in snow albedo calculations. This modified branch is available from the Met Office Science Repository Service (MOSRS)[1].

For this test, the observations of BC concentration in snow for the top 2cm of snow were used, rather than the top 10cm as JULES only uses properties from the top snow layer to calculate snow albedo. For the OS36 UKV configuration used here, the top snow layer in JULES has a thickness of 4cm so the top 2cm observation was deemed to be the closer comparator. The BC concentration values were linearly interpolated from twice weekly observations onto 1 minute timesteps for use in JULES.

Figure 2.3 shows the observed albedo and snowdepth values at Sapporo compared with values generated from JULES runs with and without the BC concentration in snow prescribed. The plots show that including BC in snow considerably improves both the JULES albedo and snowdepth

[1] MOSRS location of JULES branch for prescribing BC on snow: `https://code.metoffice.gov.uk/trac/jules/log/main/branches/dev/helenjohnson/r12869_snowBC_PrescNrSurfConc_1minTS` (registration required)

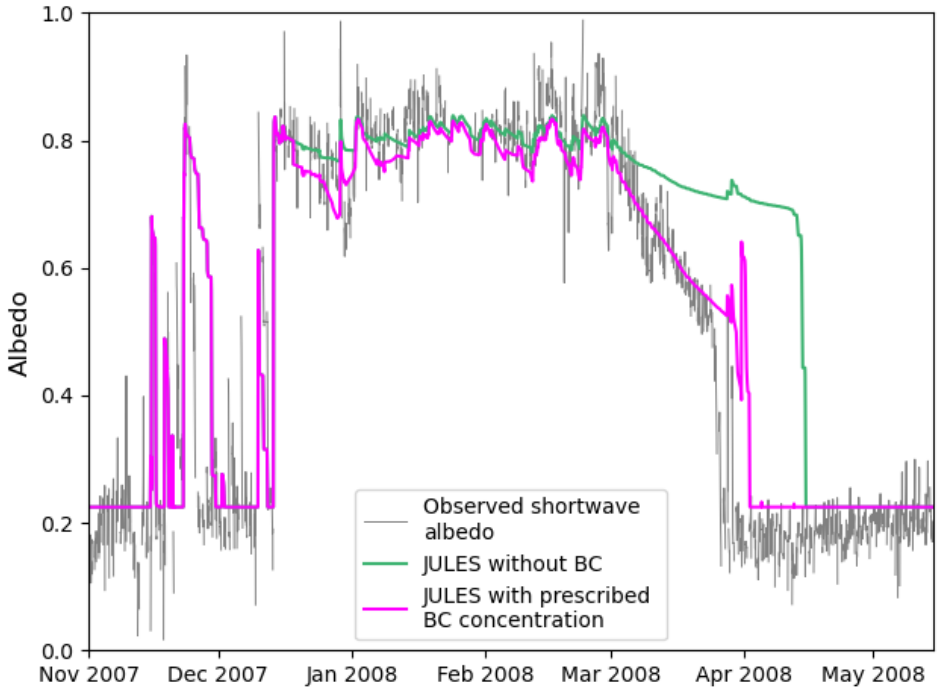

(a) Shortwave albedo

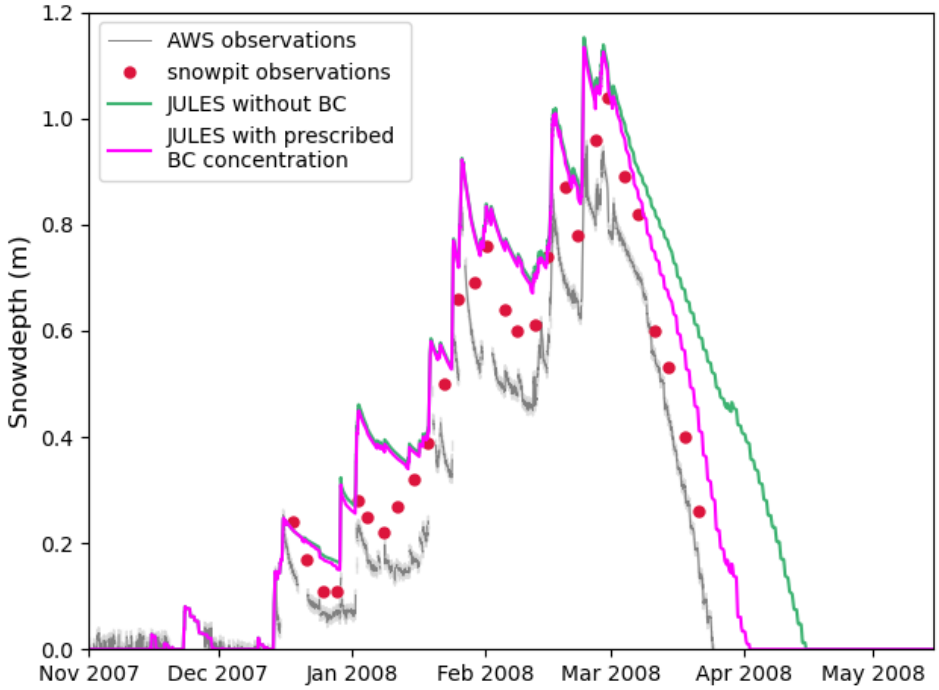

(b) Snowdepth

Figure 2.3: Modelled and observed (a) shortwave albedo and (b) snowdepth at Sapporo. Modelled values are shown at half hourly intervals to match the frequency of the observed albedo and AWS snowdepth data. For snow depth, two different sets of observations are shown - automatic weather station (AWS) and snowpit measurements. The errors associated with AWS observations are shown in light grey shading either side of the dark grey line. The snowpit measurements have an accuarcy of $\pm 0.5cm$ so errors are smaller than the markers on this plot.

during the snow melt season. The good agreement between the modelled and observed albedo values indicates that when JULES is provided with direct observations of BC concentration in snow it is able to appropriately adjust the albedo of snow to account for the presence of BC.

A note on errors in observed snow depth: For the snow depth, two different sets of observations were recorded - half hourly measurements from a Campbell SR50 ultrasonic distance sensor installed at the automatic weather station (AWS), which has an accuracy of $\pm 1cm$, and twice weekly measurements that were recorded when snow pits were dug. The instrumentational errors associated with the AWS observations are indicated by light grey shading in figure 2.3b whereas for the snowpit work they are not shown as will be smaller than the dots themselves ($\pm 0.5cm$). However, it can clearly be seen that the differences between these two sets of measurements is far larger than the instrumentational errors associated with either dataset - this is due to spatial variability in snow depth. The AWS measurements were always recorded at the same point whereas the snow pits were dug in a slightly different location each time. The fact that the snow pit measurements always appear to be greater than the AWS measurements could be due to local wind blown snow effects - perhaps the snow pit work was undertaken in a slight basin relative to the AWS so that more snow could accumulate or perhaps that the dense arrangement of instruments at the AWS shielded the area from accumulation of blowing snow somewhat.

The final snowpack clearance occurs 13 days earlier in the JULES simulation where BC is included. This result is comparable with that of *Niwano et al.* (2012) who found that, when running the model 'SMAP' for the same winter at Sapporo, including both BC and dust impurities in simulations caused snow to melt 19 days earlier. Here, the reduction in duration of snow cover is slightly smaller as only BC impurities are currently considered with the JULES albedo calculations. The large impact of BC on snow all gone date at this site is in part due to the substantial amount of snow accumulated here to begin with – locations with smaller snowpacks would take less time to melt and so would see a smaller impact from melt acceleration.

2.5 Black carbon deposition values

2.5.1 Why we need to model BC concentration rather than prescribe it

Whilst the existing albedo scheme within JULES performs well when provided with observations of the concentration of BC in snow, it is very rare that these observations are available. Only a tiny number of observation sites exist that routinely collect this data. Those that do are mainly limited to populated areas, due to the human labour required to collect the data, so do not represent the spread of different snow and BC deposition conditions across the world.

There is currently little prospect of satellite observations being capable of plugging the gaps in

spatial coverage of BC concentration measurements. *Warren* (2013) discussed a variety of reasons why distinguishing BC content in snow from remotely sensed albedo measurements would be extremely challenging. The amount of BC required to darken snow sufficiently that it impacts melting behaviour is small enough that it would be difficult to distinguish from errors in remotely sensed albedo measurements. Other physical processes that cause snow to appear darker include thin or patchy snow cover, vegetation, surface roughness, changes to snow grain size with aging, atmospheric pollution and cloud cover – all of which would be difficult to distinguish from darkening due to snow impurities. Efforts to solve these challenges are continuing with recent work focussing on extracting snow impurity concentrations as a component of determining snow cover fraction from multispectral reflectance measurements (e.g. *Bair et al.* (2021) and *Painter et al.* (2012)). However, in the near term the only accurate observations of BC concentration in snow available to us remain those collected manually at ground observation stations.

The time taken to process the observations, including the time to transport the snow sample from the observation field to the laboratory for analysis, means it will always be difficult to assimilate these observations into short term weather forecasting models. For longer term (e.g. seasonal) weather forecasting and for climate modelling it is necessary to be able to forward model what the BC concentration in snow will be in the future.

With these constraints in mind, a more practical approach instead of prescribing BC concentration in snow is instead to prescribe the BC deposition onto the snow and then model it's accumulation and evolution within the snowpack in order to predict the near surface concentration for use in albedo calculations. Observations of BC deposition onto snow are also not widely available - a methodology for directly observing black carbon deposition fluxes at the surface has only very recently (during the course of this PhD) been developed by *Emerson et al.* (2018) and has not yet been applied to snow covered surfaces. However, the ability to model BC transport through the atmosphere and deposition onto the land surface already exists within coupled climate models such as the UM. As such, this work will rely on modelled BC deposition as an input to JULES.

In order to model the accumulation and evolution of BC within the snowpack, it will be necessary to make some modifications to the snow scheme within JULES to calculate BC concentration in snow from the input deposition values. These developments will be discussed in chapter 3.

2.5.2 Coupled atmosphere-aerosol simulations with the UM and CLASSIC

The Met Office Unified Model (UM) was used to generate BC deposition values for use throughout this thesis in testing and studying the impact of including BC on snow in JULES. The UM can optionally be run with a choice of two possible aerosol schemes – the Coupled Large-scale Aerosol Simulator for Studies In Climate (CLASSIC) or the Global Model of Aerosol Processes

(GLOMAP). For this work I chose to run the UM with the CLASSIC scheme as it produces 2D fields of deposition flux at the surface.

Aerosol deposition values are generated in the UM by providing global aerosol emissions ancillary data to the aerosol scheme. The atmospheric model then advects the various species of aerosol around the globe, depending on the modelled weather systems, whilst the aerosol scheme evolves the aerosol species according to ageing characteristics, accounts for aerosol radiative effects and simulates deposition rates based on modelled weather conditions. Both dry and wet deposition processes are included. A more detailed description of the CLASSIC aerosol scheme is included in the appendix of *Bellouin et al.* (2011).

In order to produce aerosol deposition values to pass into a JULES simulation, I ran the UM globally with 85 vertical levels and an N96 horizontal resolution, meaning that the maximum number of two gridlength waves that can be represented is 96 (this works out as a gridbox width of approximately 135km at mid latitudes). The configuration used for this UM simulation was the 'Global Atmosphere / Global Land 7' (GA/GL7) standard model configuration for global coupled land-atmosphere simulations with the addition of the CLASSIC aerosol scheme. The GA/GL7 model configuration is described in detail in *Walters et al.* (2019). The model was run with a 20 minute timestep outputting daily mean aerosol deposition flux data. The aerosol emissions ancillaries input to CLASSIC were a climatology based on a ten year average from 2002 to 2011 provided by MACC/CityZEN, this dataset is available via the ECCAD-Ether project[2] and more detailed descriptions are given by *Granier et al.* (2011), *Lamarque et al.* (2010) and *van der Werf et al.* (2006).

A total black carbon deposition value is calculated by combining several of the aerosol deposition fields that are output from CLASSIC – specifically, those relating to soot (from fossil fuel and biofuel combustion) and open biomass burning. Biomass burning values are made up of both black carbon and organic carbon aerosol and so the black carbon contribution from biomass burning is a fraction of the overall biomass burning values. For both soot and biomass, CLASSIC has different output fields for the various different processes that lead to deposition. Table 2.1 lists the various different output fields that are used for calculating total black carbon deposition and the fraction of each field which is considered to be black carbon (rather than organic carbon).

For the global simulations in chapters 4 and 5 it was necessary to regrid the BC deposition fields output from the UM onto a 0.5° grid to match the resolution of the meteorological driving data that is used in those simulations, this was done using a nearest neighbour regridding method. A map of the mean BC accumulation over the course of a year generated with this method is shown in figure 2.4a. Note that the grid used here does not include Antarcticabecause driving data is not available over Antarctica in the dataset used for global simulations in this thesis. It can be seen that the areas with highest BC deposition values are found in East Asia, particularly the Brahmaputra valley region and parts of Eastern China, and in the rainforest regions of Africa.

[2] `http://eccad.sedoo.fr`

Table 2.1: Output deposition fields from CLASSIC that are used for calculating the total black carbon deposition onto the surface and fraction of the field which contributes to this total black carbon value.

Deposition field	**Fraction of which is BC**
Fresh soot dry deposition	1.0
Aged soot dry deposition	1.0
Soot rainout by large scale precipitation	1.0
Soot scavenged by convective precipitation	1.0
Soot in cloud deposition	1.0
Fresh biomass dry deposition	0.0875
Aged biomass dry deposition	0.0540
Biomass rainout by large scale precipitation	0.0540
Biomass scavenged by convective precipitation	0.0540
Biomass in cloud deposition	0.0540

These are areas that receive a lot of rainfall (allowing BC to be deposited through wet deposition), are heavily industrialised or experience open burning through wildfires or agricultural burning practices. Areas that experience the lowest deposition quantities are the desert areas such as the Sahara, Taklamakan and Gobi deserts. In part, the lack of deposition in desert regions will be due to lack of precipitation to drive wet deposition processes but the remoteness of these regions along with the lack of vegetation will also play a role due to fewer emission sources.

To get a sense of the extent to which BC deposition varies from one year to the next, the standard deviation in annual total BC deposition is shown in figure 2.4b. On the whole, the locations that see the greatest variability in deposition are the same locations that receive the largest quantities of deposition on average however the subtropical regions of Africa and South America as well as parts of Canada and Alaska also see considerable variability. Given the aerosol emissions ancillaries provided to CLASSIC are a climatology that does not vary from one year to the next, this variability is solely due to difference in modelled weather patterns from one year to the next.

2.5.3 Accuracy of CLASSIC deposition values

It's important to remember that the BC deposition fields used throughout the rest of this work are modelled rather than observed so may not be entirely accurate. There could be a number of reasons why the modelled deposition values might not be accurate so it's important to consider their limitations. Possible causes of inaccuracy include:

- Interannual variability in emissions not being accounted for when using a climatology of BC emissions.
- Undercount of emissions in the inventory used to drive the aerosol scheme.

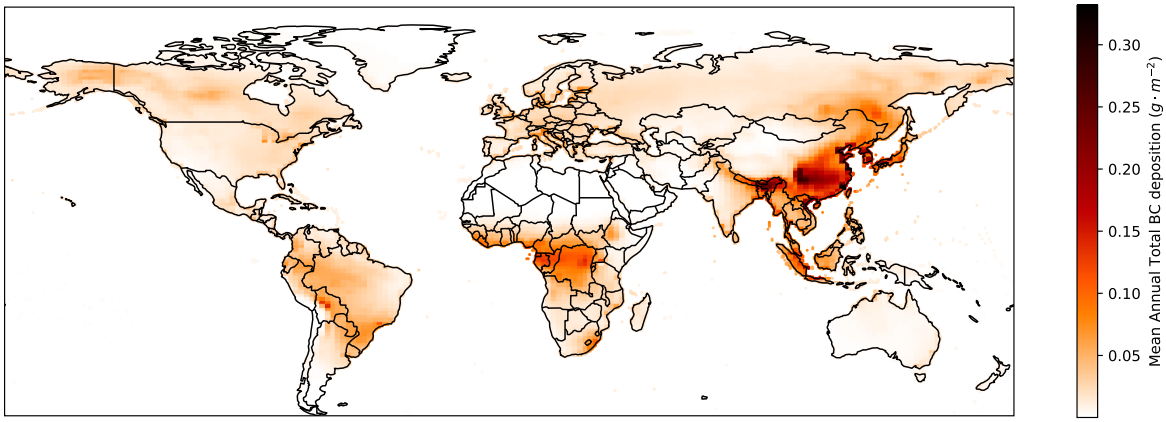

(a) Mean annual total BC deposition

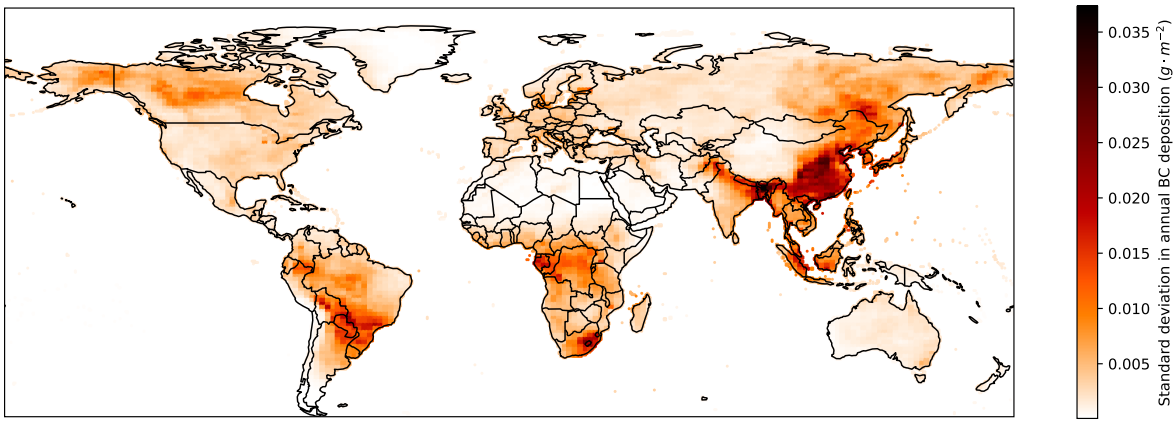

(b) Standard deviation of annual total BC deposition

Figure 2.4: Maps of mean (a) and standard deviation (b) annual total black carbon deposition output from CLASSIC over 1991–2007. Totals are accumulated over the course of a year running from 1st September to 31st August. Data has been regridded to 0.5° WFDEI grid.

- Inaccuracies in the modelled weather patterns, either due to weaknesses in model physics or driving data, would lead to inaccurate aerosol deposition values.
- Modelled atmospheric transport lifetime (linked to modelled scavenging/deposition processes).
- Local variations not being resolved by coarse model grid spacing ('subgrid variability').

Whilst validating the accuracy of the UM-CLASSIC BC deposition output globally is beyond the scope of this work, it has been possible to explore it more thoroughly at Sapporo, Japan, due to the availability of detailed snowpack measurements collected frequently throughout the snow season including measurements of the concentration of BC in the snowpack at that site. This data allows an estimate of cumulative BC deposition to be generated for the period of time when snow is accumulating.

To estimate the cumulative BC deposition, the mass of BC present in the top 2cm of snow

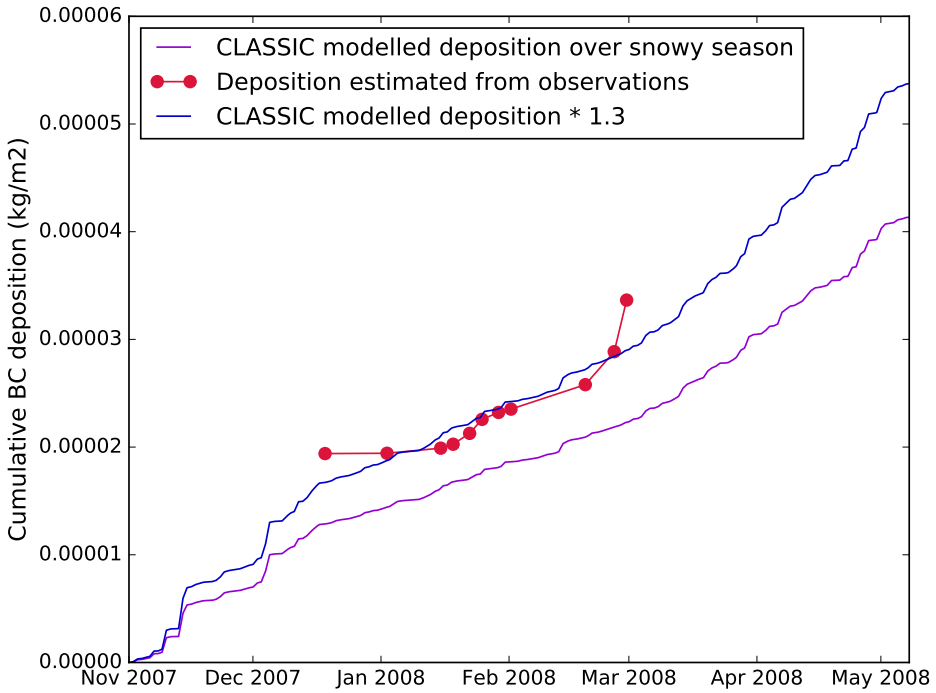

Figure 2.5: Comparison of cumulative CLASSIC black carbon deposition with estimated deposition based on observations in top 2cm of snow at Sapporo.

at Sapporo is calculated from the observations of BC concentration and snow density. Then, the mass of BC in the top 2cm of the snowpack is added to the total each time the snow depth increased by 2cm to give a cumulative timeseries of deposition. Where snow depth increased by more than 2cm between observations, it was assumed that the BC concentration in the top 2cm was the same as the concentration for all snow deposited since the previous observation. This method also relies on the assumption that no melting takes place as the snowpack accumulates.

The resulting timeseries of estimated cumulative deposition at Sapporo is shown with the red line in figure 2.5; the points indicate times at which the depth of the snowpack was observed to have increased by 2cm or more. The purple line shows the cumulative deposition from the CLASSIC aerosol scheme; the CLASSIC BC deposition is considerably lower than that suggested from the observations.

This result suggests that more BC is being deposited at Sapporo than is modelled by the CLASSIC aerosol scheme. There are a number of possible reasons for this, especially given the site's urban location. Firstly, CLASSIC is known to carry aerosols a long way from their source before depositing them – a 2014 intercomparison study showed that HadGEM2 (a UM climate configuration that uses the CLASSIC aerosol scheme) had longer black carbon global atmospheric residence times than any other model in the study (*Jiao et al.*, 2014). HadGEM2 was found to have mean BC atmospheric residence times of 17.1 days (*Samset et al.*, 2014) whereas studies based on aircraft observations have suggested that mean BC atmospheric residence times of

more than 5.5 days are unrealistic (*Lund et al.*, 2018). and whilst it is difficult to determine what the actual atmospheric residence times for BC should be, if the times produced by CLASSIC are excessive then it would likely lead to an underprediction of deposition close to source regions such as urban areas because BC is being transported further away and eventually deposited in more remote locations. Another possible consideration is that emissions that get deposited very close to their source location may be underrepresented in emissions inventories which could again lead to lower deposition rates in the model than in reality. It is possible that both of these factors play a role in the underprediction of BC deposition at Sapporo.

Yasunari et al. (2014) similarly found an underprediction of BC aerosol near the surface at Sapporo when they compared BC output from the Goddard Chemistry Aerosol Radiation and Transport module (GOCART) within the NASA Goddard Earth Observing System version 5 (GEOS-5) earth system model with observations of near surface atmospheric aerosol concentration at Sapporo. Whilst their model was using different aerosol emissions inventories to those used here, they suggested that the findings indicated an under-representation of local BC emissions. It is possible that such an under-representation could be echoed in other emissions inventories due to similarities in methods used.

It is not clear from this result whether this underestimation in BC deposition is specific to the Sapporo region, urban areas more generally or a widespread feature of CLASSIC BC deposition. To investigate this question further is beyond the scope of this thesis so going forward the CLASSIC modelled deposition values for site simulations at Sapporo shall be adjusted by a scaling factor to bring them more in line with the observed amounts of BC accumulated at the site. The scaling factor used was 1.3, based on the ratio of the means of the two cumulative deposition timeseries (blue line, figure 2.5). However, runs elsewhere will use the original CLASSIC output due to lack of further information on what (if any) scaling would be appropriate.

Chapter 3

Representing black carbon concentration in snow within JULES

3.1 Introduction

This chapter will introduce developments I have made to the snow scheme within JULES to allow black carbon (BC) to be deposited onto snow, stored within the snowpack and evolved over time. This enables the concentration of BC in the snow to be used within albedo calculations. The new developments will be tested for the site at Sapporo, Japan, and sensitivities of this scheme to relevant model parameters will be explored.

3.2 Adding infrastructure to calculate black carbon concentration in snow

I have developed a new treatment of BC within the multi-layer snow scheme in JULES to calculate the BC mass concentration in snow based on deposition values provided as an input to the model. This allows the concentration of BC in the snow to be predicted based on the amount of snowfall input to the model, the amount of snowmelt predicted by JULES and the amount of BC that has accumulated in the modelled snowpack over the course of the snow season. These code developments have been made in a branch of vn5.2 of JULES that can be viewed on the Met Office Science Repository Service (MOSRS)[1].

BC mass is stored as an additional property of snow layers and the existing snow relayering infrastructure is used to control the distribution of BC between the various layers. Figure 3.1

[1] MOSRS location of JULES branch for BC on snow: `https://code.metoffice.gov.uk/trac/jules/log/main/branches/dev/helenjohnson/vn5.2_snowBC_take3` (registration required)

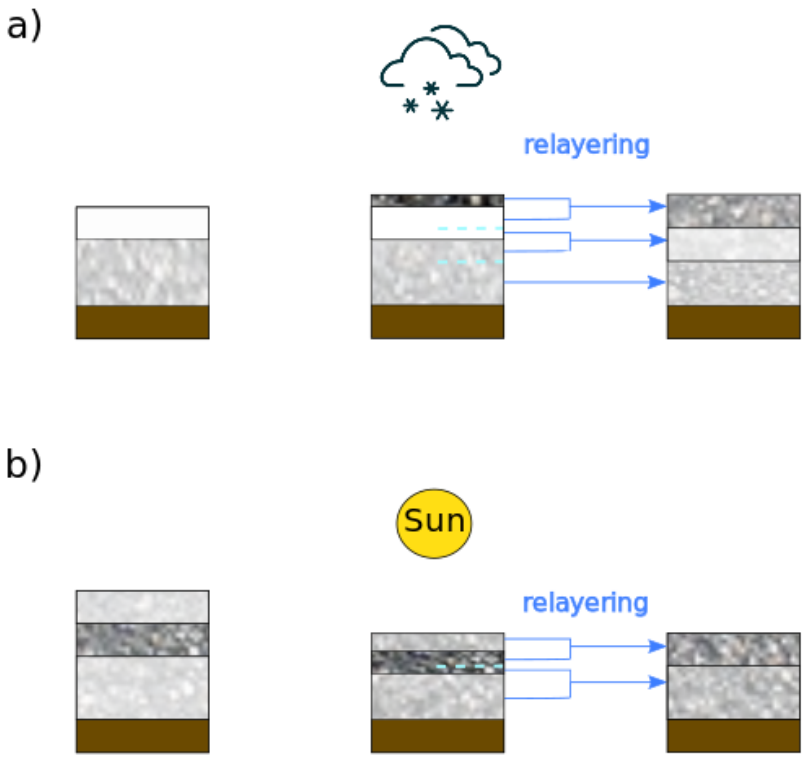

Figure 3.1: Diagram depicting how BC in snow is represented in JULES. (a) The accumulation of BC contaminated snow and the redistribution of BC as the snowpack is relayered and (b) the increasing concentration of BC as the snow melts.

shows how BC is handled by the snow scheme during (a) accumulation and (b) melting of the snowpack. Freshly deposited BC is added to the top snow layer but an increase in snow depth triggers the snowpack to be relayered in order to maintain standard snow layer depths (and a finite number of snow layers). The concentration of BC in each new snow layer is calculated as a weighted average of that in each of the previous layers which contributed to it. Thus, as the snow depth increases a fraction of the BC will move lower in the snowpack. When the snow melts and the number of snow layers decreases, BC will be shifted back towards the top of the snowpack to simulate the 'melt amplification' effect observed by *Doherty et al.* (2013). Once the snowpack has melted completely the BC mass is removed (set to zero). It is assumed that BC is evenly mixed within a snow layer and that it does not contribute to the mass of snow. The concentration of BC in a layer, s, is then simply calculated by dividing the mass of BC, m_{BC}, by the combined mass of frozen and liquid water, m_{frz} and m_{liq}:

$$s = \frac{m_{BC}}{(m_{frz} + m_{liq})}. \tag{3.1}$$

Black carbon scavenging by melt water has been included to allow BC to be redistributed within

or removed from the snowpack as the snow melts. The amount of BC removed from a snow layer by meltwater scavenging $m_{\downarrow}$ is calculated as the BC mass present in the melting snow (based on the mass concentration s within the previously frozen snow layer and the amount of melt water that is leaving the layer, $q_{\downarrow}$) multiplied by a scavenging efficiency fraction e:

$$m_{\downarrow} = e \cdot q_{\downarrow} \cdot s. \tag{3.2}$$

Melt is calculated for each snow layer starting from the top of the snowpack and working downwards, $q_{\downarrow}$ and $m_{\downarrow}$ from each layer are added to the layer below before melt is calculated for that layer. This is the same approach to meltwater scavenging of BC as is adopted by *Flanner et al.* (2007) in the SNICAR snow radiative transfer model. This ensures not all BC within the melted snow will get carried away with the meltwater. The multi-layer snow scheme in JULES allows for meltwater refreezing so it is possible for black carbon to be shifted lower in the snowpack due to meltwater scavenging without being removed from the snowpack completely. The default value chosen for scavenging efficiency fraction was $e = 0.17$, which is taken from the work of *Doherty et al.* (2013) who reported scavenging efficiencies between 14 and 20% for BC particles, based on observations taken at Barrow, Alaska.

Only the BC present in the top layer of snow is considered when calculating the snow albedo. The appropriateness of this assumption will depend on the specified thickness of the top snow layer. *Doherty et al.* (2013) discuss sunlight penetrating 3-10cm into the snowpack (depending on snow grain size). *Aoki et al.* (2011) found a seasonal variation in how deep light penetrates due to the seasonal variation in snow grain size, with light being absorbed deeper in the snowpack when the snow is melting compared to when it is accumulating. The structure of the snow scheme in JULES does not allow for seasonally or spatially varying snow layer thicknesses but instead uses constant values specified by the user. The default model configuration used in this study uses a 4cm thickness for the top snow layer which is within the range stated by *Doherty et al.* (2013).

3.3 Testing JULES BC on snow scheme at Sapporo

To test the performance of this representation of BC concentration in snow within JULES, simulations were performed for one winter (2007-2008) at Sapporo using meteorological driving data and CLASSIC simulated BC deposition values. Simulations were performed using both the original CLASSIC output and the dataset that had been multiplied by 1.3, as discussed in chapter 2, and a control run was also undertaken for which no BC deposition data was applied. Simulations were initialised from a spinup run that was performed by running JULES cyclically with meteorological driving data for the preceding year until the soil moisture and temperature converged to within 0.1% and 0.1K respectively, a process that required four spinup cycles in

this instance. This spinup simulation was performed without BC deposition applied so that all model runs have the same starting conditions and only the impacts of BC within the immediate snow season are considered. As the simulations start from the beginning of October, before the snowpack starts to form, BC deposited in previous years is not expected to be of relevance to the snow albedo, depth or BC concentration at this site.

Figure 3.2 shows the modelled concentration of BC in the top snow layer when JULES is forced with the original CLASSIC BC deposition (purple line) and the adjusted BC deposition dataset (dark blue line) compared with the observed BC concentration in the top 2cm (red dots) and the top 10cm (blue diamonds) of snow at Sapporo. As the top snow layer in JULES is 4cm thick, the BC concentration in this top layer would be expected to lie somewhere between the observations for the top 2cm and top 10cm of snow. Both of the timeseries for modelled BC concentration in snow are lower than either set of observed values, especially towards the end of the snow season, although the adjusted deposition dataset gives results that are closer to the observations. This could suggest a lack of model sensitivity to BC deposition rates, possibly related to the thickness of the top snow layer - this will be explored further in section 3.4.1.

Error bars have not been included in figure 3.2 as error estimates are not provided for the observations of BC concentration in snow at Sapporo. However, the errors are expected to be sizeable as the process for collecting these observations involves several stages, each of which offer an opportunity for errors to be introduced. *Pedersen et al.* (2015) attempted to collate and quantify

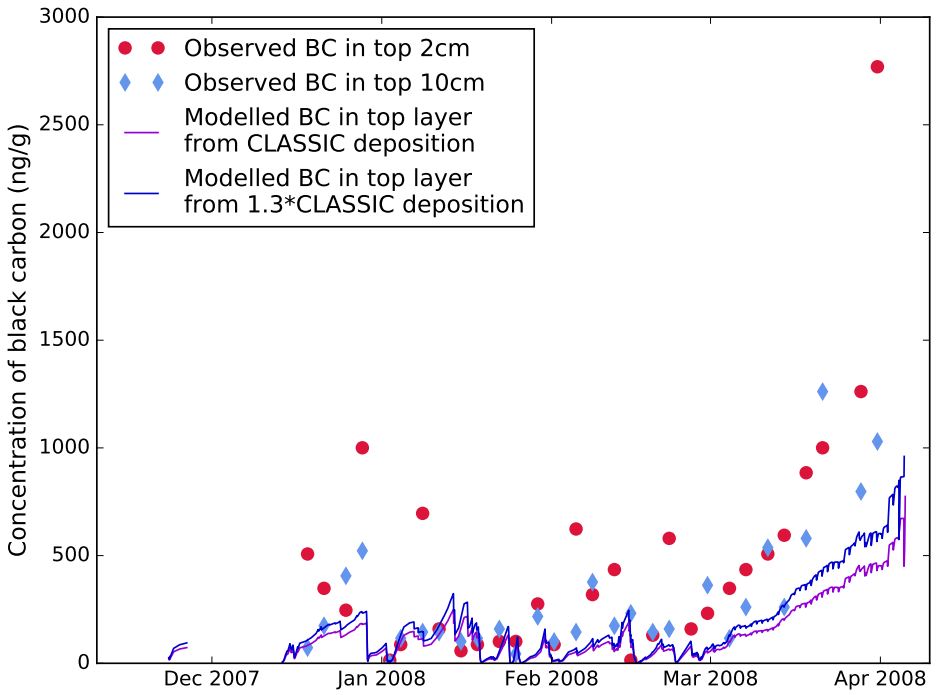

Figure 3.2: Comparison of modelled and observed BC concentration in snow near the surface of the snowpack at Sapporo.

the uncertainties and biases associated with BC concentration measurements collected using similar methodologies (see table 1 of that paper), they found that on the whole BC concentration in snow tends to be underestimated, though efforts have been made to reduce most of those biases in the observations used here by correcting measurements to account for filter undercatch and by using the 'IMPROVE' methodology for thermal-optical analysis as proposed by *Chow et al.* (2001) (*Kuchiki et al.*, 2015). The largest source of error is likely to be due to uneven loading of the filter used to collect impurities from the melted snow. Only a small section of this filter is used for the thermal-optical analysis to quantify a mass of carbon per unit area which is then used to determine the overall BC concentration in the filtered snow sample, uneven loading can therefore lead to inaccurate BC concentration values being reported. At other sites, it has been suggested that the BC mass can vary by as much as 40% between different punches from the same filter, though for larger carbon loadings this dropped to roughly 23% (*Svensson*, 2011). It should be noted that study was based on a small number of samples and a larger dataset is probably required to better understand the uncertainties introduced by uneven filter loadings. As well as possible biases and uncertainties in the measured BC concentrations, it is also likely that BC concentration in snow varies considerably at meter scales, much like for snow depth. *Forsström et al.* (2013) reported that this local spatial variability could be as much as 30%.

Using the new JULES capability to evolve the snow BC content, the concentration value from the top snow layer is used in JULES albedo calculations. Figure 3.3 shows the impact of includ-

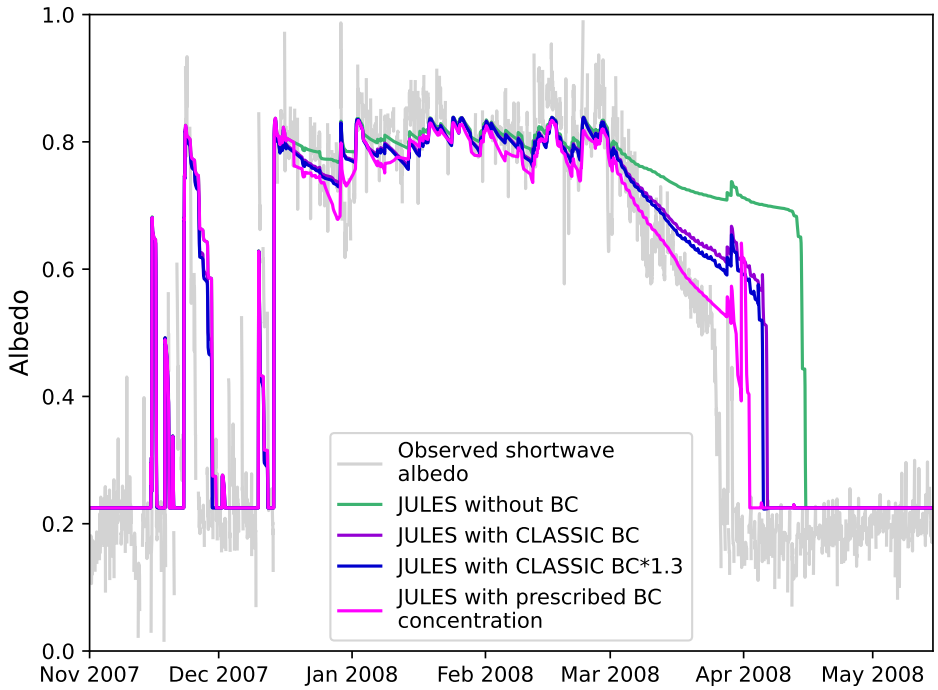

Figure 3.3: Comparison of JULES modelled shortwave albedo values with observations at Sapporo for winter 2007-2008.

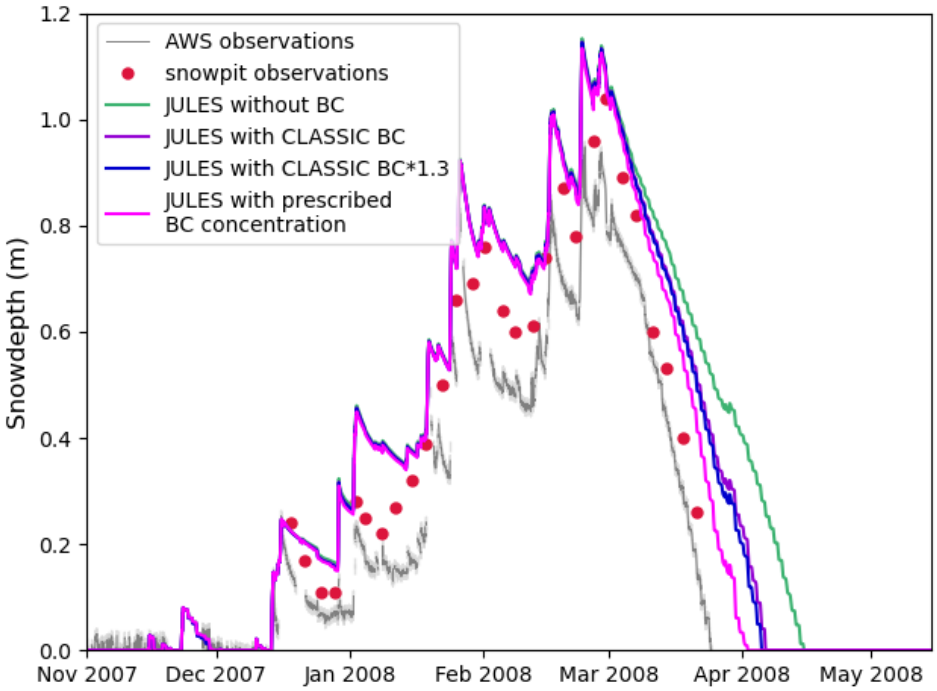

Figure 3.4: Comparison of JULES modelled snowdepth values with observations at Sapporo for winter 2007-2008.

ing modelled BC concentration in albedo calculations at Sapporo in comparison to a simulation without BC (green line) and a simulation with BC concentration prescribed as described in section 2.4 (magenta line). It is evident that the inclusion of BC improves the modelled albedos compared to the site observations. Using the adjusted deposition values (blue line) offers a slight benefit over the original CLASSIC deposition values (purple line) but the albedo values in early April are still too high compared to the observations. In figure 3.4 it can be seen that whilst the introduction of BC does cause snow to clear earlier than in the simulation without BC, snow is still persisting longer in JULES than in the observations. For both the modelled albedo and snowdepth it can be seen that when JULES is modelling the evolution of BC concentration (purple and blue lines), the underestimation in concentration towards the end of the snow season means that it cannot perform as well as when the BC concentrations are prescribed directly (magenta lines).

One thing to note from figure 3.4 is that introducing BC causes only a very small reduction in the peak snow accumulation depth and has a negligable impact on the timing of the onset of melt. The main difference seen in this plot is the rate at which snow melts.

3.4 Sensitivity to elements of model architecture

3.4.1 Sensitivity to thickness of the top snow layer

The values selected for the number and thicknesses of model snow layers in JULES do not represent physical aspects of the snowpack. In reality it may be possible to identify layers within snowpit observations associated with individual snowfall events or perhaps bulk layers associated with snowpack evolution processes such as wind slab and depth hoar. These processes are however not yet represented within the JULES snow scheme and therefore the number and thicknesses of snow layers have been selected simply to provide necessary accuracy whilst having a minimal impact on computational efficiency. As such, the OS36 configuration uses three snow layers with thicknesses of 4cm, 12cm and 34cm.

Clearly, adding more layers requires more memory and computational processing so even detailed snowpack models such as CROCUS do not maintain individual layers for each snowfall event (*Brun et al.*, 1989). Compromises between detail provided and simulation efficiency must be weighed for any model depending on resolution, time available to perform simulations and ultimately the purpose of the model.

With the introduction of BC on snow, it is considered prudent for the top snow layer thickness to be similar to the solar radiation penetration depth (e-folding depth) of snow as it is only the BC concentration in the top snow layer that is taken into account for albedo calculations. However, as the top layer thickness is used in the calculation of surface BC concentration, it is possible that it effects the albedo response to the presence of BC in JULES. It is particularly likely that the thickness of the top snow layer controls the model response to BC deposition rates if dry deposition is making up a significant fraction of total BC deposited, because if deposition occurs independently of snowfall then the concentration would vary greatly throughout the depth of the snowpack and be very stratified.

To explore this, further JULES simulations were performed where each had one additional snow layer added to the top of the snowpack and the thickness of that additional layer was varied. The thicknesses chosen were 0.5cm, 1cm, 2cm and 10cm. The impact of these changes on modelled surface snow BC content can be seen in figure 3.5. From this it can be seen that the JULES modelled surface BC concentration is highly sensitive to the thickness of the surface snow layer. Thinner top snow layers give higher concentrations of BC (because BC is mixed over a smaller amount of snow, particularly if dry deposition has occurred). The model simulation with a top snow layer thickness of 1cm (black line) appears to give BC concentration values that match the observations in the top 2cm of snow most closely. This result echoes that of *Aoki et al.* (2000) who found that, for sites in eastern Hokkaido, snow impurities were more concentrated at the snow surface due to accumulation of impurities from dry deposition between snowfall events and that a top snow layer of 1cm thickness was required to accurately simulate snow albedos

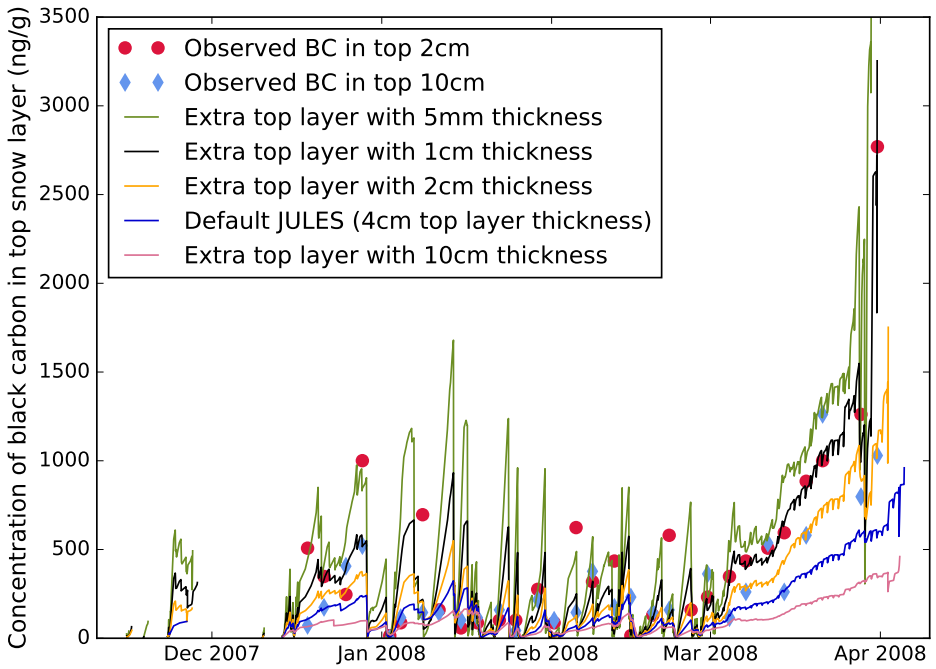

Figure 3.5: Comparison of modelled and observed BC concentration in surface snow at Sapporo. Model runs were performed with an extra top snow layer of thicknesses 5mm, 1cm, 2cm and 10cm. The default configuration with a top snow layer thickness of 4cm is also shown. Note that the y-axis is cropped at 3500ng/g but the line for the 5mm top layer thickness extends up to a BC concentration of 6491ng/g. All model runs were performed using CLASSIC BC deposition that has been multiplied by 1.3 to better match the deposition values expected for Sapporo based on observed concentrations. Observed BC concentrations are shown as points for the top 2cm and top 10cm of snow.

when considering effects of snow impurities.

Figures 3.6 and 3.7 show the impact on albedo and snow depth predictions when the additional 1cm thick snow layer is included, in comparison with the previous simulations. It is clear that this simulation produces albedo values that match observations more closely than the run with BC applied but using the default 4cm top layer thickness (blue). This is especially apparent throughout March and into April as the snowpack is melting. During this period the simulation using the thinner top snow layer produces albedo values very close to those observed. When modified CLASSIC deposition rates are applied and a 1cm thick top snow layer is used, the date of final snowpack depletion is 31st March, 15 days earlier than if no BC is applied.

The impact of the change in top snow layer thickness on the simulation without BC can be seen by comparing the solid and dashed green lines, there is a small difference in albedo and snowdepth during melting but this impact is much less than in the simulations where BC is present.

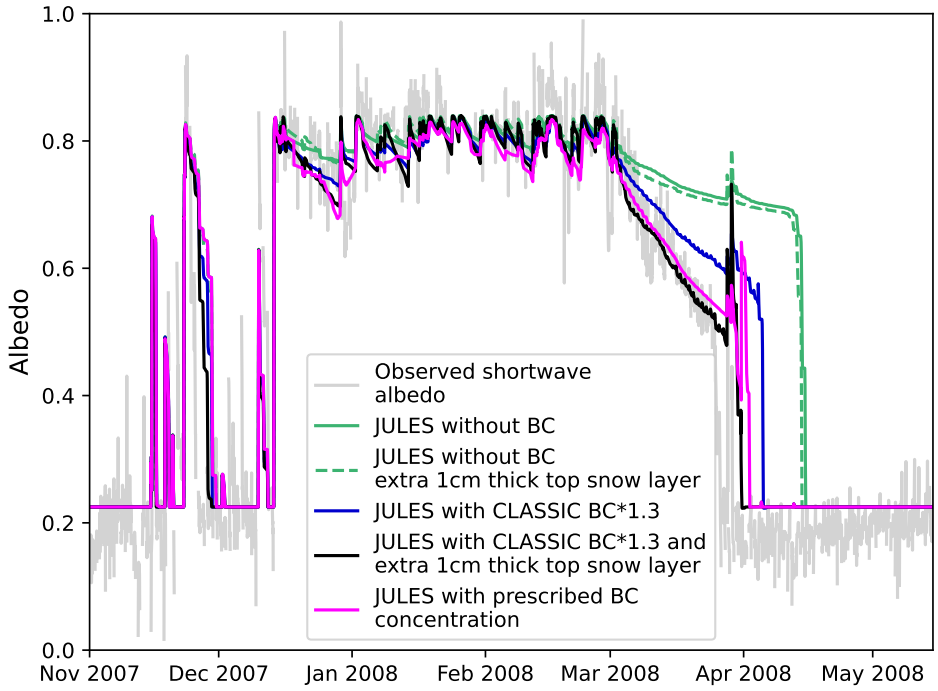

Figure 3.6: Comparison of JULES modelled shortwave albedo with observations taken at Sapporo.

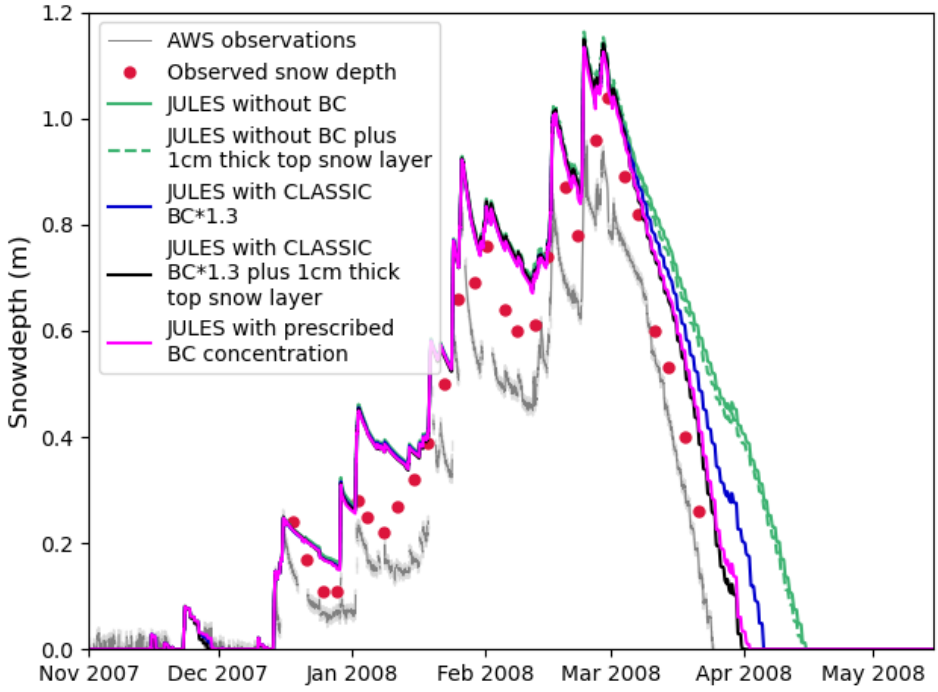

Figure 3.7: Comparison of JULES modelled snowdepth with observations taken at Sapporo.

It is apparent in figure 3.6 that when using a 1cm thick top snow layer (black line) the JULES modelled albedo responds even more quickly to periods of melt than when the BC concentration is prescribed directly from observations (pink line). At the very end of the snow season this may be due to the modelled BC concentration being slightly higher than the concentration prescribed from the observations in the top 2cm of snow (the black line in figure 3.5 exceeds the values of the last two red dots). This will also be true during the late November melt as BC concentrations were set to zero in the prescribed dataset prior to the start of the snowpit observations. However, during the first half of March, when Spring melt begins, the modelled and observed BC concentrations are in very close agreement. The differences in albedo during this time will be due to short term evolution in the modelled BC concentration values, in response to changing melt rates, vs. the linear interpolation of BC concentration between observations in the prescribed run. Interpolating concentrations between observations that are days apart doesn't allow for sudden changes due to events such as cloud cover or day and night cycles affecting the melt rate and feeding back on the BC concentration. This is also why the pink line appears smoother than the black line during January and February.

Neither the simulation with the prescribed or modelled BC concentration saw snow clearance occur quite as early as the observations. This could be due to the choice of scavenging efficiency value used for these simulations. As discussed previously, there is considerable uncertainty around what fraction of BC should be scavenged with melt water.

It is also worth noting that 1cm top layer depth is less than typical values for the e-folding depth of snow (normally between 3cm and 10cm) so the assumption that only the BC concentration in the top snow layer is relevant for calculating the albedo may be false for such a thin top layer. However, *Reay et al.* (2012) highlight that solar radiation attenuates more rapidly in snow with higher BC content so given the high BC concentrations present in this urban location, the e-folding depth is likely to be less here than elsewhere. Indeed, the surface BC concentrations in late Spring at Sapporo are several times higher than the maximum concentration considered in Reay et al.'s study. Further investigations would be required to establish whether or not a 1cm thick top snow layer is appropriate at other locations. The proportion of BC deposited through dry deposition vs. wet deposition may be a factor in determining the optimum top layer thickness for a given site. However, obtaining suitable site observations to explore this at other locations was not feasible within the timeframe of this study.

3.4.2 Sensitivity to duration of model timestep

Using thinner snow layers requires a shorter model timestep in order to maintain model stability. This does have considerable impacts on time taken to perform simulations and so users should be mindful of the compromise between model accuracy and the amount of computing resource available when selecting a timestep length for running JULES, particularly if thin snow layers

are being used.

All of the simulations above were performed with a one minute timestep in an effort to maintain accuracy but typically standalone JULES simulations would be performed at the same frequency as the meteorological driving data - often a 30 or 60 minute timestep. However, JULES does contain functionality to interpolate driving data onto a shorter timestep if needed. Any timestep length less than three hours should be sufficient for JULES to represent diurnal cycles and increased temporal resolution is more computationally expensive so that compromise needs to be considered when running with shorter timesteps. Whilst running with a one minute timestep for a single year at a single site does not take unduly long, performing global simulations for multiple years takes far longer and therefore it is worth investigating what is the longest timestep that can be used whilst still giving good accuracy when running with a 1cm thick top snow layer.

A test was performed to determine the longest timestep length one can safely use, whilst still maintaining a 1cm thick top snow layer, without considerably changing JULES results. JULES was run without BC and with the 1cm thick top snow layer using a range of different model timestep lengths - 1, 10, 15, 30 and 60 minute timesteps were tested. Figure 3.8 shows the impact on modelled albedo of varying the timestep length. Timestep lengths of 15 minutes or less converge to give approximately the same answers throughout most of the snow season. There are slight differences still apparent during periods of melt with longer timestep lengths leading to a more rapid fall in albedo. This affect can also be seen in figure 3.9 where the longer timestep lengths lead to accelerated snow melt which impacts the overall snow accumulation over the course of the season. When looking at the snowdepth, it is again apparent that results converge for timestep lengths of 15 minutes or less. Therefore, the maximum advised timestep length when using a 1cm thick top snow layer shall be 15 minutes and this shall be used in the global simulations in the next chapter.

In figure 3.8 it becomes very apparent that the JULES modelled albedos are subject to an upper limit. This is an intentional consequence of the design of equations 2.1 and 2.2 - with upper albedo limits being imposed at 0.98 for the visible waveband and 0.7 for the near infrared. As radiation is being partitioned evenly between the wavebands in these simulations this leads to a maximum albedo of 0.84. Whilst it makes sense to impose an upper limit on albedo, it is notable that the observed albedo exceeds this model limit in figures 3.3 and 3.6 suggesting that either the model limits on albedo are not high enough or that in reality there are times when there is more visible radiation received at the surface than near infrared. The latter option seems less likely given that both cloud cover and larger zenith angles lead to an increase in near infrared radiation being received relative to visible (*List*, 1949).

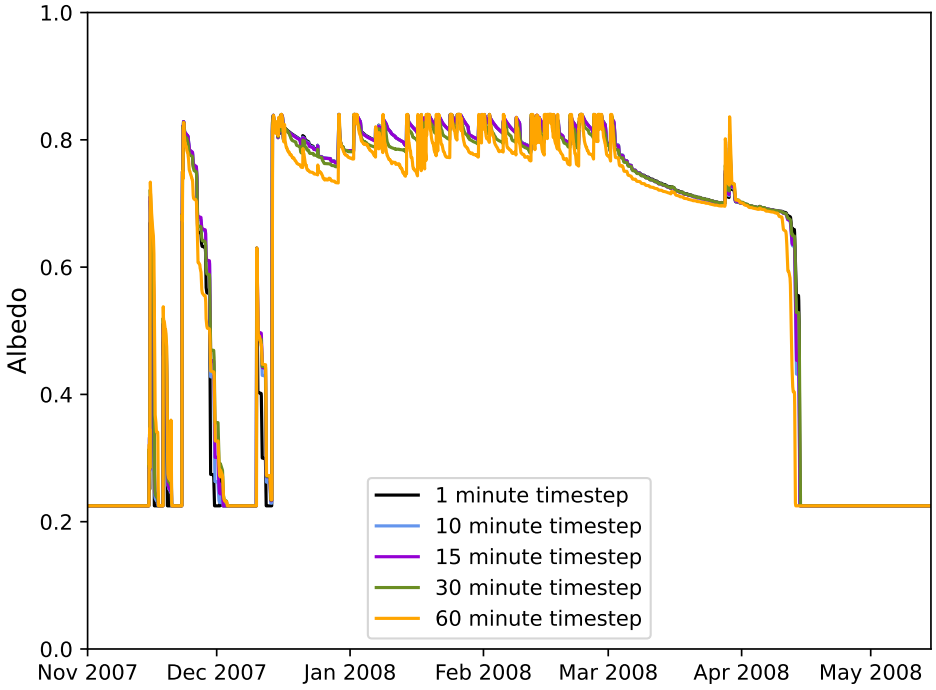

Figure 3.8: Comparison of JULES modelled shortwave albedo for simulations with different model timestep lengths. All JULES runs were performed without BC applied and with a 1cm thick top snow layer.

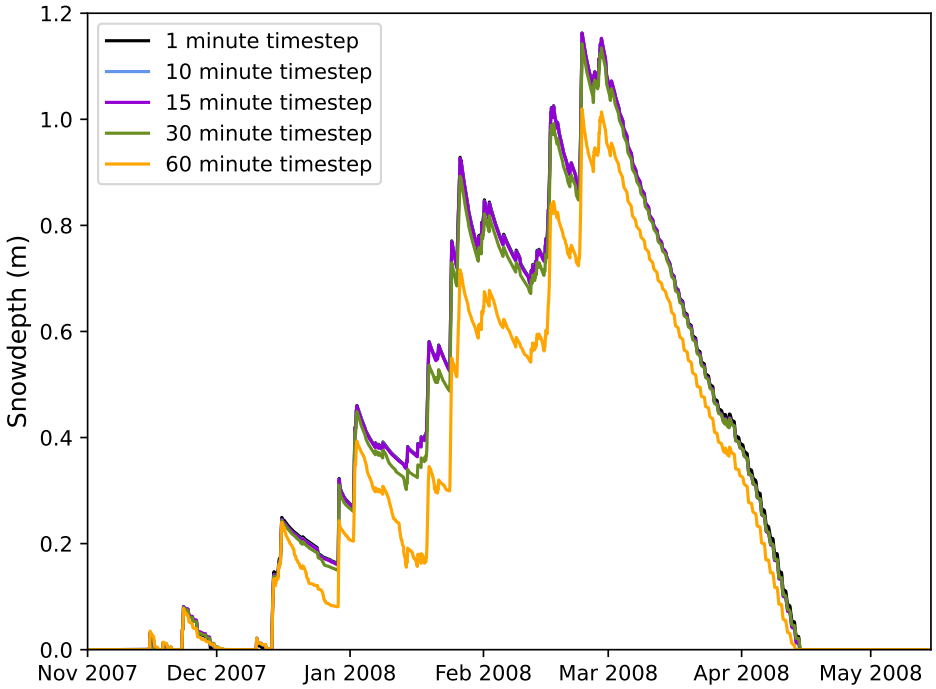

Figure 3.9: Comparison of JULES modelled snowdepth for simulations with different model timestep lengths. All JULES runs were performed without BC applied and with a 1cm thick top snow layer.

3.5 Sensitivity to meltwater scavenging efficiency

The only user specified parameter that has been added to JULES as part of the BC on snow scheme is the meltwater scavenging efficiency parameter, 'soot_scav'. Figure 3.10 depicts the impact that varying 'soot_scav' has on the simulated concentration of BC in surface snow at Sapporo. As one would expect, simulations with little or no BC scavenging experience larger concentrations of BC and these concentrations increase rapidly in spring as snow melts ('melt amplification'). The default scavenging efficiency value of 0.17 produces BC concentration values that match the observations well although this is at least in part due to the fact that the thickness of the top snow layer has been selected to perform well with this value of the scavenging efficiency. However, the huge spread in BC concentration values towards the end of the snow season highlights how sensitive JULES is to this parameter and so if a different value is chosen, perhaps due to further observational studies advancing our knowledge of this parameter, then it may be necessary to consider whether the top snow layer thickness in JULES needs to be adjusted as well.

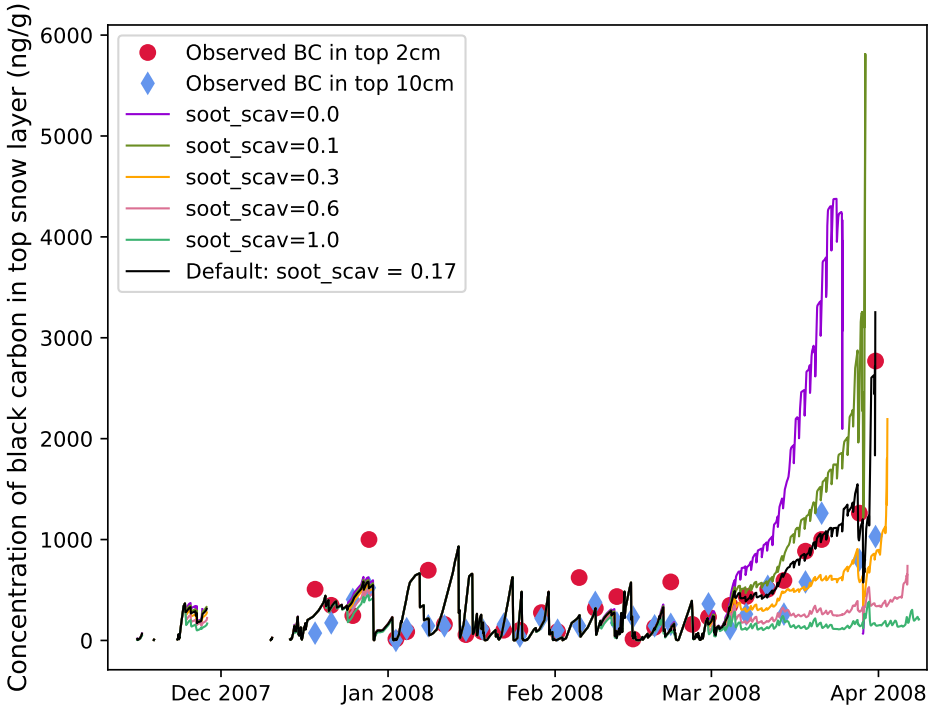

Figure 3.10: Plot showing the concentration of BC in surface layer snow in JULES when modelled with various different values of the scavenging efficiency paramenter 'soot_scav'.

In figure 3.11, the impact that varying the scavenging efficiency parameter has on albedo can be seen. The simulations with little or no BC scavenging experience greater snow darkening during the melt season and therefore the snow melts quicker than in simulations with higher values of BC scavenging efficiency. The simulation with prescribed BC concentration is shown in magenta to indicate what behaviour we expect from JULES when BC concentration is accurately

predicted.

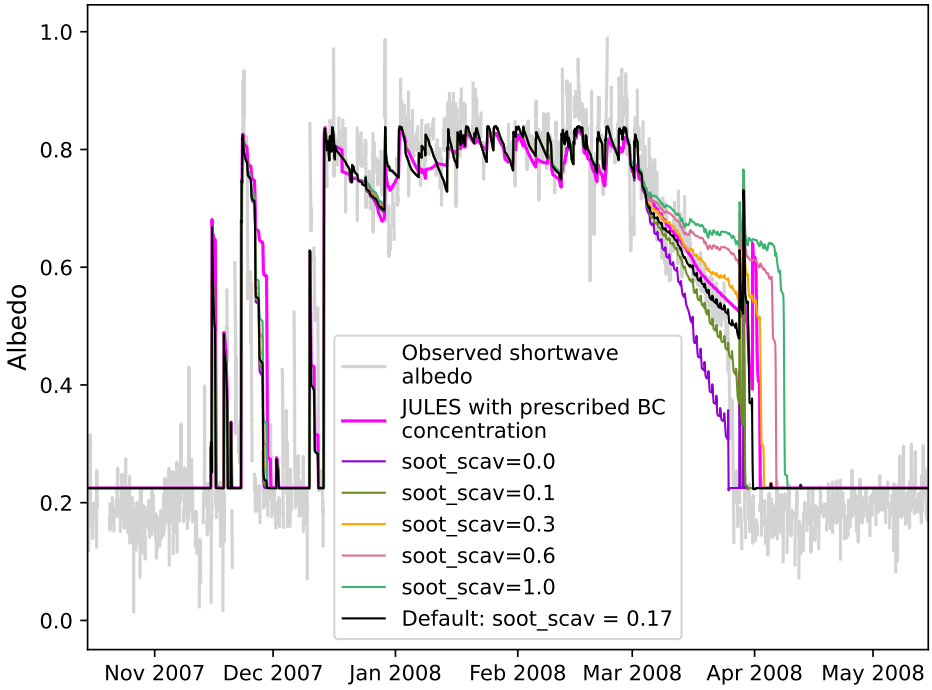

Figure 3.11: Plot showing the impact on simulated albedo of running JULES at Sapporo with different values of the BC scavenging efficiency parameter 'soot_scav'.

In reality, the BC scavenging efficiency is likely to vary from one location to another due to various factors. For instance, *Conway et al.* (1996) demonstrated that smaller BC particles are flushed more efficiently from the snowpack than larger ones and *Schwarz et al.* (2008) found that BC particle size differed depending on emission source with BC particles emitted from urban fossil fuel burning having smaller diameters than those emitted from biomass burning. These results in combination would suggest that snowpacks that receive most of their BC deposition from forest fires would see less efficient BC scavenging and therefore a stronger snow darkening impact during melt season. Particle size is also known to increase with ageing as the BC becomes internally mixed with other aerosol. This ageing process has been found to occur more rapidly in more polluted regions (*Peng et al.*, 2016). When BC particles become internally mixed they tend to transition from an initial hydrophobic state to a hydrophilic state. How hydrophobic or hydrophilic the particles are will also affect the scavenging efficiency; *Conway et al.* (1996) found that hydrophobic BC particles were scavenged more rapidly than hydrophilic ones. Whilst typically larger (*Schwarz et al.*, 2013) and more hydrophilic particles will be more readily deposited onto the snow surface, under extreme temperature or humidity conditions any particle could act as a cloud condensation nuclei and so weather conditions during snow formation can also affect the composition of BC found in the snowpack and therefore the rate at which it will be scavenged.

Given all these factors, rates of meltwater scavenging can vary considerably. For this study the value used is 0.17 - the mid-point of the range suggested by *Doherty et al.* (2013) based on observations at Arctic sites in Alaska, Greenland and Norway. However, the scavenging efficiency parameter in JULES has been set up as a namelist variable that can be edited by the user should they have a better idea of what value would be appropriate for the snowpack they are modelling.

Another element of uncertainty is whether or not the scavenging rate for BC remains constant throughout the melt season. *Lazarcik et al.* (2017) found that, for snowpacks in New Hampshire, the scavenging rate is much higher at the onset of melting and follows a similar process to the 'ionic pulse' or 'acid flushing' that has been widely observed (e.g. *Johannessen et al.* (1977)). Conversely, *Sterle et al.* (2013) observed that BC flushing only occurred late in the melt season (possibly due to mobilisation from more vigourous melt flows). For now only constant rates of BC scavenging can be accomodated by the current model setup.

3.6 Summary

The results in this chapter clearly demonstrate that including the snow darkening effects of BC in JULES model simulations improves the modelled albedo values, particularly towards the end of the snow-covered season, and in turn the timing of modelled snowmelt is improved. At Sapporo, including BC on snow in JULES simulations leads to final snow clearance occurring 15 days earlier.

The modelled BC concentration and hence albedo values were found to be highly sensitive to the thickness of the top snow layer in the JULES multi-layer snow scheme. Using a top snow layer thickness of 1cm produces modelled BC concentrations that most closely match observations and hence lead to accurate albedo calculations. However, using thinner snow layers requires consideration of the model timestep length in order to maintain model accuracy - only timesteps of 15 minutes or less should be used if the top snow layer thickness is being set to 1cm.

The model is also sensitive to the scavenging efficiency used although there remains a lot of uncertainty in the literature as to what value would be most appropriate and in reality the scavenging rate is likely to depend on many factors and processes that are not represented in this simplistic solution. Should the user wish to alter the scavenging efficiency parameter used in JULES, they may need to adjust the top snow layer thickness accordingly.

The relatively low latitude of Sapporo means that a reduction in albedo at this site will have a greater impact during the winter months, when snow is accumulating, than at higher latitude sites due to the greater insolation received at lower latitudes. However, the reverse may be true during the melt period due to the increased day lengths at high latitude sites in late spring. It remains to be seen the extent of the impact that including BC snow albedo affects will have

at other sites. The next two chapters will explore the impact of including BC in global JULES simulations.

Chapter 4

Assessing the impacts of adding BC to snow in JULES

4.1 Introduction

Having demonstrated the capability to model the evolution of black carbon (BC) concentration in snow and its impacts on albedo and snow melt at Sapporo, it is important now to explore the geographical variability of BC's effect on snow and the wider implications for the land surface system. This chapter will use global JULES simulations to investigate the impacts of including BC on snow across different geographical regions. Later, in chapter 5, the performance of JULES in these global simulations will be validated against a satellite albedo product.

4.2 Global model simulations

4.2.1 Model setup

For the simulations in this chapter and the next, an updated branch of JULES was used[1]. This vn7.0 branch of JULES is broadly similar to the branch used in chapter 3 but also expands the BC on snow scheme to operate on canopy snow tiles as well as tiles that don't use the canopy snow scheme. These changes do not affect the results at Sapporo because the Sapporo simulations used a grass tile that does not include the canopy snow scheme. However, in these global simulations the canopy snow scheme will be used in gridboxes that contain needleleaf trees.

[1] MOSRS location of JULES branch for BC on snow: `https://code.metoffice.gov.uk/trac/jules/log/main/branches/dev/helenjohnson/vn7.0_snowBC` (registration required)

Two JULES simulations were performed - one with (denoted “experiment”) and one without (denoted “control”) black carbon applied. These simulations were driven by the WFDEI dataset (WATCH Forcing Data methodology applied to ERA-Interim reanalysis data, *Weedon et al.* (2014)) which contains the necessary atmospheric forcing fields to drive JULES - namely shortwave and longwave downward radiation, rainfall and snowfall, near surface air temperature, wind speed, air pressure and specific humidity. These fields are available at 0.5° spatial resolution and 3 hourly temporal frequency. In particular, this driving data set made use of the GPCC gridded product of monthly rainfall and snowfall totals based on rain gauge observations to correct the ERA-Interim reanalysis so that the number of wet days per month and the monthly total precipitation better match observed values *Weedon et al.* (2011). The GPCC data has been corrected for precipitation gauge undercatch but it has not been corrected for undersampling of mountinous areas — due to orographic effects on precipitation, such as those discussed by *Adam et al.* (2006), this may lead to precipitation quantities being underestimated in mountainous areas(*Schneider et al.*, 2014). The GPCC rain gauge network is also sparse at high latitudes so accuracy in these regions may be more limited. Another thing to note about this WFDEI driving dataset used is that it excludes Antarctica.

The simulations were run from 1991 - 2008, the same period that the UM-CLASSIC simulation introduced in chapter 2 was run for as the deposition fields output from that simulation are used again here to prescribe BC deposition onto the snow in JULES for the experiment simulation. The CLASSIC BC deposition field was regridded from N96 resolution to 0.5° using a nearest neighbour interpolation method.

4.2.2 Spinup

When initialising a land surface model simulation, it can take some time for the model to adjust to the initial conditions provided and settle to a stable state. For example, if one were to initialise a soil column to be fully saturated in an arid location, it may take several years of drying out before the model converged on a stable soil moisture level. The model is unlikely to give realistic output until it is running in a stable state. To account for this, one would typically use the first year of available driving data to repeatedly cycle the simulation until a stable state is achieved. An entire year is used as it provides a complete cycle of both diurnal and seasonal patterns of variation so the start point and the end point are expected to occur under very similar climatological conditions meaning there will be minimal shock to the model from restarting the beginning of the year using output from the end of the year as the new ‘initial state’.

Within JULES there are four possible variables that can be examined to test whether or not the model has successfully spun up to a stable state after the requested number of spinup cycles. These are the temperature of each soil layer, the moisture content of each soil layer, the amount of soil carbon in each soil layer and the carbon content of vegetation. The later two of these

are only used for long climate simulations where dynamic vegetation (and soil carbon) schemes are selected. Most JULES simulations just test the first two spinup criteria, values from the current and previous spinup cycles are compared to see if they have converged to within a user specified threshold. Typically threshold values are set to differences of less than 0.1K for soil temperature and 1% for soil moisture.

For the global simulations used here, a year-long spin up (starting from saturated soils) was cycled 30 times. There were still various gridboxes that did not pass the standard soil temperature and moisture spinup threshold tests after 30 spinup cycles, these locations are shown in

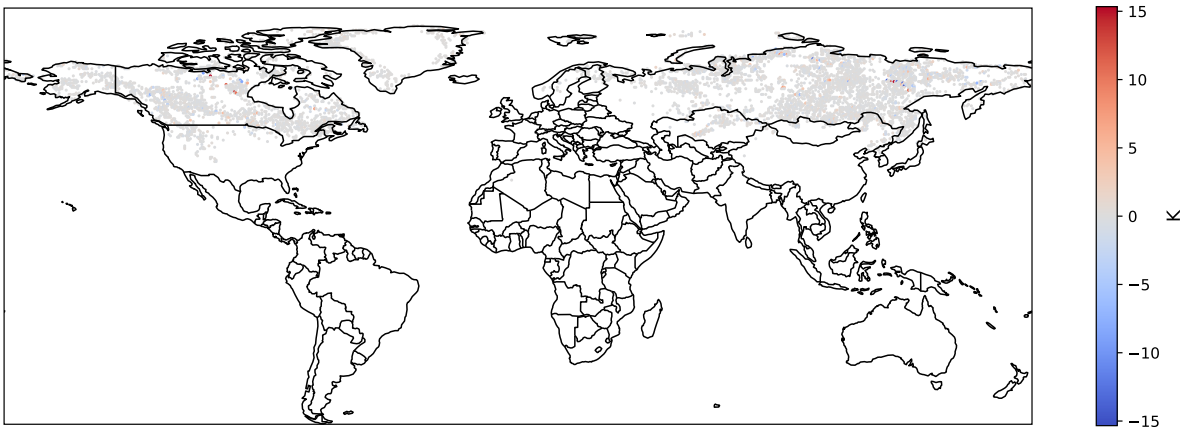

(a) Points that have a soil temperature difference of more than 0.1K in the top soil layer between the output at the end of the 29th and 30th spinup cycles. Colourbar indicates temperature difference.

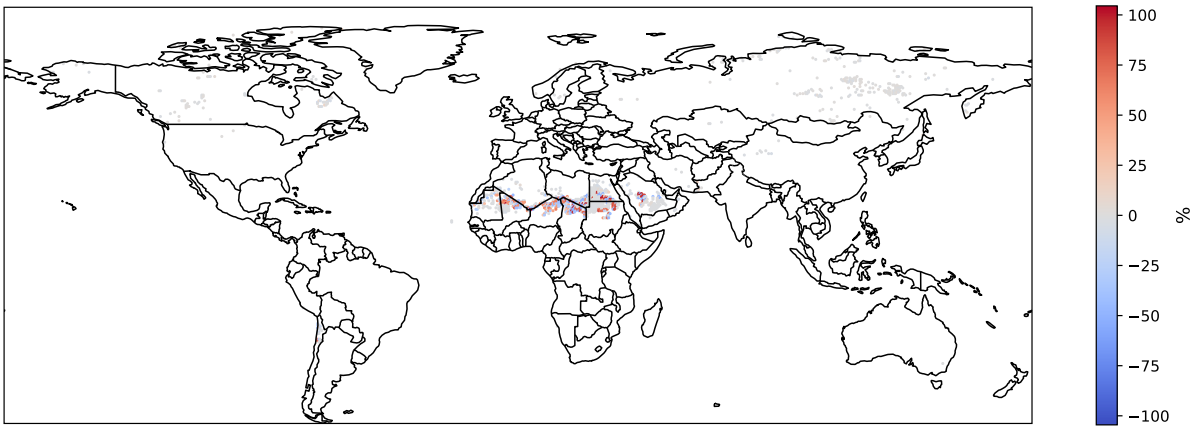

(b) Points that have a soil moisture difference of more than 1% in the top soil layer between the output at the end of the 29th and 30th spinup cycles. Colourbar indicates percentage difference.

Figure 4.1: Points that still haven't passed the standard spinup threshold tests in the top soil layer after 30 years-worth of spinup cycles. a) soil temperature test, b) soil moisture test.

figure 4.1. In the case of soil moisture, many of these gridpoints occurred in very arid locations that would likely not receive much snow and therefore not be especially relevant to this study. As these simulations are forced with atmospheric driving data rather than being coupled to a simulated atmosphere there is no opportunity for the impacts of a poor spinup in one location to feed back to results in other locations so it was decided that gridboxes that failed to pass the soil moisture convergence test after 30 cycles would simply be excluded from the results analysis later.

For soil temperature, the number of gridboxes which experience significant snow cover that would be excluded with this threshold test was too large to exclude all of them. Almost all the points were showing only small soil temperature differences but the number of points failing the spinup did not seem to be reducing significantly with additional spinup cycles (5531 gridboxes out of a total of 67209 failed to meet the spinup threshold after 20 cycles but this only reduced to 5259 gridboxes after 30 cycles - a less than 5% reduction in the number of failing gridboxes). Running a longer spinup was unlikely to yield a better set of starting conditions within a reasonable timeframe. As most locations had only small differences in soil temperatures between spinup cycles after 30 years, even a small relaxation in the spinup threshold would greatly increase the number of gridpoints that could be included without having large implications for results. An alternative soil temperature spinup threshold of 0.5K was selected, this small change in the spinup threshold led to the number of points that 'fail' the spinup reducing from 5259 to 730 points out of a total of 67209 land points. The locations that are still considered to have not spun up are shown in figure 4.2, these points will be excluded from analysis along with those that failed the soil moisture test shown in the lower plot of figure 4.1.

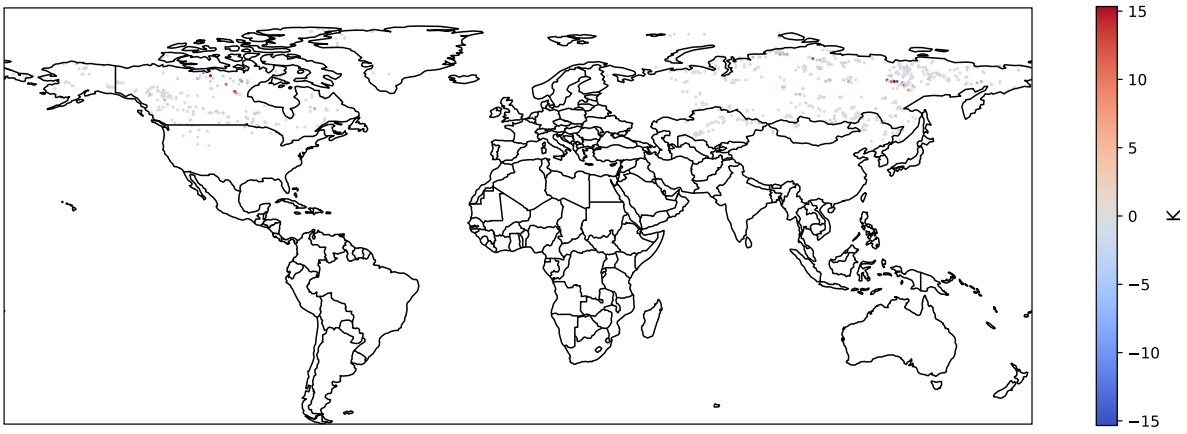

Figure 4.2: Points that still have differences in soil temperature greater than 0.5K after 30 years-worth of spinup cycles. Colourbar indicates difference in temperature of the top soil layer between the 29th and 30th spinup cycles.

It is worth noting that the points shown in figures 4.1 and 4.2 only consider the temperature and moisture content of the top soil layer. On the whole, the differences between spinup cycles were greater in the upper soil layers. Whilst JULES would normally check that all soil layers had spun up before proceeding to the main run, only points that fail to spinup in the surface soil layer will be excluded from further analysis.

4.3 Defining a seasonal snow cover mask to simplify analysis

Some consideration has been given to which gridboxes to analyse. Working with large datasets such as these, some of the analysis performed in this study is rather time consuming to process and therefore it is preferable not to process gridboxes where the output would be meaningless and would either be ignored or worse, misinterpreted. To this end, masks were generated that were used to exclude unnecessary gridboxes from analysis processes.

Firstly, any gridboxes that failed to meet the spinup thresholds described previously were excluded. All other criteria depended on the presence of snow so it was necessary to define when a gridbox was snow covered. It was found in earlier simulations that some locations that would only experience occasional snow cover in reality, e.g. Southeast England, were unrealistically modelled as having persistent very thin snow cover all year round[2]. Whilst this thin snow cover was assessed as not affecting albedo or surface temperature, it did require a threshold limit to be set for minimum snow amount to be considered snow covered when deciding which points to analyse. Although the specific issues causing these spurious thin snow amounts have been fixed in this JULES version, it seems prudent to maintain a minimum snow threshold in case of other as yet undiagnosed issue with small or negative snow amounts. A minimum snow mass value of $0.001\,\mathrm{kg\,m^{-2}}$ was used. Any gridboxes that do not receive snow accumulations above this thin snow threshold are not of interest in this work and therefore can be disregarded during analysis.

Much of the focus of this study is looking at the impacts on timing of melt of seasonal snowpacks. It is common for locations that experience an extended period of snow cover during winter to also experience shorter duration snow covers at the start and end of the winter. To help with this, the longest snow covered period was identified for each gridbox each year. Here, a year was defined as running from 1st September to 31st August so that Northern Hemisphere winter is not split between two years. This approach does mean that the 'longest snow covered period' for Southern Hemisphere gridboxes in a given year may be shorter than the actual snowpack duration due to it being split between years. For this reason, many of the figures in this work will only show the Northern Hemisphere, if both hemispheres are shown then the 'longest snow

[2]The cause of this issue has since been identified by Martin Best as being due to a problem with the fractional snow cover calculations being rounded due to reaching the limits of machine precision. A fix has been provided in JULES version 7.0, ticket #1279.

covered period' has not been used to calculate values in that figure.

For the purposes of calculating the longest snow covered period, and particularly taking averages across years of values that depend on longest snow covered period, it was necessary to only consider gridboxes that experienced at least some snow cover every year but also at least some snow free days every year. These gridboxes were selected on the basis of the snow mass quantities output from the experiment simulation rather than the control as this will include locations that experience year round snow cover in the control simulation but have snow free summers in the experiment simulation (these gridboxes will be discussed further in section 5.5). Figure 4.3 shows the mask that was generated to exclude gridboxes that either didn't experience seasonal snow cover and snow clearance or weren't sufficiently spun up.

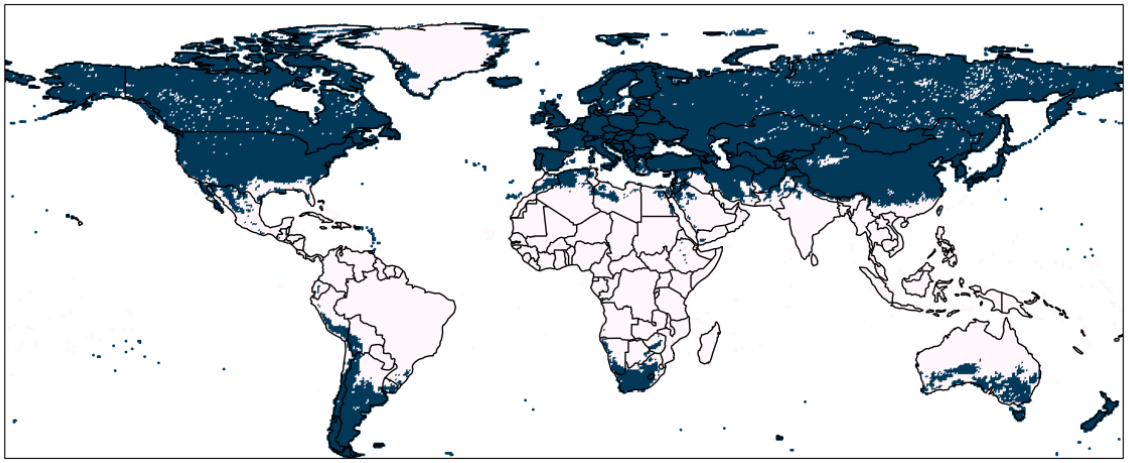

Figure 4.3: Mask of gridboxes that that will be excluded from analysis due to either not having seasonal snow cover in the experiment simulation or failing to spinup after 30 cycles. Locations that will be analysed are shown in dark blue, locations that will be excluded are shown in off-white.

4.4 Impacts of black carbon on modelled snow

4.4.1 Impacts on duration of snow cover

For each of the gridboxes shown in figure 4.3, the longest snow covered period was identified each year. Figure 4.4 compares the duration of the longest snow covered period in the experiment simulation with the control simulation. It can be seen that snow durations are shorter in the simulation with BC (experiment) than in the control simulation, as is expected. Most of the changes to snow duration are small reductions - the points lie close to but slightly below the one-to-one line.

There are however a small number of gridboxes where the experiment simulation shows longer

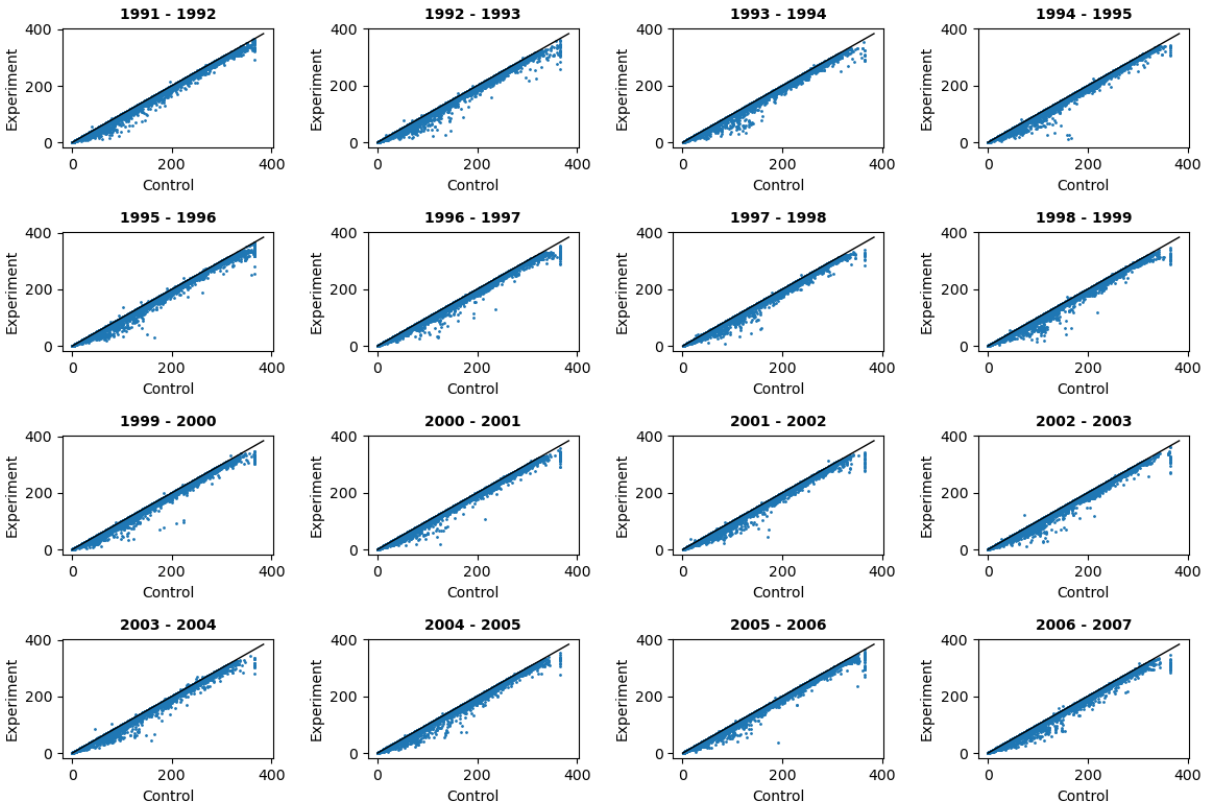

Figure 4.4: Scatter plot comparing duration (number of days) of the longest snow covered period each year between the experiment simulation (with BC) and the control simulation (without BC). Each point represents one gridbox (only Northern Hemisphere gridboxes are shown), the black line is the one-to-one line of matching durations.

snow duration, this behaviour was not expected so it was explored further. In total there were 1033 gridbox years (0.18%) that displayed this behaviour. On the whole, increased snow durations only occurred for one year rather than many or all years at each of the affected gridboxes. Of these cases the mean difference in snow duration is 1.24 days but the maximum increase in snow duration was 46.92 days.

The greatest increases in snow duration were found to be caused when two snowpacks broken by a brief snow clearance in the control simulation merged into one longer lasting snowpack in the experiment simulation. A few snow free timesteps in the control simulation were sometimes replaced with a very shallow snowpack in the experiment simulation. An example of this is shown in figure 4.5. The lefthand panel shows the timeseries for the entire year, where two main snowpacks can be identified, along with a smaller one at the end of the season. Differences between the simulations with and without BC appear to be relatively small and at first glance none of the snowpacks in the experiment simulation appear to persist 46 days longer than those in the experiment simulation. Indeed, for the central snowpack, the snow appears to persist slightly longer in the simulation without BC. However, when the righthand panel is examined,

which shows the shaded section of the first panel in closer detail, it becomes clear that in the experiment simulation the snow mass does not drop below the thin snow threshold and therefore instead of there being two separate snowpacks, they merge into one snowpack of much longer duration.

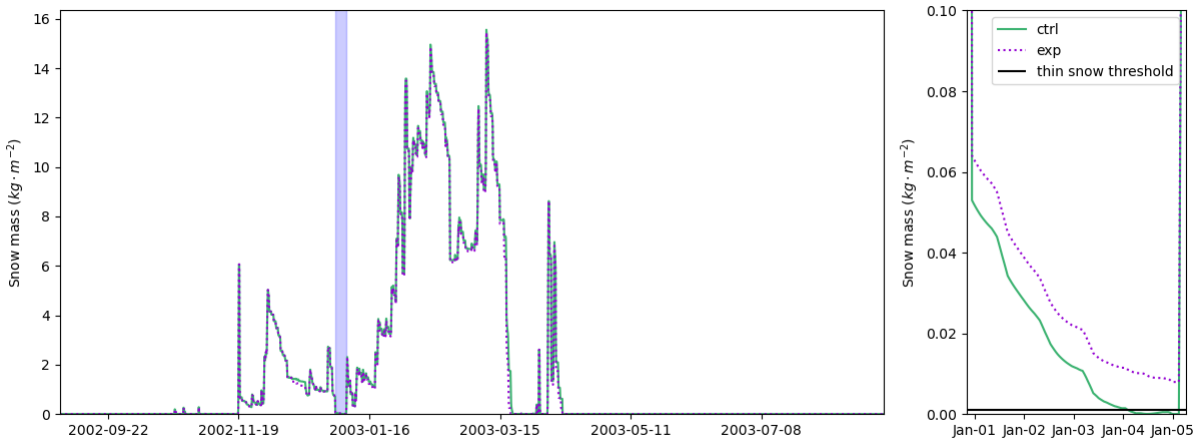

Figure 4.5: Snow mass timeseries for the gridbox year that experiences the greatest increase in snow duration, the simulation without BC (ctrl) is shown in green and the simulation with BC (exp) is shown in dotted purple. The lefthand panel shows the timeseries for the entire year whilst the righthand panel shows a more detailed look at the section that is shaded in the left panel. The black horizontal line in the righthand panel indicates the thin snow threshold, snow quantities beneath this amount were excluded from snow masks and snow duration calculations.

Whilst it is still unclear why the snow would melt slower in the experiment simulation, the differences in snow mass are very small and therefore unlikely to have substantial impact on overall results.

The vertical cluster in figure 4.4 at 365 days on the control axis highlights a group of gridboxes that had multi-year snow durations or perpetual snowpacks in the control simulation but transitioned to having seasonal snow with (brief) summertime snow clearance when BC was introduced to the modelled snow. As snowpack duration has been calculated on an annual basis, these gridboxes were considered to have a snow duration of 365 days each year when in fact the snow may have persisted for much longer prior to the addition of BC.

These scatter plots also show that whilst there are some differences in the impact of BC on snow duration from year to year, the overall trend remains the same. Differences from one year to the next will be due to differences in the meteorological driving data - mainly variations in the amount of snowfall and incoming radiation.

Figure 4.6 shows a histogram of the differences in snow duration caused by introducing BC on snow. The biggest difference in snow duration was -153.79 days but the mean value is -2.26 days. The largest snow duration differences are associated with gridboxes where the longest persisting snowpack in the control simulation was broken up into several shorter-lived

snowpacks once black carbon was included.

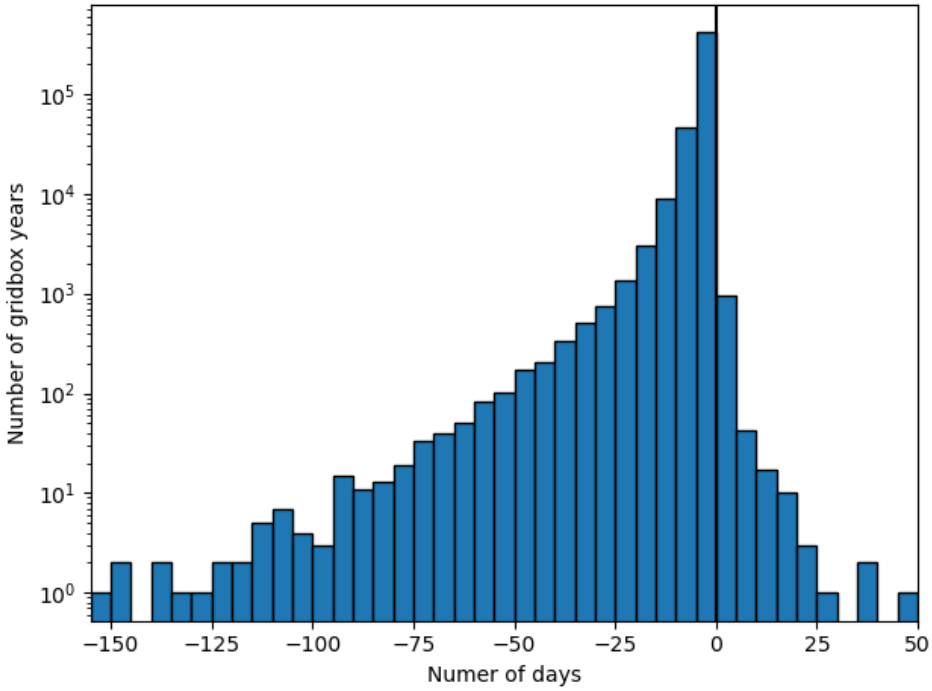

Figure 4.6: Histogram of differences (experiment minus control) in duration of longest snow covered period for each gridbox and each year (September-August). Note the logarithmic scale. Gridbox years that experienced zero difference have been excluded from this plot to aid interpretation, they constitute 13.13% of the dataset.

To explore how the impact of including BC varies geographically, a map of mean difference in snow duration is shown in figure 4.7. This shows that many locations only see small differences. The biggest impacts are seen in the Himalayas but also some other mountainous regions such as Alps, the Chucotka mountains in far Eastern Russia, the Kamchatca and Korean Peninsulas and the Pacific Coast ranges of North America. The area around the Eastern border of China and Russia is also considerably affected, this (along with the Himalayas) is an area that received relatively high BC deposition rates (see figure 2.4a).

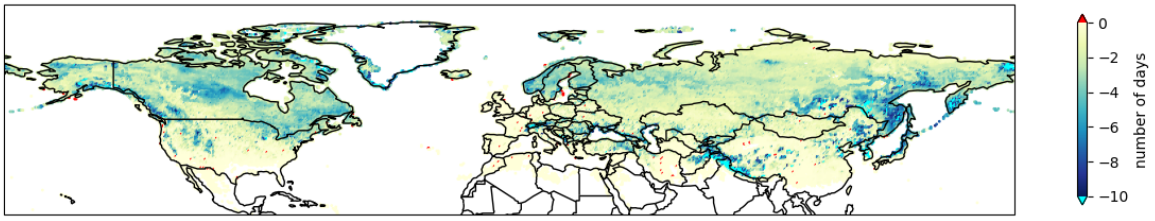

Figure 4.7: Map of mean difference (experiment minus control) in snow duration across all model years.

A notable area which does not see a large impact from the introduction of BC is the Tibetan Plateau. This is because of the relatively small amounts of both snowfall and BC deposition in this region (see figures 4.8 and 2.4a). It has been suggested that light absorbing impurities in snow in the Tibetan Plateau region have the potential to significantly impact water availability in Southeast and East Asia (e.g. *Qian et al.* (2011) and *Usha et al.* (2022)). The concern is born out of the fact that several of East Asia's biggest rivers are fed from the Tibetan Plateau region, which has relatively low latitude, and therefore receives more insolation than higher latitude regions so will be more sensitive to albedo changes. However, this result highlights that it is the mountain ranges neighbouring the Tibetan Plateau that are most affected so rivers fed from mountain runoff, such as the Ganges and Indus, are likely to see the biggest hydrological impacts.

The red gridboxes in figure 4.7 indicate the locations that saw an increase in snow duration. It has already been noted that these gridboxes were few in number but this map also highlights that there is no apparent geographical trend to their locations.

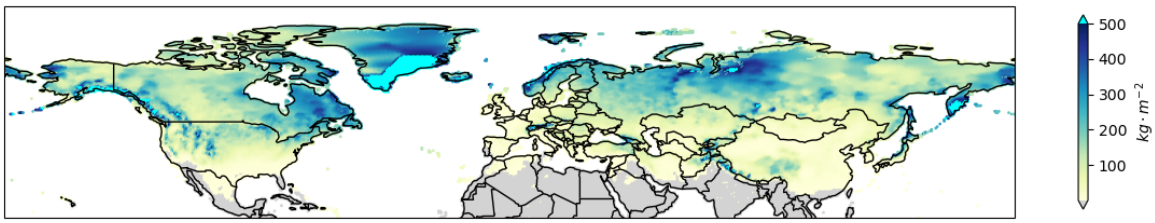

Figure 4.8: Map of mean annual total snowfall driving data. Gridboxes in grey are areas that receive a negligible amount of snow ($0.001\mathrm{kg\,m^{-2}}$ per year).

4.4.2 Impacts on peak snow quantity

As well as causing earlier snow clearance, the introduction of BC to the snow in JULES also triggers earlier melt onset and exacerbates any melt events during the snow accumulation season leading to reduced overall peak snow quantities.

Figure 4.9 shows a histogram of the peak snow mass values in the simulations with and without BC. There is a clear trend of a reduction in peak snow mass quantity when BC is added to the snow. The only column which increases in height in the experiment simulation is the left-most column, the change is sufficiently small as to be hard to distinguish on the logarithmic scale. Across the Northern Hemisphere, the mean percentage difference in peak snow mass is -0.33% of the mass in the control simulation.

The map in figure 4.10 shows how the impact of BC on peak snow mass varied across the Northern Hemisphere. As with changes to snow duration, the main impacts are seen in the Himalayas/Hindu Kush region but now coastal areas around the Black Sea and Caspian Sea

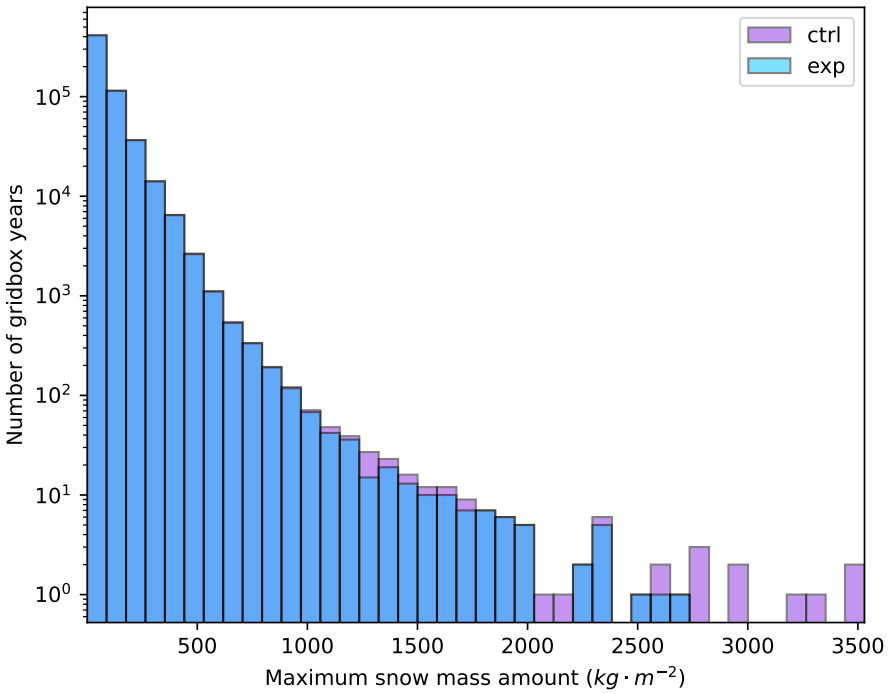

Figure 4.9: Histogram of peak snow quantities found in Northern Hemisphere gridboxes for the control simulation (without BC, purple) and the experiment simulation (with BC, light blue).

along with the Aral Sea region also stand out. There appears to be much more latitudinal dependence in these results than there was for snow duration changes, with lower latitudes seeing bigger impacts. This is likely due to differences in the amount of incoming radiation during the snow accumulation period - albedo changes at high latitudes will not have an impact during polar night so mainly affect the melt season.

There are more gridboxes that experience an increase in peak snow mass than overall snow duration. 17.62% of gridbox years show an increase in peak snow mass, though the maximum increases remain small relative to the maximum decreases. Not all of these increases relate to consecutive snowpacks merging together. It is still not clear why introducing BC to the snow

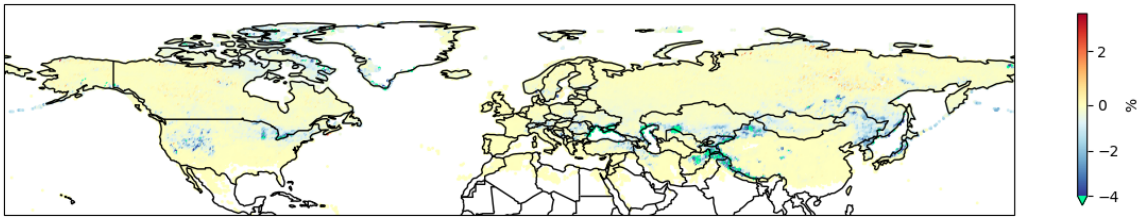

Figure 4.10: Map of percentage difference in peak snow mass averaged across all model years. The negative colour scale is limited to -4%, the actual limits of the data were $+3.38\%$ and -70.58%.

sometimes increases the snow mass in JULES, there are various complex relationships within JULES, e.g. between surface temperature and snow density or snow grain size, that could be factoring into this behaviour but there has not been sufficient time to explore all the possible mechanisms fully in order to explain this unexpected result.

4.5 Impacts on energy balance

The changes in snow melt patterns highlighted above are driven by changes in the fraction of incoming radiation that is reflected vs. absorbed by the snow surface when BC is introduced to the snow and the consequent changes in surface temperature. It is therefore worth further exploring the impact that adding BC to snow has on the various components of the energy balance within JULES as these are the primary effects of this change. These fields interact with many other aspects of the earth system so any changes to the energy balance will have the potential to trigger wide ranging hydrological, meteorological and ecological impacts.

Figure 4.11 shows how the various components of the energy balance are impacted by the addition of black carbon to snow. These results are averaged by month and by latitude band to highlight both the seasonal and latitudinal variations in response to the inclusion of BC. For all of the variables it can be seen that there is a strong seasonal dependence to their response to BC with the main impacts being seen in spring and early summer. At higher latitudes the effects occur later in the year. The largest differences are seen at higher latitudes where the majority of gridboxes experience long snow durations rather than just the gridboxes in mountainous regions as is seen at lower latitudes (figure 4.12).

The introduction of BC leads to increases in temperature, sensible heat flux and net radiation as more of the incoming radiation is absorbed by the land surface. Latent heat flux is more nuanced due to it's relation to the water cycle: it increases during spring, as snow melt and runoff occur earlier in the year, and then decreases during summer when there is less water available to evaporate because snow has already finished melting. However, the spring increase in latent heat appears to be greater than the summer decrease so introducing BC causes an overall increase in latent heat flux over the course of a year, though this increase will be less-so than those seen for the other components of the energy balance.

The surface temperature changes in figure 4.11 are an order of magnitude smaller than the changes in 2m air temperature found by *Flanner et al.* (2007) when they used the SNICAR model to introduce BC and organic carbon (OC) snow darkening effects to version 3 of the NCAR Community Atmosphere Model GCM (CAM3). Whilst it might be expected for there to be some difference between surface temperature and 2m air temperature, especially in a coupled GCM where air is free to advect and atmospheric feedbacks can take place, the scale of the differences between these two results is likely due to differences in the BC emissions used in

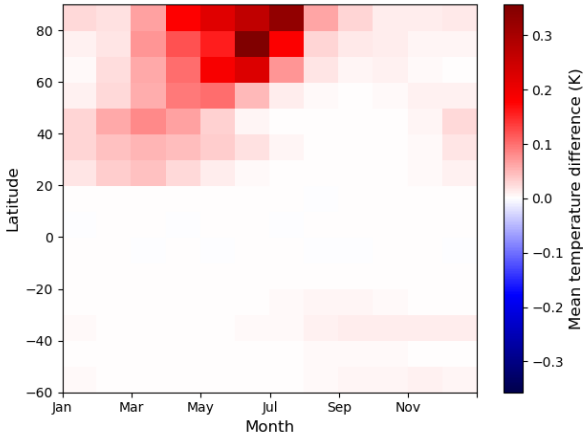

(a) Monthly mean surface temperature

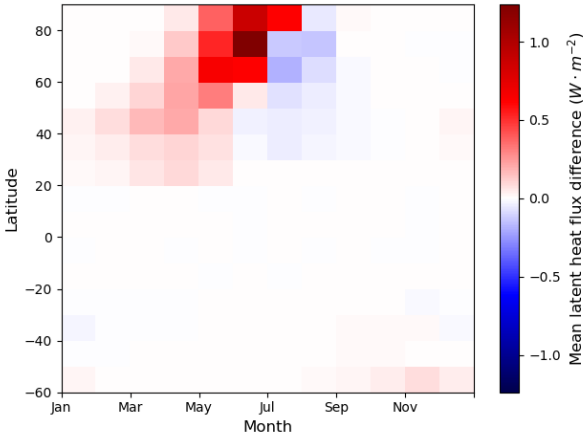

(b) Monthly mean latent heat flux

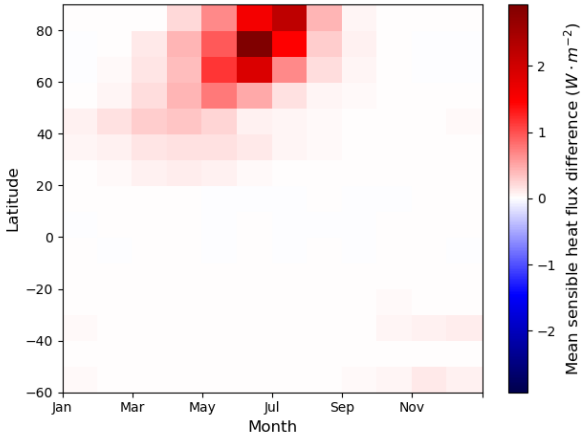

(c) Monthly mean sensible heat flux

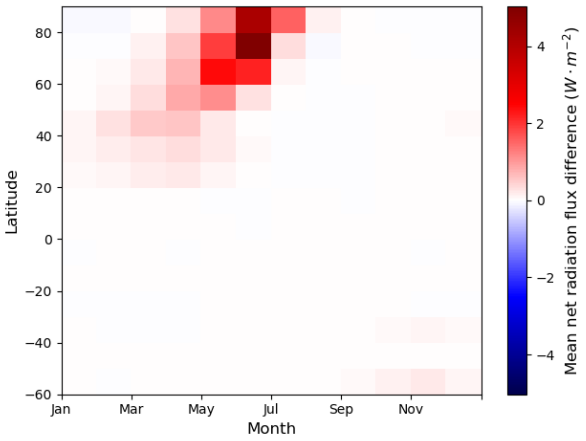

(d) Monthly mean net radiation flux (the positive direction is taken to be downwards)

Figure 4.11: Differences in monthly mean values, averaged by latitude band, of the various components of the energy balance. Note that these plots each have different colour scales.

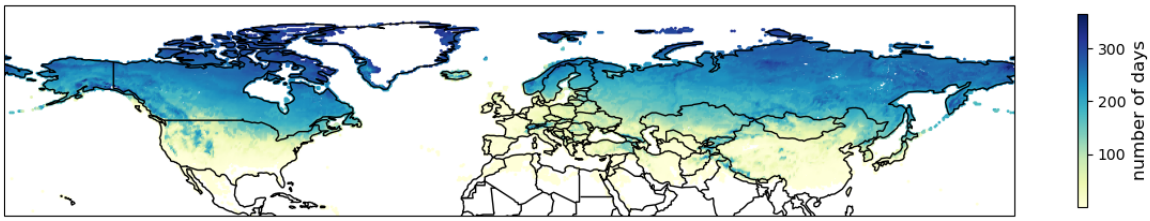

Figure 4.12: Northern Hemisphere map of the mean duration of the longest lived snowpack in a year (September - August) in the control simulation.

the studies and other factors affecting model sensitivity to BC such as representation of aerosol scavenging processes, snow aging and optical properties. The results of *Flanner et al.* (2007) show less of a seasonal cycle to the impacts of BC on air temperature than is seen in the surface temperature results here, this is particularly true for the year with high boreal forest fire

emissions. Their results agree with the findings here that the greatest temperature impacts are found at high latitudes.

Similarly to *Flanner et al.* (2007), a study by *Lau et al.* (2018) also found that the introduction of light absorbing particles (LAPs) to snow in the GEOS-5 GCM increased spring time surface temperatures by as much as 3K. Their study showed a seasonal-latitudinal pattern similar to that produced by the JULES simulations here (i.e. a spring time warming trend that progresses to higher latitudes as spring turns to summer), although the greatest temperature differences they found were at mid latitudes, around 50°N rather than the at Arctic latitudes as seen here. That study incorporated dust as well as BC and organic carbon to the snow so the warming effect might be expected to be greater than in both the simulation shown here and those of *Flanner et al.* (2007) (which did not include dust).

Another aspect that may possibly be enhancing the temperature differences seen in those two studies is that atmospheric feedback processes in coupled GCM simulations may further enhance the warming effect of BC in snow. For instance, *Sang et al.* (2019) found that including aerosol snow darkening in the GEOS-5 model resulted in increased spring time precipitation - if this fell as snow, and scavenged more BC, then it could potentially enhance the impacts of introducing snow darkening aerosol beyond what is seen in standalone land surface model simulations and if it fell as rain on top of snow that could accelerate snow clearance further. Indeed, when *Yasunari et al.* (2015) compared their free running climate simulations to ones where certain atmospheric fields were replaced by reanalysis to force the atmospheric trajectory, they noted that the effects of LAPs were amplified in the free running simulations due to feedback interactions.

Various studies consider changes to radiative forcing when BC is introduced to the snowpack however there are many different definitions of radiative forcing, most relate specifically to fields in a coupled atmospheric model so are not directly comparable to standalone land surface model simulations. Instead in this instance it is more practical to consider the changes to net radiation at the surface. Whilst not entirely equivalent to radiative forcing, the fields are closely related and therefore are expected to exhibit similar trends. When *Flanner et al.* (2007) examined the seasonal impacts of BC on surface forcing, they found a very similar pattern of variation by month and latitude band to that seen for net radiation impacts here.

Figures 4.13 and 4.14 show the geographic variability in the monthly mean values of the temperature and radiative flux fields. When these two sets of maps are compared it can again be seen that the higher latitudes experience the greatest differences later in the year, with the Canadian shield region particularly affected by the introduction of BC. At lower latitudes, the main impacts are more apparent in March (figure 4.13) but at these latitudes the impacts are less widespread as fewer areas experience long lived snowpacks. The biggest impacts are found in the Himalayas, as seen with the snow impacts, but also, less expectedly, in the North American Great Lakes and the Aral sea region and also in coastal areas around the Black Sea

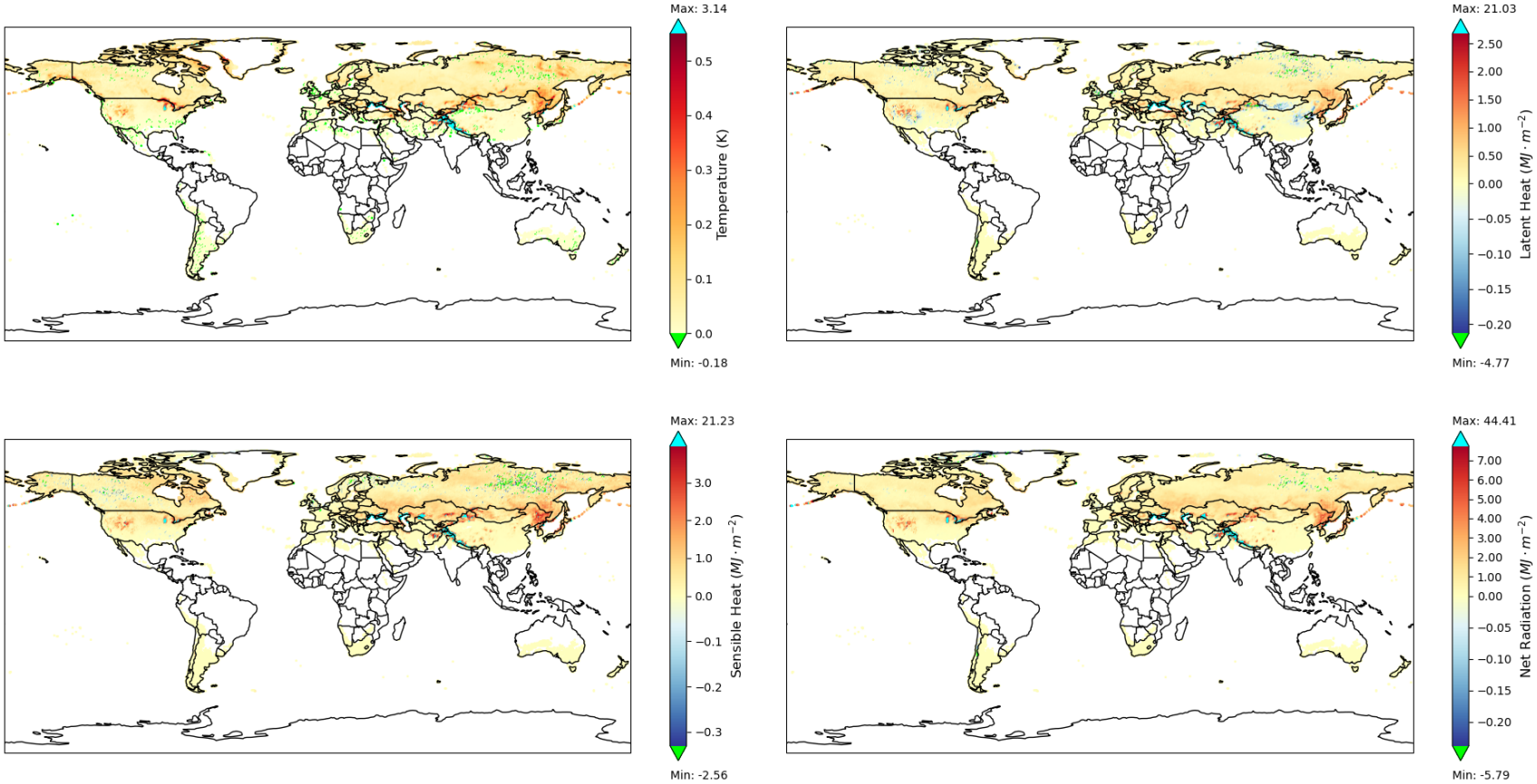

Figure 4.13: Maps for March of differences in monthly mean temperature and monthly total latent heat, sensible heat and net radiation. Colourbar limits have been set to cover the 0.5%-99.5% range, except for the lower limit of temperature which has been set to zero as all negative temperature values were very small. Absolute minimum and maximum values are given at the top and bottom of the colourbars. Note that each variable has different colourbar scales and that negative portions of colourbars are scaled differently to positive portions as the values tend to be much smaller.

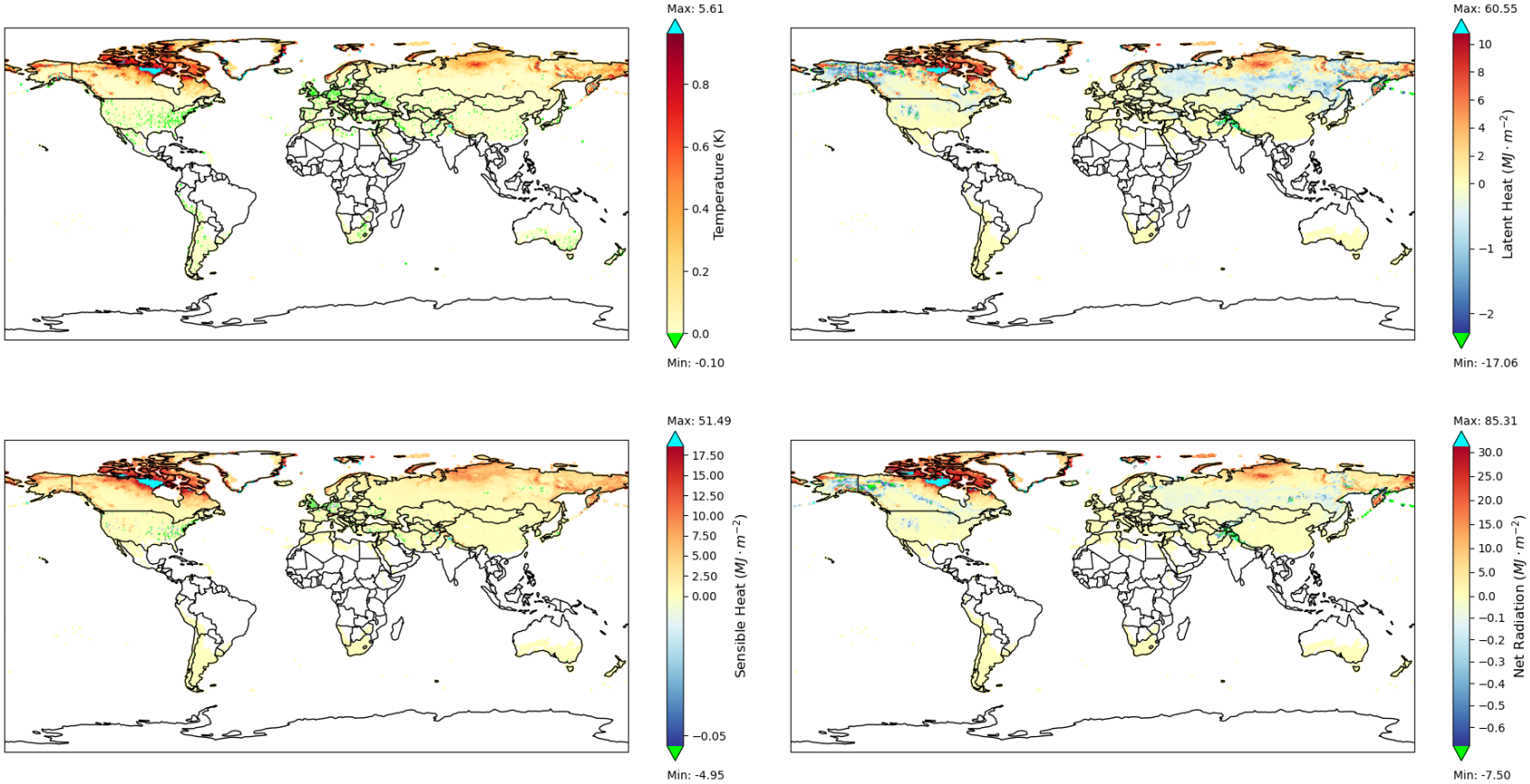

Figure 4.14: Maps for June of differences in monthly mean temperature and monthly total latent heat, sensible heat and net radiation. Colourbar limits have been set to cover the 0.5%-99.5% range, except for the lower limit of temperature which has been set to zero as all negative temperature values were very small. Absolute minimum and maximum values are given at the top and bottom of the colourbars. Note that each variable has different colourbar scales and that negative portions of colourbars are scaled differently to positive portions as the values tend to be much smaller.

and Caspian Sea. The reason for the large impacts in these non-mountainous areas is that they all have high lake surface tile fractions. The lake representation currently used in JULES is very basic and does not represent ice formation[3]. This means that snow is able to form on the lake surface whether or not the surface is frozen in reality. This, combined with the fact that the lake tile has very low roughness length, means it can experience high snow cover fractions for extended periods. In reality, the duration of snow cover on lakes is far shorter than that seen in JULES so the impact of black carbon would likely be much less than seen here. Another area that experiences fairly large increases in temperature and radiative fluxes is Northeast China and the border region with Russia, as well as the west coast of Japan - areas that experience moderately high black carbon deposition.

It is also apparent from these maps that whilst the vast majority of gridboxes experience increases in temperature, sensible heat and net radiation, the opposite is true for some gridboxes. Whilst the negative differences are less frequent and of smaller magnitude, they represent an unexpected result so should not be ignored. It was found that there were no decreases in net shortwave radiation, it is only the longwave component, which depends on surface temperature, that contributed to the reduction in net radiation. Sensible heat flux is also largely controlled by surface temperature. Unsurprisingly then, the areas that experience decreases in sensible heat and net radiation broadly correspond to areas that see a reduction in surface temperature. It appears that many of these negative differences occur at lower latitudes in areas that wouldn't necessarily be associated with extended snow cover duration such as Southeast United States, Western Europe and North Africa but there is also a number of these gridboxes in the Yakutia region of Eastern Siberia.

One possible explanation for this behaviour is that earlier snow clearance allows for easier heat transfer between the soil and the atmosphere. If the soil is warmer than the atmosphere this would lead to a reduction in surface temperature over the period of difference in snow duration. In order to see an overall reduction in temperature over the course of a month, this extra heat loss from the soil would need to outweigh any extra heat absorbed by the surface due to reduced snow albedo so it is possible that short-lived snowpacks are more prone to this situation arising.

Another possible explanation is that this behaviour is caused by some bug within JULES. For example, there are a number of known bugs that cause small negative snow mass values to occur, JULES ticket #1396 is currently being developed to address some of these. At one gridbox in Southeast England it was found that the introduction of BC caused a reduction in surface temperature despite the gridbox receiving very little snowfall. On closer inspection it transpired that the temperature reduction coincided with the occurrence of negative snow amounts. However, whilst the coincidence of temperature reduction with occurrences of negative snow is not unique to that one gridbox, it is not found in all cases of surface temperature reduction. It may

[3]The lack of representation of lake ice formation and clearance is a known problem in JULES and work is underway to remedy the issue by introducing the FLake model to better represent lake tiles (*Rooney and Jones*, 2010).

well be that a number of factors can cause this behaviour and it is not clear what proportion of gridboxes are affected for legitimate physical reasons and what proportion are due to model faults. If this scheme were to be adopted for regular use in future, it would be worth further investigating the causes of this behaviour but for now the focus remains on the majority of gridboxes which instead experience an increase in surface temperature and radiative fluxes.

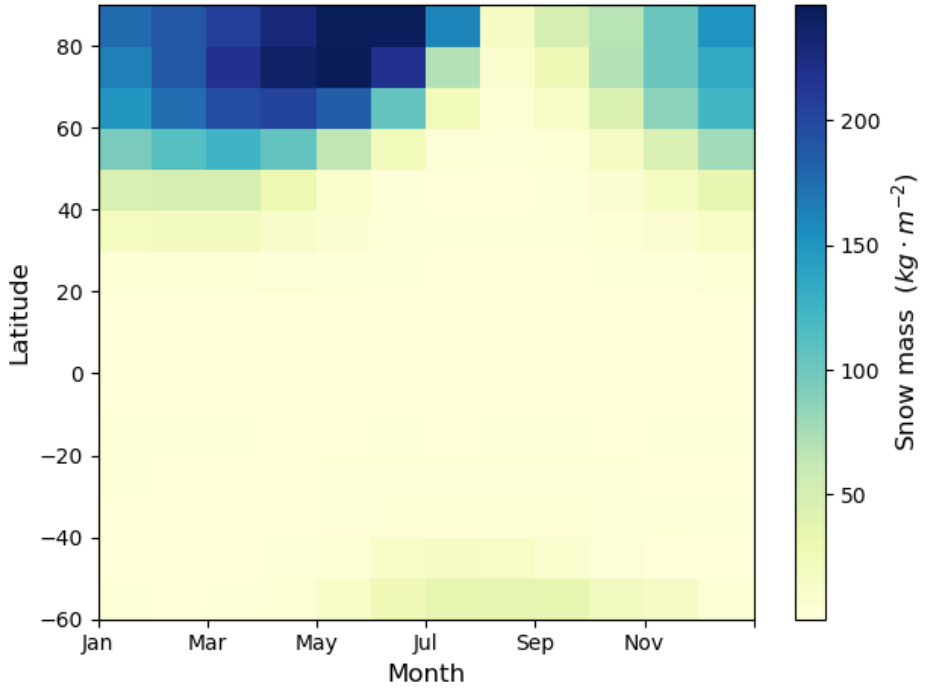

Figure 4.15: Zonal mean gridbox maximum snow mass each month in the control simulation (without BC).

The plots shown in this section are the first results from this study that also consider the Southern Hemisphere (as they look at monthly values rather than values analysed over an entire year). It is therefore worth highlighting that the impacts of BC on snow in the Southern hemisphere appear to be much smaller than in the Northern hemisphere. The Southern Hemisphere experiences considerably less snow cover than the Northen Hemisphere (figure 4.15) with the greatest snow masses occurring in the Southern part of the Andes mountains. Due to the westerly prevailing wind direction, the air mass in this region originates from the South Pacific Ocean and therefore carries very little black carbon. Similarly, BC deposition in New Zealand and Australia are very low. Whilst South Africa does experience moderate BC deposition around Durban (figure 2.4a), this area is not generally affected by seasonal snow (figure 4.3). Therefore, snow in the Southern Hemisphere is much cleaner than snow in most of the Northern Hemisphere and so is only minimally affected by the inclusion of BC snow darkening affects in JULES.

4.6 Impacts on water balance

The previous sections highlighted that introducing BC to the snow in JULES leads to earlier snow melt and a shift in the seasonal cycle of latent heat flux. Both of these changes are likely to have wider hydrological effects so the impacts on the various components of the water balance will now be explored further. For this analysis, the water input to the surface comes from precipitation, P, and water is lost via evaporation, E_{evap}, sublimation, E_{sublim} and surface and sub-surface runoff, R_{surf} and R_{sub}. Water is also stored in both the snowpack and the soil so it is possible that the losses may not completely balance the inputs on any given timestep. Therefore the budget equation can be formed as thus:

$$\Delta S = P - E_{evap} - E_{sublim} - R_{surf} - R_{sub} \tag{4.1}$$

where ΔS is the water storage term. The precipitation supplied to the surface is the same in both the simulations with and without BC but the differences in the other five components of the water balance are shown in figure 4.16.

The presence of BC in snow causes surface runoff from snow melt to shift earlier in the year. Increases in spring time surface runoff are mirrored by a decrease shortly after as snow melt ends. *Lau et al.* (2018) refer to this behaviour as the 'wet-first-dry-later' effect. At higher latitudes this trend occurs later in the year but the magnitudes of the differences are greater. A similar pattern is seen with evapotranspiration, which very closely matches the differences seen in latent heat flux in the previous section, the only variation between these two plots is associated with sublimation, which is not included in the evapotranspiration term in JULES. The differences in evapotranspiration are not as great as for surface runoff. Sublimation sees smaller increases than evapotranspiration, though they follow a similar pattern, just fractionally earlier in the year, before the snow melts. Unlike evaporation, there is no discernible decrease in sublimation later in the year, likely because in many cases final snow clearance will still have occurred in the same calendar month as before and there was never sublimation after snow clearance. These increases in sublimation are a feature of a warmer snow surface, especially during spring.

Water storage experiences the opposite pattern to surface runoff and evapotranspiration. There is a reduction of water being stored in the snowpack during spring, due to the reduced accumulation and earlier melt, and an increase in water storage within the soil column in summer.

The one field which does not see a strong latitudinal component to the timing of impacts is the sub-surface runoff. This field experiences a slight increase during spring followed by a reduction the rest of the year, although the magnitude of the change is much smaller than the other fields. The reduction in sub-surface runoff suggests a slightly drier soil column as a result of the earlier and more rapid snow melt. There is very little change at the highest latitudes, likely because the soil is frozen for much if not all the year - hindering water transport through the soil column.

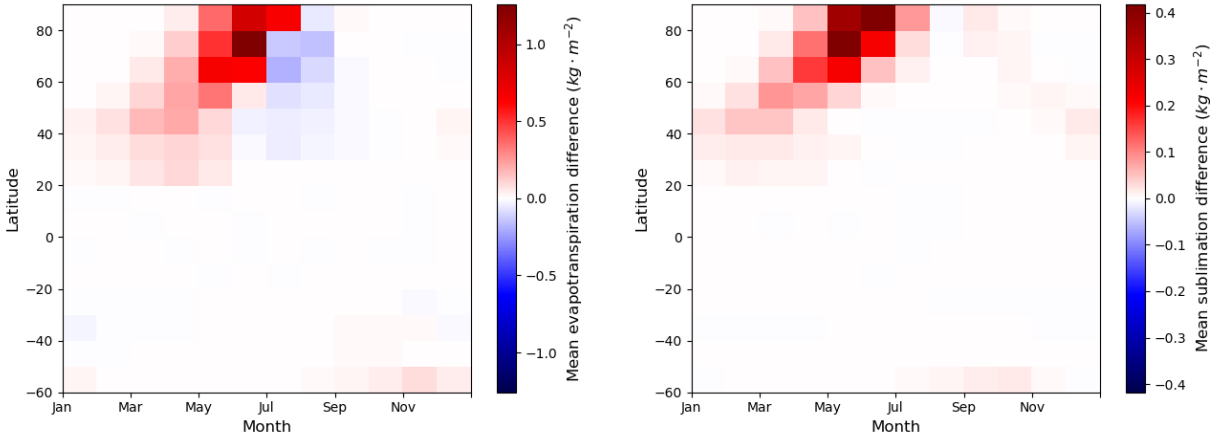

(a) Evapotranspiration

(b) Sublimation

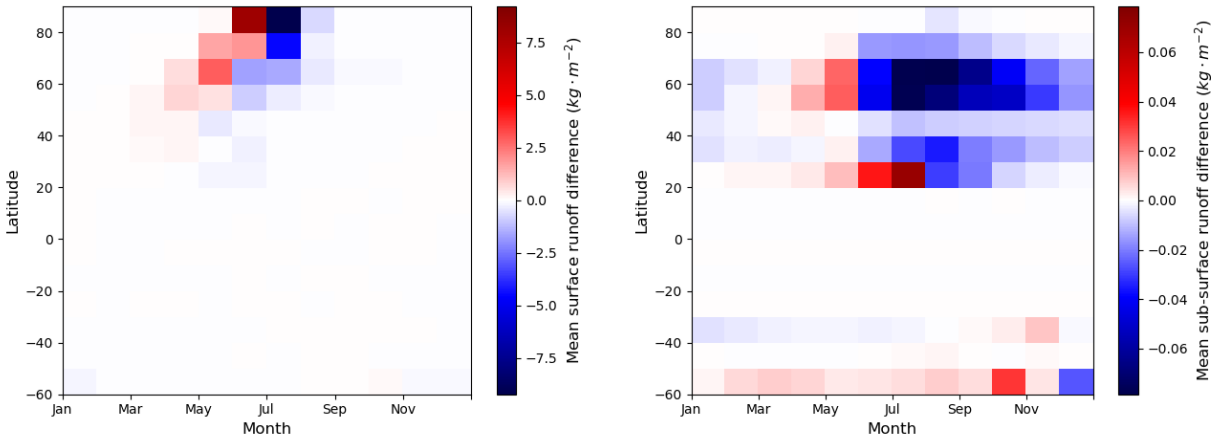

(c) Surface runoff

(d) Sub-surface runoff

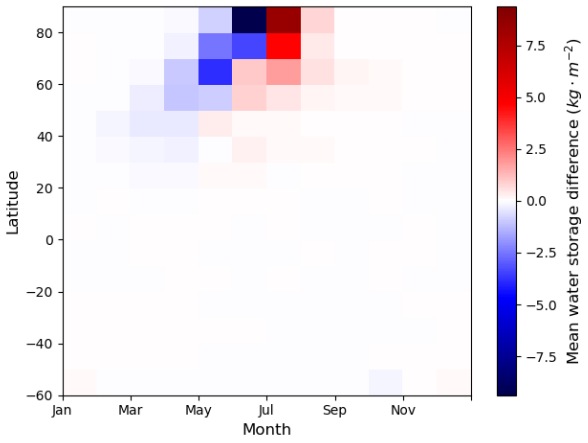

(e) Water storage (i.e. snow or soil moisture)

Figure 4.16: Differences in mean monthly totals, averaged by latitude band, of the various components of the water balance. Water storage is a residual term rather than a model diagnostic, it encompasses changes to snow mass or soil moisture. Note that these plots each have different colour scales.

Whilst the changes to snow cover and melt are localised mainly to high latitude and high elevation regions, the wider impacts on the water cycle can be far reaching as evaporation affects humidity and precipitation and runoff affects river flow. In order to better understand the scale of the hydrological impacts it may be beneficial to consider the cumulative impacts across entire river catchments. Surface runoff is of particular interest because it drives river flow. Whilst river routing is not turned on in these JULES simulations, considering catchment area totals still helps to build a picture of the potential impacts of BC on hydrology.

In order to calculate river catchment totals, the gridbox totals were integrated over river catchments as defined by version 2 of the Total Runoff Integrating Pathways (TRIP) river basin templates (*Oki and Sud*, 1998) which defines areas of major river catchments at a resolution of 0.5° (the same resolution as these JULES simulations). For this study, 53 of the largest snow fed river catchments in the northern hemisphere were selected to evaluate.

The seasonal cycle of differences in catchment total surface runoff is shown in figure 4.17 for the catchments that experience the greatest monthly differences in surface runoff. As with individual gridboxes, here it can be seen that across the entire river catchment there is an overall trend of runoff being shifted earlier in the year with an increase in the spring followed by a decrease as the snowmelt season passes. The exact timing of these differences varies depending on the latitude or elevation of the catchment and the magnitude of the differences depends both on the size of the catchment and the amount of snowfall within it but the pattern of runoff shifting earlier is consistent across all catchments.

The magnitude of the increase does not always match the magnitude of the decrease. As a result, some catchments experience an overall change in total annual surface runoff. These changes are shown in figure 4.18 as a percentage of the overall catchment runoff in the simulation without BC. Considering the percentage change in catchment runoff rather than absolute values means the values are not dependant on catchment size. It can be seen that some catchments experience an overall decrease in surface runoff, as the warmer surface leads more water to evaporate or sublimate, whilst other catchments experience an increase in total annual runoff as increased melt rates cause soils to saturate and water to flow away before it has chance to evaporate.

The catchments which experience the greatest changes in surface runoff are the high latitude Siberian rivers that drain into the Arctic Ocean and some of the river catchments that are fed from the High Mountain Asia region (made up of the Himalayas, Hindu Kush, Pamir Mountains, Karakoram and Tian Shan). Rivers that originate on the Tibetan Plateau (the Yangtze, Yellow, Mekong and Salween rivers) do not appear to be particularly affected by the introduction of BC in terms of their annual surface runoff. Whilst it's possible that other snow darkening contaminants, such as dust, may play a larger role on the Tibetan Plateau, as suggested by *Yasunari et al.* (2015), runoff in these catchments is likely dominated by rainfall rather than snowmelt.

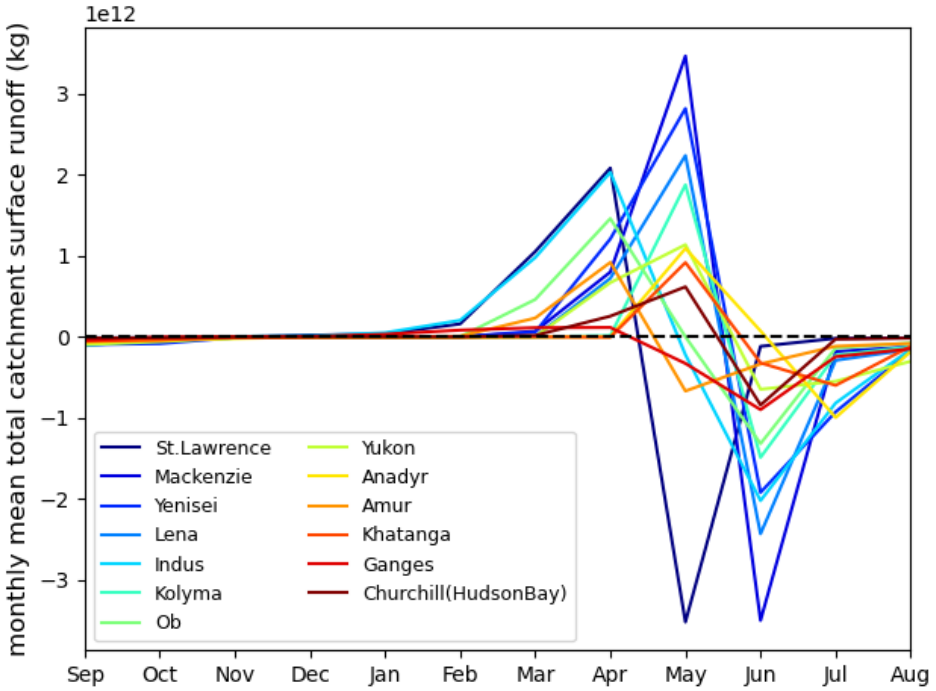

Figure 4.17: Timeseries of differences (exp minus ctrl) in monthly mean catchment total surface runoff for 13 catchments that see the greatest changes in monthly surface runoff quantity. The locations of these catchments are highlighted on the map in figure 4.18.

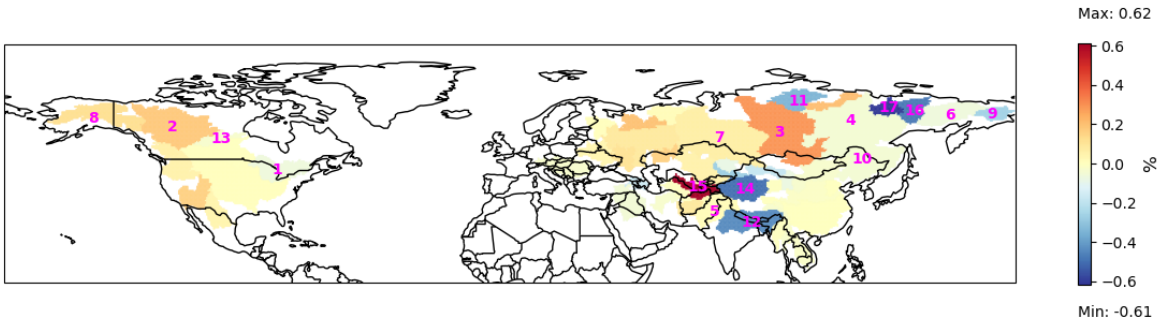

Figure 4.18: Map of percentage difference in annual mean river catchment total surface runoff for major Northern Hemisphere rivers. Numbered river catchments: 1. St. Lawrence, 2. Mackenzie, 3. Yenisei, 4. Lena, 5. Indus, 6. Kolyma, 7. Ob, 8. Yukon, 9. Anadyr, 10. Amur, 11. Khatanga, 12. Ganges, 13. Churchill (Hudson Bay), 14. Tarim, 15. Amu-Darya, 16. Indigirka, 17. Yana.

It is interesting that the river which experiences the greatest increase in surface runoff when BC is included is the Amu-Darya river – a river that in recent decades (along with the Syr-Darya) has experienced such high water extraction for irrigation that it has led to the drying up of what was once the world's fourth largest lake, the Aral Sea, and the desertification of the surrounding area (*Yang et al.*, 2020). Climate change already poses a threat to populations that depend on the Amu-Darya river as glaciers retreat and melt water from the Pamir mountains reduces. The

result here suggests that any reduction BC emissions, e.g. due to transition away from fossil fuel usage, could lead to further reduction of water availability in this region.

Both the Amu-Darya and the Tarim basins flow through extremely arid regions for much of their length so the surface runoff in these basins is more heavily dominated by snow melt from the upstream mountains than is the case in basins where the lowlands also experience significant quantities of precipitation. This is likely a factor in why these two rivers are so strongly affected by the introduction of BC snow darkening.

Whilst the impacts on overall annual surface runoff trends are mixed, the same is not true for evapotranspiration. Figure 4.19 shows that the vast majority of catchments experience an overall increase in annual total evapotranspiration with the greatest impacts typically being found in high latitude catchments but also in the Indus and Ganges catchments. In reality, and if this scheme were included in a coupled atmospheric model, these increases in evapotranspiration would likely alter precipitation patterns, as was found by *Sang et al.* (2019). It's possible that this may cancel out some of the reductions in annual runoff shown in figure 4.18.

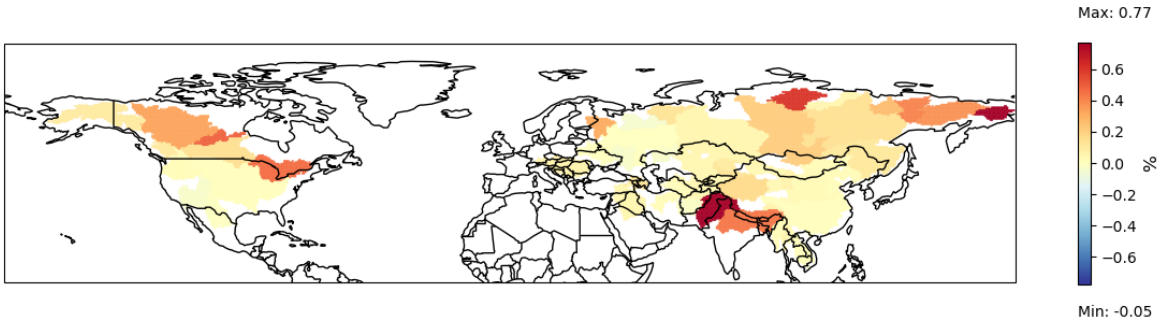

Figure 4.19: Map of percentage difference in annual mean river catchment total evapotranspiration for major Northern Hemisphere rivers.

4.7 Summary

This chapter has explored the impacts of including BC on snow in JULES across the Northern Hemisphere. It has been found that there is a strong trend of BC on snow causing snow to clear earlier in the spring although the mean reduction in snow duration was 2.26 days - far less than the 15 day reduction in snow duration found at Sapporo in chapter 3. The biggest reductions in snow durations were seen in gridboxes where one continuous snowpack was broken into several shorter lived snowpacks when BC was introduced, the most extreme case of this led to a reduction in snow duration of 153.79 days.

Introducing BC on snow also causes a clear trend of reduction in the peak snow amount, the mean reduction being 0.33% of BC-free snow mass. This effect is stronger at lower latitudes

due to the greater insolation received during the period of snow accumulation.

A minority of gridboxes experience an increase in snow mass when BC is introduced. This increase is usually small but it is an unexpected behaviour that it has not yet been possible to identify the cause of so further investigation would be prudent before using this scheme more widely.

Adding BC to snow generally leads to increased surface temperatures as more incoming radiation is absorbed by the surface. This is especially true in spring when the snow surface is at its darkest due to the melt amplification effect and then earlier snow clearance reveals an even darker surface and so even more radiation is absorbed. This increased surface temperature leads to an increase in sensible heat flux and outgoing longwave radiation. There is a latitudinal dependence on the timing of these impacts as the snow melt line progresses north gradually over the course of spring and summer. However, the strongest impacts are eventually felt at the higher latitudes where snow persists for extended periods.

Some gridboxes show a reduction in surface temperature. It is not clear if this is for genuine physical reasons, most likely relating to the insulating properties of the snowpack due to its low thermal conductivity, or if this behaviour relates to some form of model fault. As with the increased snow mass quantities, this should be investigated further before this scheme is adopted for more routine use.

Evapotranspiration, latent heat flux and surface runoff all show an increase in the spring as snow melt season shifts earlier followed by a decrease once the snow has cleared.

The High Mountain Asia region (Himalayas, Hindu Kush, Pamir Mountains, Karakoram and Tian Shan) experiences some of the greatest differences in snow duration and peak snow mass when BC is introduced to snow, this is likely due to the surface being exposed to greater insolation at such low latitudes as well as the relatively high BC deposition in this region compared to high latitude locations. This also leads to changes in annual total surface runoff across river catchments fed from these mountains, particularly the Amu-Darya (0.62%), the Tarim (-0.50%) and the Ganges (-0.44%) rivers, as well as increases in annual evapotransirarion, particularly for the Indus (0.77%) and Ganges (0.44%) rivers.

This study only considers standalone JULES simulations. More work is required to couple the BC in snow scheme in JULES directly to aerosol deposition fields within the UM without the need for offline processing as discussed in section 2.5.2. Work by *Yasunari et al.* (2015) found that coupling an aerosol snow darkening scheme to an atmospheric model led to positive land-atmosphere feedback processes that exacerbated the radiative and hydrological impacts of the change. Given the patterns of changes to surface temperature and latent heat flux found in this chapter, it is reasonable to assume that the similar feedbacks would be found if this scheme were coupled to the UM.

These results suggest that mountainous regions are particularly sensitive to the inclusion of BC snow darkening effects. It may be worth improving the representation of orographic effects within JULES when using this scheme. For example, slope gradient and orientation effects on snow melt are not currently accounted for in JULES but it may be beneficial to do so in this context. It is also important to remember when considering these results that GPCC precipitation driving data used in this study may be less accurate in mountainous regions due to orographic affects. In the context of coupled atmospheric modelling, *Oaida et al.* (2015) and *Sarangi et al.* (2019) both argued that it is necessary to use higher resolution models to represent the effects of complex mountainous terrain on snow processes, including aerosol snow darkening processes, as coarser resolutions fail to capture orographic effects on precipitation.

A remaining uncertainty is the accuracy of the BC deposition fields that were generated using CLASSIC. As shown in chapter 2, CLASSIC underestimates the deposition in some areas although it is not clear how widespread that issue is. One theory is that deposition is underestimated in source regions and overestimated in remote regions. If true then impacts of BC snow darkening may be even greater in the High Mountain Asia region but less so in high latitudes. Fully examining the global accuracy of CLASSIC BC deposition is beyond the scope of this work but these results do highlight the need for accurate aerosol modelling when considering aerosol induced snow darkening.

Other studies that examine the impacts of BC on snow also consider other snow darkening aerosols such as organic carbon and dust. It would be beneficial to expand the snow darkening scheme in JULES to account for other light absorbing snow contaminants such as these. Different particles affect different regions to differing extents, for instance *Gleason et al.* (2022) found that BC was the dominant snow contaminant, in terms of radiative absorption, in snowpacks in the Rocky Mountains whereas *Sterle et al.* (2013) found that dust dominated at a site in the Sierra Nevada mountains of California. In order to accurately predict snow albedo, surface temperature, snow melt timing and the consequent downstream hydrological effects globally it will be necessary to include all snow contaminants that have a discernible impact on radiative absorption. This work demonstrates a methodology that could be expanded to incorporate other aerosols within JULES. Work in this chapter has demonstrated that seasonal snowpacks within JULES are sensitive to even relatively small BC depositions with some of the biggest impacts being seen in remote high latitude locations. Including other snow contaminants within JULES would likely lead to darker, warmer snow surfaces than shown here and thus even earlier snow melt, even more evaporation and greater impacts to water availability.

Chapter 5

Validating performance of BC on snow scheme globally

5.1 Introduction

In chapter 3, the BC on snow scheme was validated at a single site but it is important to assess the performance of any new scheme at a range of different locations as it may perform differently under different conditions. Given the challenges of maintaining ground based weather stations in snowy conditions, due to instruments freezing or becoming buried in snow, the most readily available data for validating model performance across a wide variety of locations are those obtained from satellites. In this chapter a satellite albedo product is used to assess the spatial variability of the impact of including BC on snow.

5.2 Satellite validation data

5.2.1 Choice of satellite product

Whilst satellite data are available in remote locations and are not subject to the same instrument maintenance issues under snow conditions that ground based measurements are, they do still face many weather and geography related limitations. For example, when observing the surface, one must discard optical measurements that were obscured by cloud cover. Distinguishing snow cover from cloud cover is not always straightforward. Additionally, the elevation of the surface can in some instances affect the measurements obtained. For instance, *Savoie et al.* (2009) found that remotely sensed passive microwave snow covered area products needed to be corrected to account for the thinner atmosphere over the Tibetan Plateau in order to avoid

overestimating snow extent in this region.

For this study, the main interest was the timing of snow clearance. This can be seen in both products that measure snow amount/extent and products that measure surface albedo. The snow amount/extent product that was considered was Globsnow. Globsnow makes use of ground based measurements of snow depth to help constrain remotely sensed passive microwave measurements of snow water equivalent (SWE) (*Takala et al.*, 2011). *Takala et al.* (2011) and *Hancock et al.* (2013) found that this approach enabled Globsnow to perform better than other satellite SWE products. However, *Hancock et al.* (2013) also found that both Globsnow and the other passive microwave SWE products studied did not perform well at predicting the day of snow melt (Globsnow had a mean bias of +5.7 days and an RMSE of 21.1 days), probably due to difficulties sensing shallow or wet snow with a passive microwave instrument. For this reason it was decided that a product measuring albedo would be more appropriate for studying the introduction of BC to snow in JULES, where the biggest impacts are expected to be on the timing of snow clearance. The product selected for use in this chapter was the MODIS MCD43C3 albedo product.

5.2.2 How the MODIS MCD43C3 v6.1 albedo product is produced

The MODerate Resolution Imaging Spectroradiometer (MODIS) is an instrument onboard NASA's Terra and Aqua satellites that measures surface reflectance in seven different narrow spectral wavebands. A Bidirectional Reflectance Distribution Function (BRDF) can be fitted to these surface reflectance measurements. Assuming data are available at a sufficient range of viewing and irradiance angles, it is then possible to obtain a value of albedo by integrating the BRDF over these angles. MODIS has been reporting albedo values in this way since Terra began operating in 2000.

In the case of the MODIS MCD43 products, the BRDF used is based on the linear kernel-driven formulation proposed by *Roujean et al.* (1992):

$$\rho(\theta_s, \theta_v, \phi, \lambda) = \sum_{k=1}^{3} f_k(\lambda) K_k(\theta_s, \theta_v, \phi). \tag{5.1}$$

Here, $\rho(\theta_s, \theta_v, \phi, \lambda)$ is the reflectance, as can be observed from a satellite. It depends on the solar illumination angle, θ_s, the viewing angle, θ_v, their relative azimuth angle, ϕ and the wavelength of the light being observed, λ. These angles are illustrated in figure 5.1. There are three different 'kernels', K relating to different modes of scattering. The first kernel represents isotropic scattering off a Lambertian surface, as this scattering has no directional dependence the value of K_1 is 1. The second kernel represents geometric scattering - this accounts for undulations in the surface or opaque protrusions such as thick vegetation and the shadowing effects that they cause. Finally, the third kernel represents volumetric scattering as might be seen from leaves

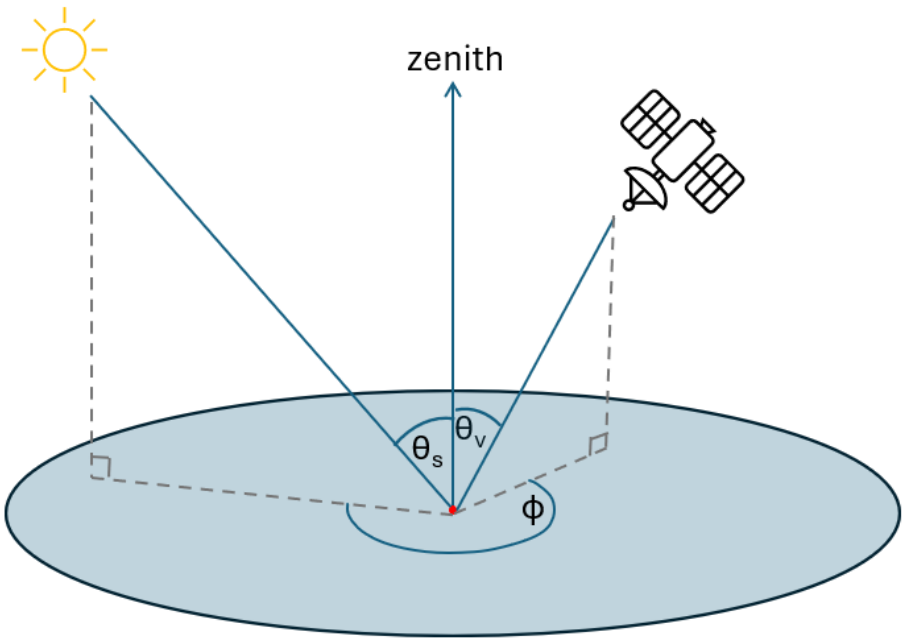

Figure 5.1: Diagram illustrating the solar illumination angle, θ_s, the viewing angle, θ_v, and their relative azimuth angle, ϕ, in relation to a point on the Earth's surface.

in a vegetation canopy or from microstructures such as soil pores. For each kernel there is also an associated kernel weight parameter, f.

Wanner et al. (1995) collated and derived several different options for the volumetric and geometric kernels that could be used in this BRDF model. The kernels that were selected for use in the MODIS MCD43 BRDF and albedo products were the Ross-thick kernel to describe the volumetric scattering and the reciprocal form of the Li-sparse kernel to describe the geometric scattering. The Ross-thick kernel is based on the radiative transfer modelling approach of *Ross* (1981), that treats the surface as a medium consisting of randomly spaced and orientated facets above a lambertian plane. It was derived by *Roujean et al.* (1992) and relies on assumptions of a single scattering approximation and that vegetation canopies are optically thick - i.e. they have a large leaf area index ($LAI \gg 1$). The Li-sparse kernel was derived by *Wanner et al.* (1995), it is based on the approach of *Li and Strahler* (1986) and considers a canopy of randomly located ellipsoids above the ground that results in illuminated and shaded patches of both canopy and ground. The surface is assumed to be sufficiently sparsely vegetated that mutual shadowing from adjacent vegetation crowns can be neglected. The reciprocal form of this kernel was introduced by *Strahler et al.* (1999). The Ross-thick Li-sparse kernel combination has been found to perform well over a range of surfaces (*Privette et al.*, 1997).

The kernel values can be determined from the positions of the satellite and the sun relative to the surface, a least squares errors approach can then be used to obtain values of the f parameters from observations of ρ (*Strahler et al.*, 1999; *Lucht et al.*, 2000).

The directional hemispheric albedo, also known as the 'black sky albedo', is the fraction of direct incident radiation reflected from the surface. It can be obtained by integrating equation 5.1 over all viewing angles θ_v but it remains dependent on the solar illumination angle θ_s. The linear nature of the BRDF formulation means that the kernels can be integrated separately and the parameters f_k remain unchanged as they have no angular dependence.

Lucht et al. (2000) defined the integral of the model kernels with respect to viewing angle and relative azimuth angle as

$$h_k(\theta_s) = \frac{1}{\pi} \int_0^{2\pi} \int_0^{\pi/2} K_k(\theta_s, \theta_v, \phi) sin(\theta_v) cos(\theta_v) d\theta_v d\phi, \tag{5.2}$$

such that the black sky albedo can then formed as a sum thus:

$$\alpha_{bs}(\theta_s, \lambda) = \sum_{k=1}^{3} f_k(\lambda) h_k(\theta_s). \tag{5.3}$$

The diffuse bihemispherical 'white sky' albedo is then obtained by further integrating over the incidence angles of solar irradiance so the kernel integral becomes

$$H_k = 2 \int_0^{\pi/2} h_k(\theta_s) sin(\theta_s) cos(\theta_s) d\theta_s \tag{5.4}$$

and then the white sky albedo is given by the sum

$$\alpha_{ws}(\lambda) = \sum_{k=1}^{3} f_k(\lambda) H_k. \tag{5.5}$$

The values K_k in equation 5.1 as well as h_k and H_k can all be determined from the positions of the sun, satellite and surface pixel being observed. The observation of surface reflectance ρ is then used to solve 5.1 to find values of the f_k parameters. By combining all these values, the black and white sky albedos become known.

Finally, to obtain a broadband albedo, the individual spectral albedos calculated for each waveband observed are combined as a weighted sum:

$$\alpha_{bs} = \sum_{i=0}^{n_\lambda} q_i \alpha_{bs}(\lambda) \tag{5.6}$$

$$\alpha_{ws} = \sum_{i=0}^{n_\lambda} q_i \alpha_{ws}(\lambda) \tag{5.7}$$

where n_λ is the number of wavebands and q_i are spectral to broadband conversion weights that have been determined from models (*Liang et al.*, 1999). In cases of pure snow a different set

of weights is required (*Stroeve et al.*, 2005). Three different broadband albedos are produced - a visible band (0.4-0.7μm), a near infrared band (0.7-5.0μm) and a total shortwave band (0.25-5.0μm). Because BC is strongly absorbing only at visible wavelengths and because the white sky albedo is independant of sun angle, it is the visible white sky albedo that will be used in this chapter for comparison with the diffuse visible component of the JULES modelled albedo.

In order to sample a sufficient range of irradiance and viewing angles, reflectance observations are collected over a 16 day rolling window and combined as a weighted average, heavily weighted towards the day of interest (the centre day, day 9), the quality of the values is also factored into the weighting. If snow is detected on the day of interest then only the observations made under snowy conditions are included, otherwise the snowy observations are discarded (*Wang et al.*, 2018)[1]. Observations made under cloudy conditions are also excluded. Where insufficient observations are available, a backup algorithm is employed based on a priori information combined with any observations that are available, albedos generated using this method are considered to be of lower quality, this is reflected in their quality flag value.

The standard MODIS BRDF products (MCD43A) are supplied at 0.5km resolution on a sinusoidal grid but a 0.05° resolution albedo product is also supplied on a lat/lon 'climate modelling grid' by averaging the albedo values of all the 0.5km pixels that make up the 0.05° grid box (*Gao et al.*, 2005). This is the MCD43C product that shall be used in this chapter. The coarser resolution means that files are smaller and easier to handle than the 0.5km product and as it is being compared to the 0.5° JULES simulation the additional resolution would be of no benefit.

5.2.3 Accuracy of the MODIS MCD43 albedo products

The accuracy of these albedo values does depend on the surface being observed and how well the BRDF model describes that surface. They cannot be considered direct observations due to the number of assumptions and amount of modelling required to convert from the surface reflectance measurement to the albedo value. One must always use caution when comparing one modelled value with another and so the reliability and weaknesses of this albedo product shall now be explored.

Numerous studies have attempted to assess the validity of the MODIS albedo products, it is important to note that the product has been updated several times over the lifetime of the Terra and Aqua satellite missions and so there may be small differences in performance between the versions. For instance, reflectance measurements from Aqua (which launched later) were incorporated at v5 (*Wang et al.*, 2012) and at v6 corrections were made to account for sensors aging over the lifetime of the satellites (*Wang et al.*, 2018). Where possible, studies that evaluate the latest version (v6.1) are discussed but it is sometimes also necessary to consider the history

[1] In previous versions (v5 and earlier) this was determined by snow conditions on the majority of days rather than the day of interest.

of evaluation of this product. This is especially true as there are fewer studies available that specifically focus on the performance of the MCD43 products over snowy surfaces.

Other points to note when comparing different evaluation studies are that whilst some studies look at the coarser 'climate modelling grid' product, most studies choose to focus on the finer resolution MCD43A product, especially when comparing to data from ground observation stations which tend to have a much smaller footprint (of the order of a few tens of meters). Even then, some studies choose to only focus on ground stations that are in spatially homogeneous locations. Ground stations in these locations are more likely to have albedos that are representative of the entire view seen by the satellite pixel. Indeed, *Stroeve et al.* (2013) and *Wang et al.* (2014) both found that when comparing the satellite product to ground observations in less homogeneous locations greater biases were seen, with ground albedos being brighter than was seen by the satellite product. *Urraca et al.* (2022) (when evaluating v6 and v6.1 of MCD43C) avoided this issue by limiting their study to ground stations which were assessed to be in locations that were sufficiently spatially homogeneous in both vegetation cover and snow cover that the ground station measurements were expected to give a good representation of the entire satellite pixel. It's worth noting that even locations that are very homogeneous in terms of surface type and vegetation cover are likely to experience heterogeneous albedos during periods of snow melt due to snow cover becoming patchy. In terms of validating JULES, using an albedo value that represents a wide area rather than a single point is beneficial because the global JULES simulations model large gridboxes rather than single points. Whilst JULES calculates separate albedos for individual surface types ('tiles'), these are averaged to give an overall albedo for the gridbox.

Whilst MCD43C3 is able to represent the spatial variability of a gridbox by including multiple albedo values from the higher resolution MCD43A product, the temporal variability of snow cover is a bit less straightforward. Because the high resolution product will only accept either snow covered or snow free reflectance observations within the 16 day window, periods of snow accumulation or melt can be less well represented than periods that are completely snow covered or snow free. This was found to be the case by *Stroeve et al.* (2013), *Wang et al.* (2018) and by *Urraca et al.* (2022). The fact that the MODIS products are available daily (from v6 onwards) does help with this and as a consequence MCD43C3 was found to perform better in periods of partial snow cover than other less frequently available satellite albedo products (*Urraca et al.*, 2022). From version 6 onwards, the snow conditions on the day of interest (9th day) are used rather than the snow conditions on the majority of the days in the aggregation window (*Wang et al.*, 2018), this helps to avoid a lag in snowpack formation and clearance compared to reality and also allows the product to include short durations of snow cover (1-7 days) that were previously excluded.

It must be noted that this product is not always available, reflectances cannot be collected during periods of polar night and must be excluded during periods of cloud cover (using cloud masking

algorithms). *Gao et al.* (2005) noted when reviewing v4 of the MCD43C product that the cloud cover masking was not always perfect and occasionally some spurious albedos were produced due to cloud contamination - this mainly affected tropical regions and the cloud masking algorithms have since been improved (*Wang et al.*, 2018). Excluding cloud covered periods will of course mean that albedo cannot be sampled during snowfall events so there may be fewer values available during the snow accumulation period but the snow melt season is less likely to be affected.

Another consideration is that at the very high solar zenith angles (SZA) sometimes seen at high latitudes, the MCD43 albedo products may be less accurate. *Stroeve et al.* (2013) found that the MCD43A (v5) albedo values remain realistic for SZA $\leq 75^{\circ}$ but that the lower quality backup algorithm is sensitive to SZA and when albedo values from this algorithm are used at high SZA a low bias is seen. Similarly, *Urraca et al.* (2022) found a negative bias of -0.042 at stations between 68°N and 75°N when evaluating the more recent MCD43C3 v6.1 product but this was not apparent at Antarctic stations.

When comparing satellite albedo products to ground observations it is necessary to convert the black and white sky albedos to a blue-sky albedo - i.e. the albedo as seen at the surface given the relative amounts of direct and diffuse radiation. Most studies simply calculate this as

$$\alpha_{blue-sky} = \alpha_{ws}k + \alpha_{bs}(1-k) \tag{5.8}$$

where k is the ratio of diffuse to total radiation. *Wang et al.* (2012) suggested an alternative approach for converting black-sky and white-sky albedos to the blue-sky albedo. Their full expression for blue-sky albedo attempts to account for the anisotropic illumination and increased multiple scattering seen under high SZA. This formulation gives much better results (see table 5.1) but has not been adopted in later studies. The fact that so much improvement is seen from adjusting the blue-sky conversion method suggests that the issue is mainly related to atmospheric affects to do with the increased optical path length at high latitudes rather than assumptions in the underlying black and white sky albedos produced by the RossThick-LiSparse-Reciprocal model. As white-sky albedo shall be used for comparison with JULES rather than blue-sky albedo, issues at high latitudes may be less of a concern.

Table 5.1 summarizes the results of several studies of MCD43 albedo products under snowy conditions. As already discussed, it can be seen from *Wang et al.* (2012) and *Urraca et al.* (2022) that higher latitude locations have much larger low biases than other locations. Studies that compare fully snow covered conditions with partially snow covered conditions (*Stroeve et al.*, 2013; *Urraca et al.*, 2022) find that partially snow covered periods have a smaller bias than fully snow covered periods but larger RMSEs. *Wang et al.* (2014) found that performance was surface type dependant with forested surfaces performing much better under snowy conditions than grassland and agricultural surfaces. They also separated out results where there was enough reflectance observations to perform a full inversion from results where a lack of obser-

vations meant the backup algorithm had to be used to retrieve an albedo value. Unsurprisingly, the lower quality backup inversion produced larger biases and RMSEs although the impact of using the lower quality albedo values seems to be less than the impact of high latitudes on the quality of the retrieval.

Study	**Product version**	**resolution used**	**Conditions**	**Bias**	**RMSE**
Wang et al. (2012)	v5	MCD43A	16-day daily variant, standard isotropic conversion to blue-sky albedo, high latitude (71°), snow covered	-0.064	0.079
			16-day daily variant, full expression for conversion to blue-sky albedo, high latitude (71°), snow covered	0.004	0.047
Stroeve et al. (2013)	v5	MCD43A	Year round snow cover	-0.026 ± 0.057	0.052
			Seasonal snow cover	0.016 ± 0.078	0.077
Wang et al. (2014)	v5	MCD43A	16-day daily variant, snow covered grassland, full (high quality) inversion	± 0.027	0.041
			16-day daily variant, snow covered grassland, backup (low quality) magnitude inversion	± 0.027	0.046
			16-day daily variant, snow covered forest, full (high quality) inversion	± 0.005	0.005
			16-day daily variant, snow covered forest, backup (low quality) magnitude inversion	± 0.023	0.025
Wang et al. (2018)	v6	MCD43A	Snow covered	-0.0163	0.0471
Urraca et al. (2022)	v6.1	MCD43C3	Snow covered	-0.017	0.004
			Snow covered, high latitude ($> 68^{\circ}$)	-0.042	
			Partially snow covered	-0.013	0.023

Table 5.1: Summary of biases and RMSEs found in various studies comparing MODIS albedo products to ground based albedo measurements under snowy conditions.

5.3 Methods for comparing JULES and MODIS albedos

5.3.1 Processing MODIS MCD43C3 albedo product for comparison with JULES

In order to compare the MODIS albedos with JULES output it was necessary to regrid the MCD43C3 product to the same resolution as the JULES output (0.5°). This was done using an area weighted mean interpolation method. The missing data tolerance was set to 0.5 such that if more than half of the source data within a target grid cell was missing then the overall value for the grid cell would be set to missing data.

Whilst some of the studies mentioned in table 5.1 only include albedo values where a full inversion of the BRDF model has been possible, here both albedo values generated with the main BRDF algorithm and the backup 'magnitude' inversion are included. Whilst the lower quality albedos generated with the backup algorithm have been found to have a low bias (*Jin et al.*, 2003a; *Stroeve et al.*, 2013), they have still been found to correlate very highly ($r \geq 0.94$) with albedos generated via the main algorithm (*Jin et al.*, 2003a). Given the database of backup values has since been updated (*Wang et al.*, 2018), the performance of the magnitude inversion is expected to have further improved.

5.3.2 Calculating albedo comparison statistics

The MODIS albedo values are available daily, valid at local solar noon, whilst the JULES simulations output albedo values every hour. Determining which modelled albedo value is closest to local solar noon each day for each gridbox is not entirely straightforward so instead the maximum albedo value each day was chosen for comparison with MODIS albedos. Whilst this would not be appropriate for the direct (black sky) albedo, which tends to have larger values at larger solar zenith angles (*Jin et al.*, 2003b), it should be sufficient for the diffuse (white sky) albedo that is used in this chapter as white sky albedo has no dependence on solar zenith angle.

When calculating statistics comparing JULES and satellite albedo values, only the period of snow cover and snow clearance is of interest. The purpose of this chapter is not to validate snow free albedo and so for each gridbox each year statistics are calculated only over the longest snow covered period in the control simulation (as determined in chapter 4) plus two weeks either side. The control simulation was chosen for the reference duration as it is known to have longer snow durations than the experiment simulation (figure 4.4) but two weeks is added to either side of this temporal window to ensure that the entire snowpack accumulation and clearance is captured, including any differences in timing between the modelled snowpack and that observed by the satellite. Two weeks is towards the upper end of the differences in snow duration seen when BC is added; as mentioned in section 4.4.1, 99.1% of all gridboxes see a reduction in snow duration between 0 and 14 days when BC is added so by considering a period of interest of

the entire duration of snow cover in the control simulation ± 14 days, the snow accumulation and clearance is expected to be fully captured in most cases. The main exceptions would be cases where there are several short-lived snowpacks in a season and which one lasts longest changes with the addition of BC. In order to focus on gridboxes where the 'main' snowpack each year is clear and avoid confusion caused by ephemeral snowpacks, only gridboxes where the longest snow duration exceeds 14 days have been considered in this chapter.

The Mean Absolute Error (MAE) between the satellite albedos and the albedos from each of the JULES simulations was calculated. These values were calculated for each gridbox for the snow covered part of each year (September - August) as follows:

$$MAE = \frac{\sum |\alpha_{sim} - \alpha_{sat}|}{n_{days}}. \tag{5.9}$$

Where α_{sim} is the albedo value for the JULES simulation and α_{sat} is the satellite albedo value for the same day. n_{day} is the total number of days that the values are being compared over (snow duration $\pm$ two weeks). Whilst this doesn't give information about the bias of the simulated albedos, it does allow the errors to be compared by calculating MAE separately for each of the two simulations and then taking the difference (experiment minus control). Mean Bias Error (MBE) was also considered but taking the difference of the MBEs for the two simulations would just have given the mean difference between the two simulations as the satellite albedos would cancel out. For this reason, MBE is only used to quantify the biases in the two simulations. The equation for mean bias error is

$$MBE = \frac{\sum (\alpha_{sim} - \alpha_{sat})}{n_{days}}. \tag{5.10}$$

5.4 Global comparison with satellite albedos

5.4.1 JULES without black carbon

Before examining the impact of adding black carbon to JULES, it is worth first examining the capability of the existing snow scheme within JULES to replicate the MODIS albedo values. Figure 5.2 shows the mean bias error maps comparing the control simulation with MODIS. These mapsshow large areas where JULES underpredicts albedo during the snow season, often by quite a considerable amount. Albedo values range between zero and one, typically snow would have an albedo > 0.7 and a snow free surface might be more of the order of 0.2 so an error of the order of -0.5 is very large and suggests that JULES is often reporting that a surface is snow free when in fact it should be snow covered. Given the limitations of the satellite product discussed in section 5.2.3 tend to lead to low biases in reported albedo rather than high biases, it is unlikely that the MBE values shown in figure 5.2 can be due to inaccuracies in

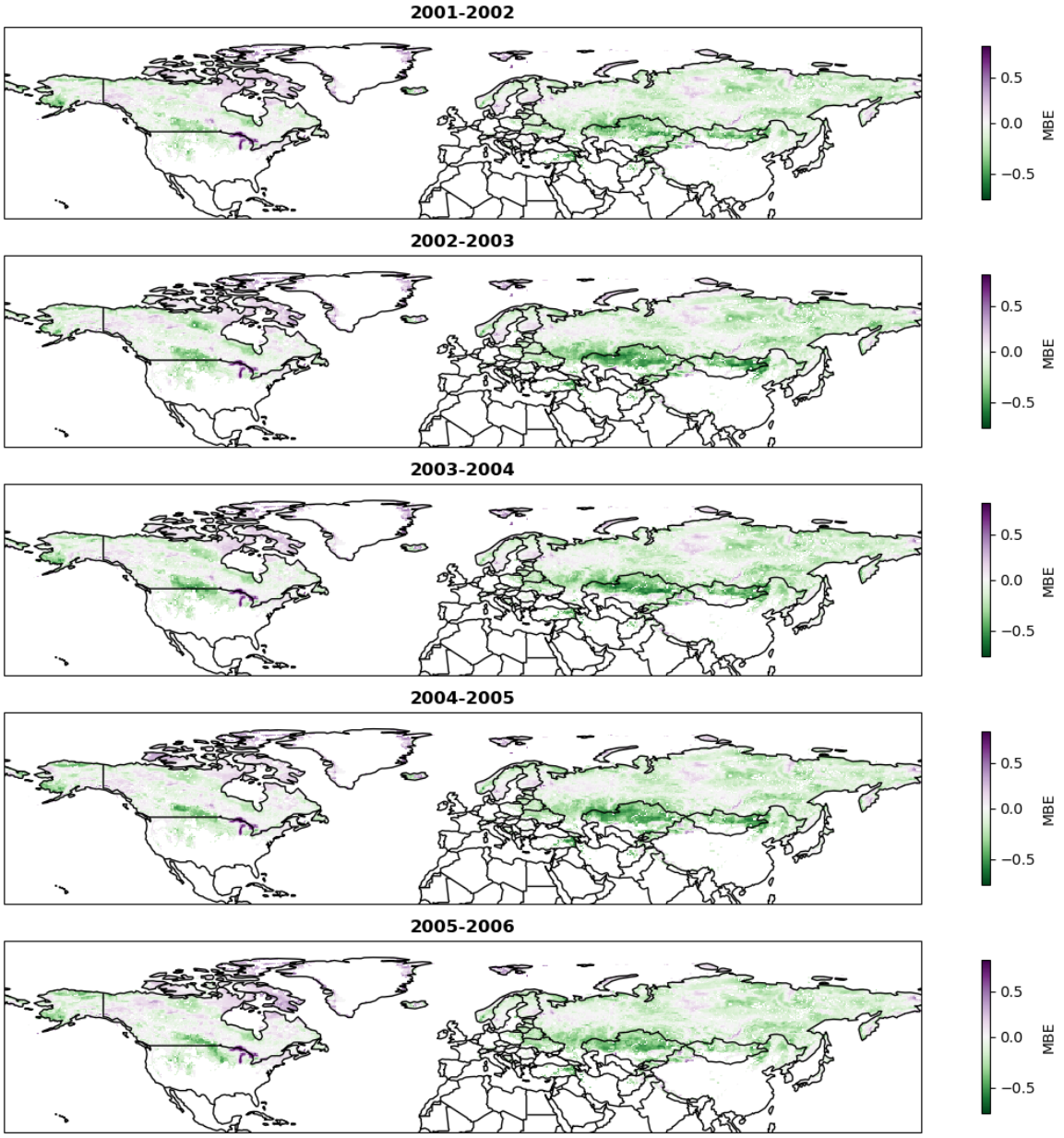

Figure 5.2: Maps of mean bias errors in the control simulation when compared to the MODIS MCD43C satellite product.

the albedo product used for comparison. The extent to which JULES underpredicts winter-time albedo has only become apparent here by carefully selecting the snow covered period of each gridbox each year and examining albedo performance specifically for that time window.

Adding BC to the snow in regions where snow albedo is already underpredicted will likely result in even larger errors but in regions where snow albedo is currently overpredicted, such as the area to the North of Hudson Bay, it may still offer some benefit.

5.4.2 JULES with black carbon

Figure 5.3 shows the MAE difference maps for five years where the JULES simulations and the MODIS albedo datasets overlap. Note that the scale of the colorbar has been capped as a small number of locations have much larger differences in MAE than most, aqua and fuchsia are used to highlight locations with large differences in MAE. Negative differences in MAE (displayed in green and aqua) indicate gridboxes where including BC in the JULES simulations has improved albedo prediction. There are a mixture of locations that have an improvement in albedo prediction and locations where including BC reduces the accuracy of the modelled albedo. However, when we look at the more extreme differences, there are more places that see big improvements (aqua) than big deteriorations (fuchsia).

Figure 5.4 shows a histogram of the MAE values seen in Northern hemisphere gridboxes each year. It can be seen that when BC is added to JULES, the peak of the histogram shifts to lower MAE values, suggesting that overall there is a reduction in absolute albedo errors. There is a reduction in the number of gridbox years showing errors in the 0.1-0.22 range, whilst most of these shift to lower MAE values when BC is added, there are also some small increases in the number of gridbox years experiencing higher MAE values once BC is included (slight increases in the height of bars in the 0.24-0.44 range). Overall, the mean Northern hemisphere MAE value for the simulation without BC was 0.1715 and the mean MAE value for the simulation with BC was 0.1710 - a reduction in absolute error of 0.0005 (or 0.3%).

The Mean Bias error histogram in figure 5.5 again highlights that in the control simulation, the albedo in JULES tends to be too low – the peak value indicates a negative bias. Adding black carbon exacerbates this by increasing the number of gridbox years experiencing low biases and reducing the number of gridbox years experiencing high biases.

As might be expected, there are various reasons for the different results seen here and many of them are to do with other underlying weaknesses in JULES's ability to model snow rather than being directly related to the need to include snow contaminants in albedo calculations. For example, one feature that stands out in the maps in figure 5.3 is that large lakes (e.g. the North American Great Lakes) see big improvements in snow albedo when BC is included. This is because of a lack of representation of ice formation on lakes in JULES. As mentioned previously,

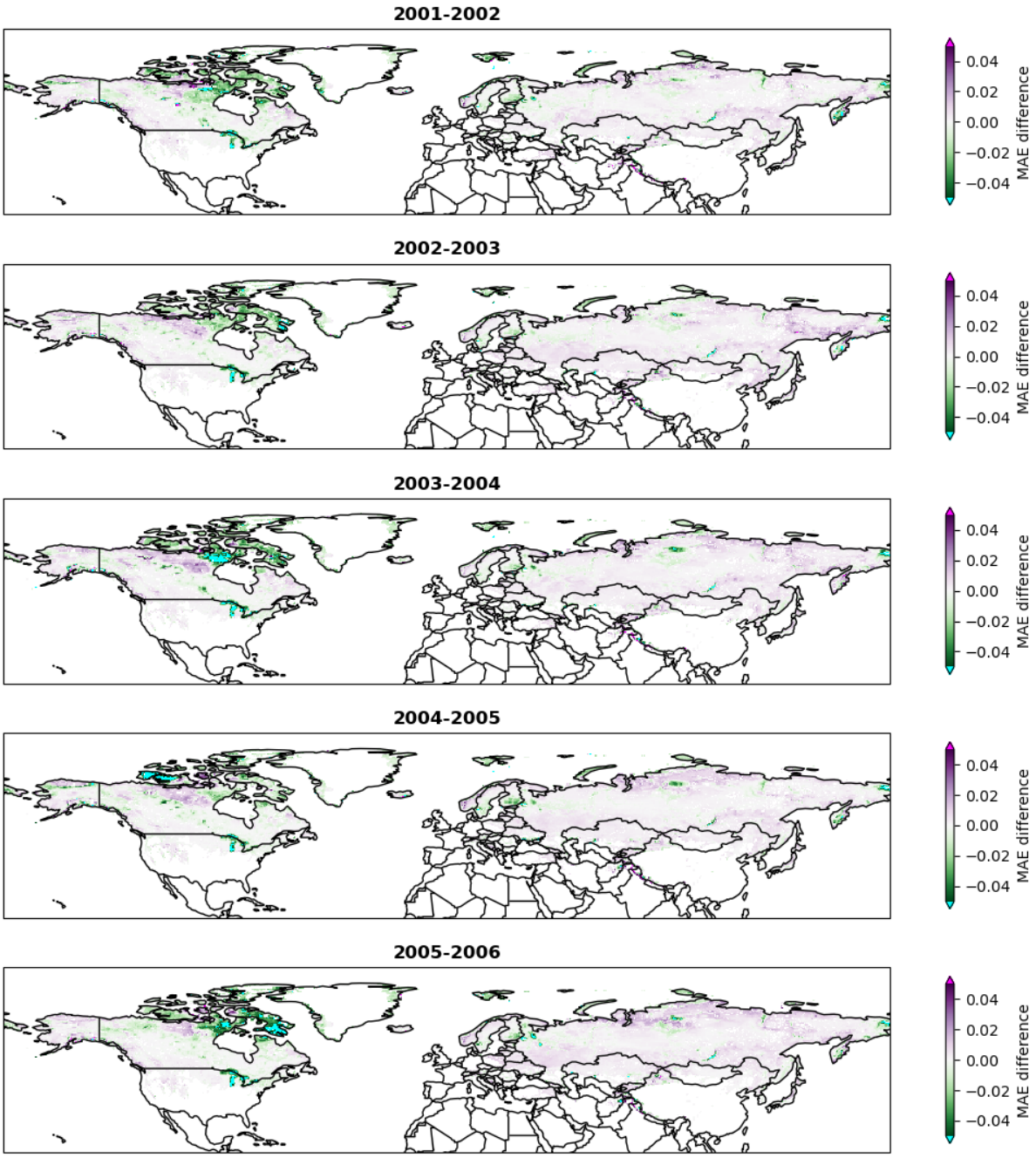

Figure 5.3: Difference in mean absolute error in albedo (experiment MAE minus control MAE) for the snow period of five years. Negative differences in MAE (displayed in green and aqua) indicate gridboxes where including BC in the JULES simulations has improved albedo prediction.

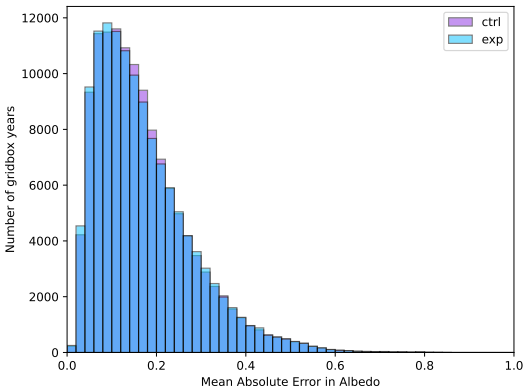

Figure 5.4: Histogram of values of Mean Absolute Error in albedo each year (2001 to 2006) across northern hemisphere gridboxes for the control simulation (without BC, purple) and the experiment simulation (with BC, light blue) each compared with the MODIS satellite albedo product.

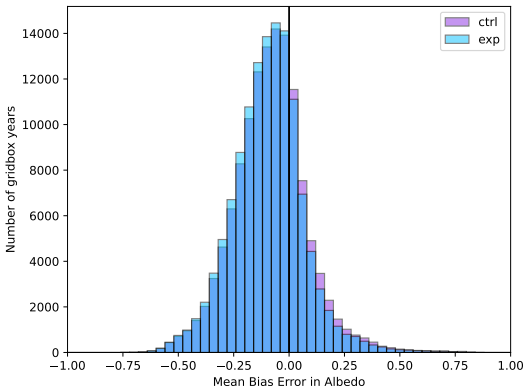

Figure 5.5: Histogram of values of Mean Bias Error in albedo each year (2001 to 2006) across northern hemisphere gridboxes for the control simulation (without BC, purple) and the experiment simulation (with BC, light blue) each compared with the MODIS satellite albedo product.

JULES will allow snow to settle on lakes whether or not ice is present. As such, lakes in JULES tend to experience far more snow cover than real world lakes so any reduction in winter time albedo is likely to bring the modelled albedos closer to observations.

It is clear that there are some differences from one year to the next but many features remain broadly similar. To begin with, much of Asia and parts of North America see an adverse impact from including black carbon - this is not the expected result and needs further exploration. Some of the biggest impacts are seen in Northern Canada, the Himalayas and far Eastern Russia. There is a sharp transition in the Canadian Shield region between an area where including BC brings JULES results much closer to the satellite albedos and an area where the opposite is true. All of these features will be further examined in the sections that follow in order to understand what determines whether introducing BC has a positive or negative impact on JULES's albedo modelling performance.

5.5 Transition to snow free summers

There are a small number of gridboxes (384) where the introduction of black carbon makes the difference between snow persisting year round in the control simulation and snow clearing in the summer in the experiment simulation. These gridboxes see some of the most extreme differences in MAE results - mostly a reduction in MAE indicating that the snow should indeed be clearing in the summer but also a few points where the opposite is true and JULES now falsely clears snow in summer. The locations of points where the number of fully snow covered

years reduces when BC is introduced are shown in figure 5.6. Most of these points are clustered around the fringes of the Greenland ice sheet and the mountainous islands of the Canadian Arctic Archipelago but there are also a few gridboxes in mountainous regions of Southern Alaska and far Eastern Russia. These locations suggest that this behaviour is seen when the introduction of BC causes the snow line to be nudged slightly further up a mountain or slightly further inland.

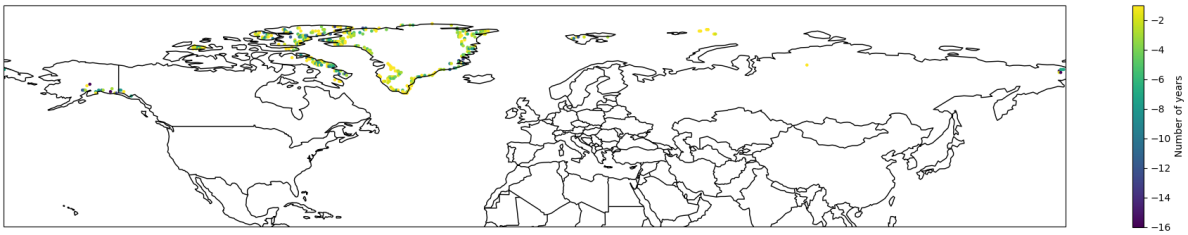

Figure 5.6: Difference (experiment minus control) in the number of years that experience year-round snow cover in JULES simulations.

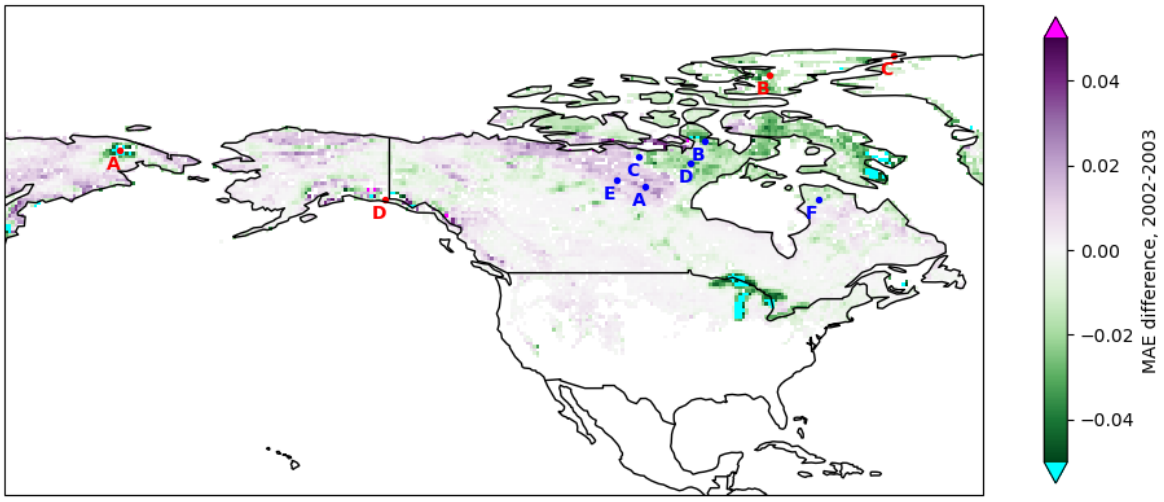

Figure 5.7: Locations of gridboxes for which albedo timeseries are shown in figure 5.8 (red) and figure 5.10 (blue). The shading reflects the MAE difference values for the snow season of 2002-2003 for reference.

Four of these gridboxes have been selected as examples of this behaviour, their locations are shown in red in figure 5.7, the albedo timeseries' for these gridboxes are shown in figure 5.8. In each case it can be seen that in the control simulation (blue line), the albedo remains high during summer months - suggesting that the snowpack never clears. When BC is introduced (yellow line), the albedo is seen to drop sharply in summer months indicating snow clearance.

For the first three locations shown, the MODIS gridbox mean albedo is also seen to drop in summer - suggesting that the snow does indeed clear in reality and therefore introducing BC on snow to JULES allows a more realistic snowpack behaviour at these sites. This is reflected in the MAE difference values shown at the bottom of the plots. The simulation that includes BC matches the MODIS albedo timeseries much more closely (has a lower MAE value) than the control simulation and so, when comparing the MAE values from the two simulations, large negative MAE difference values are found at these sites.

The difference in summertime albedo is clearly the starkest effect of introducing BC at sites A-C but it can also be seen that the peak wintertime albedo is slightly reduced when BC is added, this is particularly apparent at site B. This behaviour is expected and again helps to bring the modelled albedo closer to that reported in the satellite product, again improving MAE values.

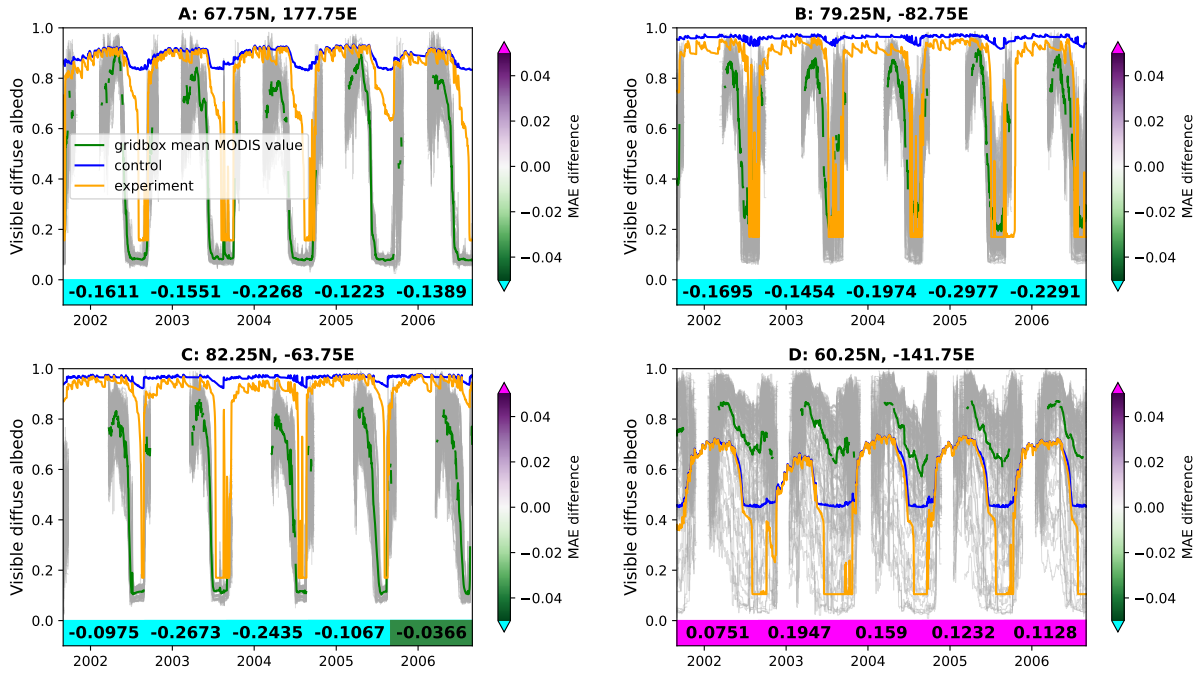

Figure 5.8: Timeseries of visible diffuse albedo from JULES simulations with (yellow) and without (blue) BC on snow for four gridboxes where the inclusion of BC triggers summertime snowmelt. Also shown is the gridbox mean MODIS white sky albedo (green) along with the MODIS white sky albedo timeseries for each of the satellite pixels that contribute to that gridbox mean value (grey). The colour shading and numbers along the bottom of the plots indicates the MAE difference that was calculated for each of the years shown.

On the other hand, at site D (located in the mountains of Southern Alaska), the introduction of BC has the opposite result on MAE difference values. Here, the introduction of BC takes the modelled albedo values further away from the satellite values in part because JULES was underestimating the wintertime albedo to begin with and in part because the gridbox mean satellite albedo value never gets low enough to indicate snow clearance. Examination of the ensemble of individual satellite pixel timeseries (grey lines) that contribute to the gridbox mean MODIS

value suggest that within the gridbox there is a mixture of pixels that do report snow clearance and ones that don't, this explains how the gridbox mean MODIS value shows some reduction in snow albedo during the summer but not enough to suggest full snow clearance. Whilst the modelled albedos of both the control and experiment simulations fall well below the mean satellite albedos, it is reassuring to see that they still remain within the spread of albedos measured for that gridbox. From the ensemble of satellite pixel time series it can be inferred that this is a very heterogeneous location, likely due to differences in elevation of the mountainous terrain. JULES is unable to represent this heterogeneity of snow cover within the gridbox. JULES can account for differences in snow cover on different surface types within a gridbox but other causes of sub-grid hetrogeneity of snow cover, including orographic affects, are not considered. The other three sites show much more agreement amongst the component satellite pixels indicating more homogeneous snow cover within these gridboxes.

To get a sense of where experiences the most heterogeneity in MODIS satellite albedo vales, a map of the 10th–90th percentile range of satellite values within each model gridbox is shown in figure 5.9. This map is just a snapshot of the heterogeneity on one date but it can be seen that areas with the highest heterogeneity include the Himalayas/Pamir Mountains/Hindu Kush region, the Caucasus mountains, coastal regions of Southern Alaska and British Colombia, Norway and Iceland. Many of these are mountainous regions. It is also possible to see a thin line across central Kazakhstan, given this area does not correspond to any obvious geographical features (such as mountains, rivers, varied vegetation) it is likely that this line indicates the snow extent on that date - it stands out so clearly here because of the otherwise homogeneous landscape.

The JULES configuration used for these simulations does not consider elevation. There is however an option available in JULES ('l_mask_snow_orog') to reduce snow albedo depending on the standard deviation of orography so that more mountainous regions would appear darker. This option would not have helped at point D as it seems that JULES was already underestimating the fraction of snow cover within the gridbox but it may have been beneficial in other mountainous areas such as the Brooks range of North Alaska and the Chukotka and Kamchatka

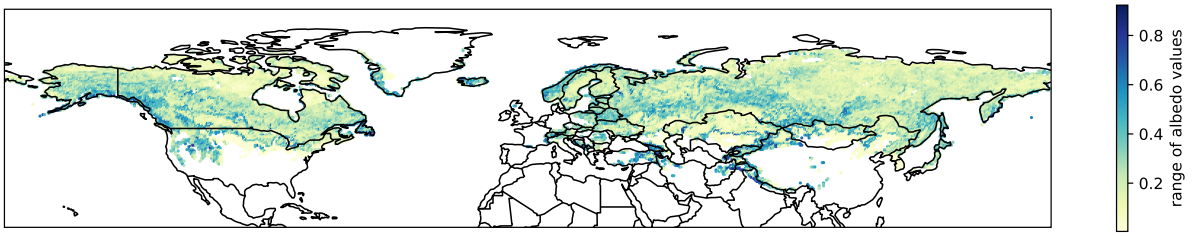

Figure 5.9: Map of 10th to 90th percentile range of satellite albedo values within each model gridbox area on the 5th March 2006 (the mean date of peak snow mass in the Northern hemisphere that year, according to the simulation that included BC).

mountains of Eastern Russia - these areas were all found to have positive mean bias errors in the control simulation (see figure 5.2), suggesting that JULES overpredicts snow albedo. This is in contrast to most of the northern hemisphere where JULES underpredicts albedo. Introducing BC did improve albedo errors compared to the satellite product in these regions (figure 5.3) but it is not clear if snow in these regions is darker in reality because of BC, slope effects in mountainous areas, heterogeneity of snow cover or a combination of all of these.

What's not clear from the results in figure 5.8 is whether or not BC is responsible for the summertime snow clearance at sites A-C in reality or if this is a case of a change enabling the model to get 'the right answer for the wrong reason'. It is however clear that at the boundaries between snow covered and snow free areas within JULES, the exact positioning of the snow line is sensitive to small changes in snow albedo.

5.6 Canada transition

The MAE difference maps (figure 5.3) show a sharp boundary in North-Eastern Canada between an area where adding black carbon improves modelled albedo (green/aqua) and an area where it makes it worse (purple/magenta). This boundary is also seen in figure 5.2 as a transition between one of the few areas where the control simulation overpredicts albedo to an area where albedo is underpredicted. Understanding the causes of this transition may lead to wider understanding of the controls and limitations on albedo modelling performance in JULES. To study this area further, three gridboxes were selected either side of this transition for further examination; their locations are shown in blue in figure 5.7 and their albedo timeseries are shown in figure 5.10.

In the area where adding BC makes the albedo worse (left-hand column of figure 5.10), we see that JULES consistently underestimates peak wintertime albedo. Adding BC will further reduce snow albedo values and so exacerbate this problem. In this region we also see that although JULES's timing of snowmelt was fairly accurate, if anything the albedo tends to drop fractionally early in the control simulation and so even earlier once BC is included. In the years where this is not the case, we see positive MAE difference values. Conversely, further East, in the region that routinely sees positive MAE differences (gridboxes in the right-hand column), not only is JULES slightly overpredicting peak wintertime albedo values but it also predicts the timing of snowmelt to be slightly later than is seen in the satellite data. Adding BC improves both of these behaviours.

It was considered whether the underestimation of albedo in some areas could be due to differences in the way JULES calculates albedo for different surface types, perhaps relating to snow interactions with vegetation. For instance, areas with high bare soil fractions tend to correspond with the areas where JULES snow albedo is overpredicted rather than underpredicted

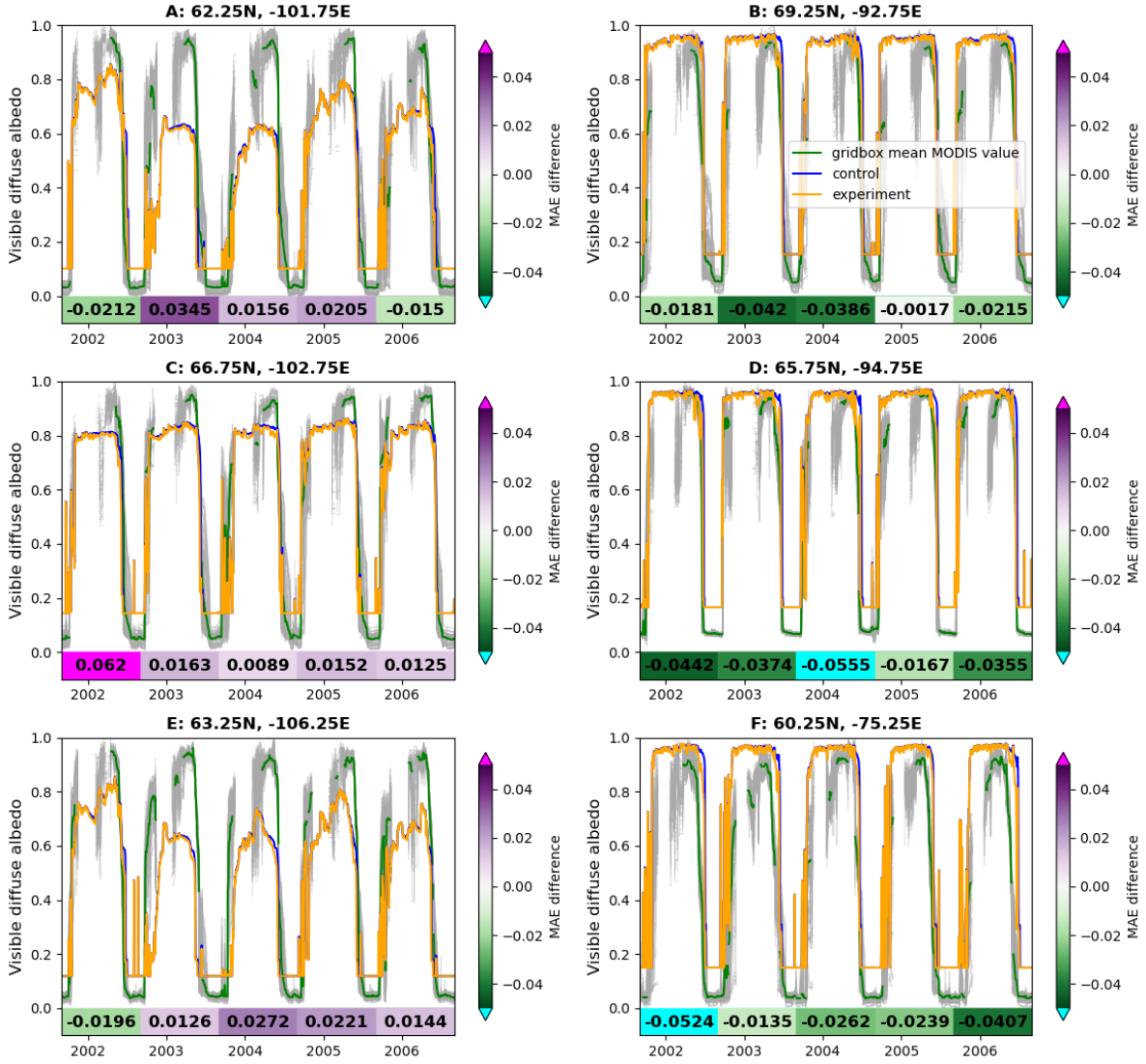

Figure 5.10: Timeseries of visible diffuse albedo from JULES simulations with (yellow) and without (blue) BC on snow for six gridboxes in North Eastern Canada. Also shown is the gridbox mean MODIS white sky albedo (green) along with the MODIS white sky albedo timeseries for each of the satellite pixels that contribute to that gridbox mean value (grey). The colour shading and numbers along the bottom of the plots indicates the MAE difference that was calculated for each of the years shown.

(see figure 5.11, compare to 5.2). Figure 5.12 looks in detail at the albedo timeseries of the control simulation for the six Canada gridboxes. As before, the dark green line shows the mean satellite albedo and the dark blue line indicates the overall gridbox albedo but the other lines indicate the albedos of the individual surface tiles present in each gridbox. As you can see, the vegetation albedos are far darker than the bare soil albedos and so drag down the overall gridbox albedo considerably. The three gridboxes that are made up of only lake and bare soil tiles (B,D,F) have albedo value close to and slightly higher than the MODIS satellite albedo values whereas the gridboxes containing vegetation (A,C,E) have albedos considerably lower than the

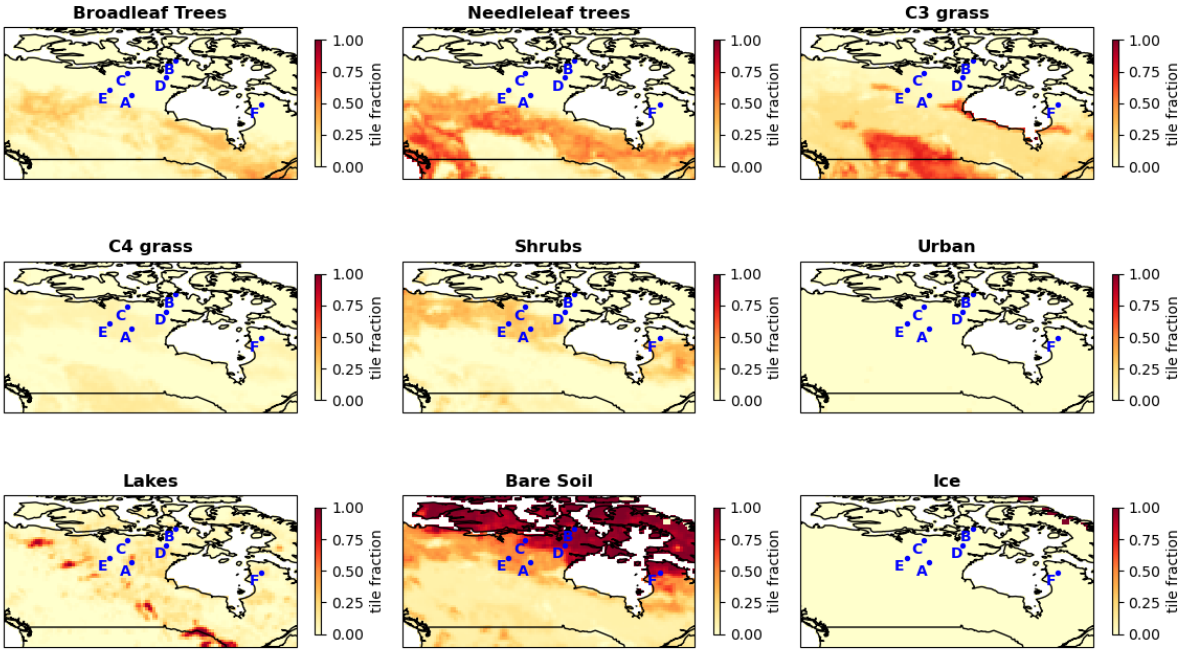

Figure 5.11: Map of surface tile fraction ancillaries used in global JULES simulations. These values remain constant throughout the simulations. Points marked in blue indicate locations of the six gridboxes which have been studied in detail in this section.

satellite albedos.

However, when we compare MAE difference maps for different years, (figure 5.3) we see that the boundary between the green and purple regions moves between years which suggests that the differences in JULES's ability to predict snow albedo cannot be solely related to vegetation tile fractions (or other ancillary fields) which remain the same from one year to the next and so must be at least in part related to the model driving data. As we have seen from equation 2.6, the albedo very much depends on snow depth and years with deeper snow do indeed have higher albedos on vegetated tiles (figure 5.14) although these albedos are still far from being high enough to bring the overall gridbox albedo in line with the satellite albedos.

It is plausible that the underestimation of albedos in some areas may be due to JULES failing to accumulate sufficient snow over the course of the winter. Smaller snow packs would also be likely to melt earlier. Underprediction of snow accumulation could be due to either bias in the precipitation driving data or problems with the representation of snow processes within JULES.

Whilst the GPCC precipitation data used to drive JULES is already bias corrected for rain gauge undercatch, the sparsity of rain gauges in remote high latitude regions may reduce its reliability in these areas. *Robinson and Clark* (2020) found that even after accounting for any under-reporting of precipitation in the driving data (of which WFDEI-GPCC has less than other com-

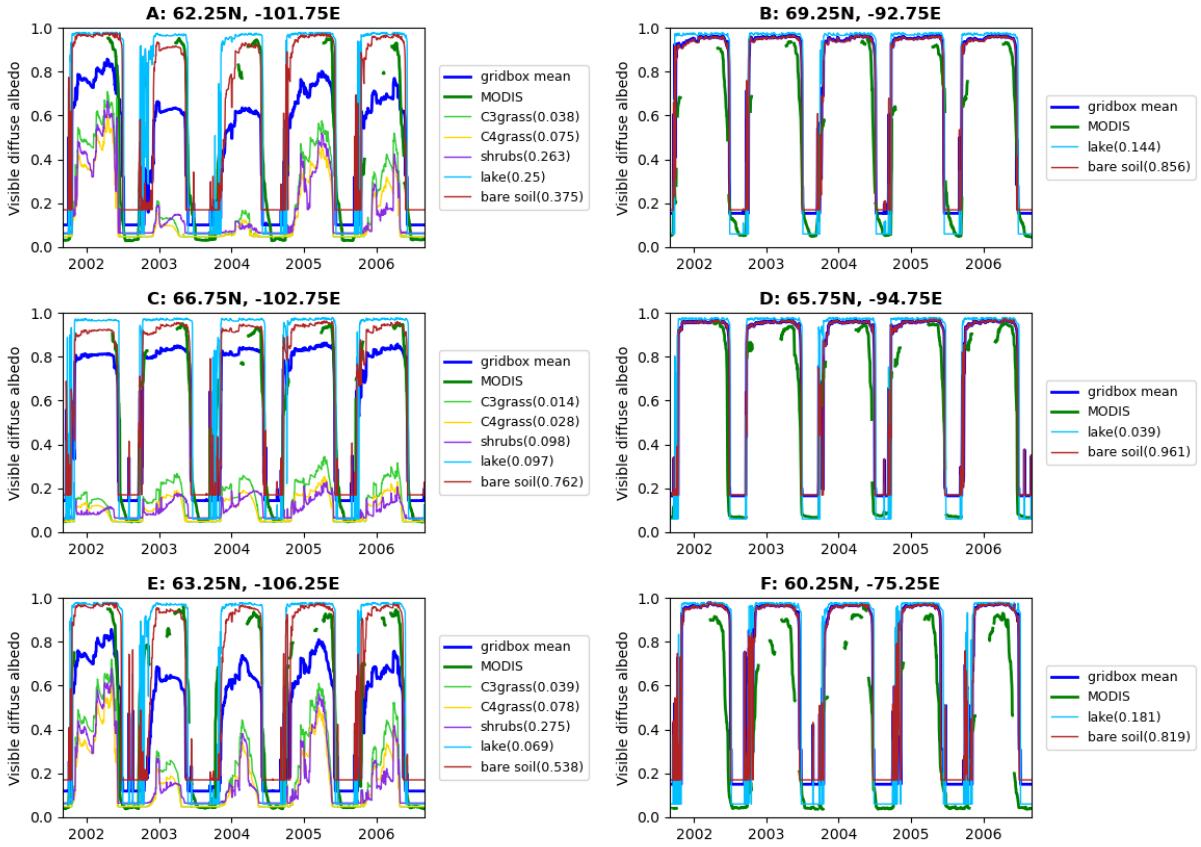

Figure 5.12: Timeseries of modelled visible diffuse albedo on surface tiles in the JULES control simulation, for six Canada gridboxes, along with overall gridbox albedo (blue line) and MODIS satellite white sky albedo (dark green line). Only surface tiles that have a non-zero tile fraction are shown for each gridbox, exact tile fractions for each surface type are shown in brackets in the legend.

monly used precipitation driving datasets), JULES tends to underpredict seasonal snow accumulation. This suggests that precipitation driving data is not exclusively to blame for low snow depths and therefore under-accumulation of snow must also partly be due to weaknesses in representation of physical snow processes within JULES.

When we examine the equation used to calculate the snow covered fraction of a surface tile in JULES (equation 2.6) we see that vegetated tiles can never be completely snow covered, this is illustrated in figure 5.13. For shrubs and grasses in this JULES configuration it transpires that the tile will only have a snow covered fraction of 0.5 when the snow depth is equal to the canopy height. This is leading to grass and shrub surfaces being far too dark in the presence of snow. This expression of snow covered fraction is taken from the Biosphere-Atmosphere Transfer Scheme (BATS) model and has previously been found to underestimate snow cover fraction compared to observations on grass surfaces (*Yang et al.*, 1997). Some researchers have suggested that different expressions of snow covered fraction are required for different

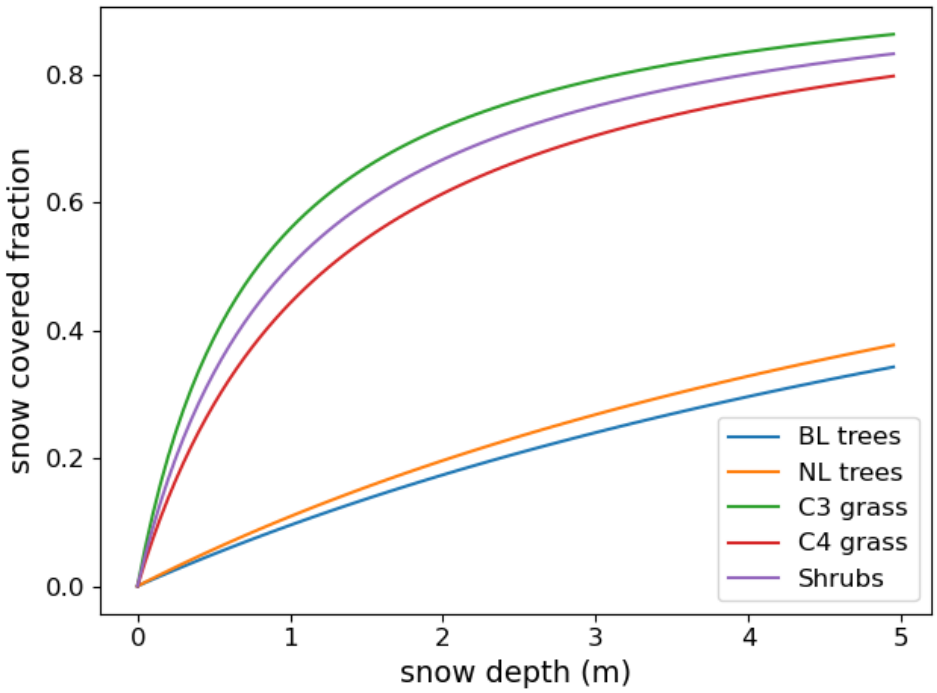

Figure 5.13: Relationship between snow covered fraction and snow depth on different vegetation tiles according to equation 2.6

vegetation types to account for the various ways they interact with snow. For instance, *Ménard* (2010) proposed an alternative expression of snow covered fraction for the shrub tile in JULES to account for the fact that shrubs, particularly at high latitudes, tend to bend under the weight of snow so can become completely covered even before the snow depth reaches the (summertime) height of the canopy.

Figure 5.14 shows the control simulation snow depth on surface tiles for the three vegetated gridboxes relative to the canopy height that has been specified for the different vegetation types. It can be seen that snow depth is often close to or beneath the canopy height at these locations. Years where the snow depth exceeds the canopy height (e.g. 2002 in gridboxes A and E) correspond with modelled albedos being closer to the satellite albedo values and thus allow for an improved MAE when BC is introduced due to the improved melt timing (compare to figure 5.10).

In the two stream embedded snow albedo scheme, instead of calculating an overall albedo as a sum of snow covered and snow free albedos weighted according to some snow covered fraction, the leaf area index of vegetation is adjusted to account for partial snow cover before the overall albedo above the canopy is calculated. The expression for this adjustment was given in equation 2.10, because the exponent n is set to 1.0 in most configurations this scheme can be said to have a snow covered fraction of $\frac{d}{h}$ (the snow depth divided by the canopy height). If the snow depth exceeds the canopy height in this scheme then the effective LAI is simply set

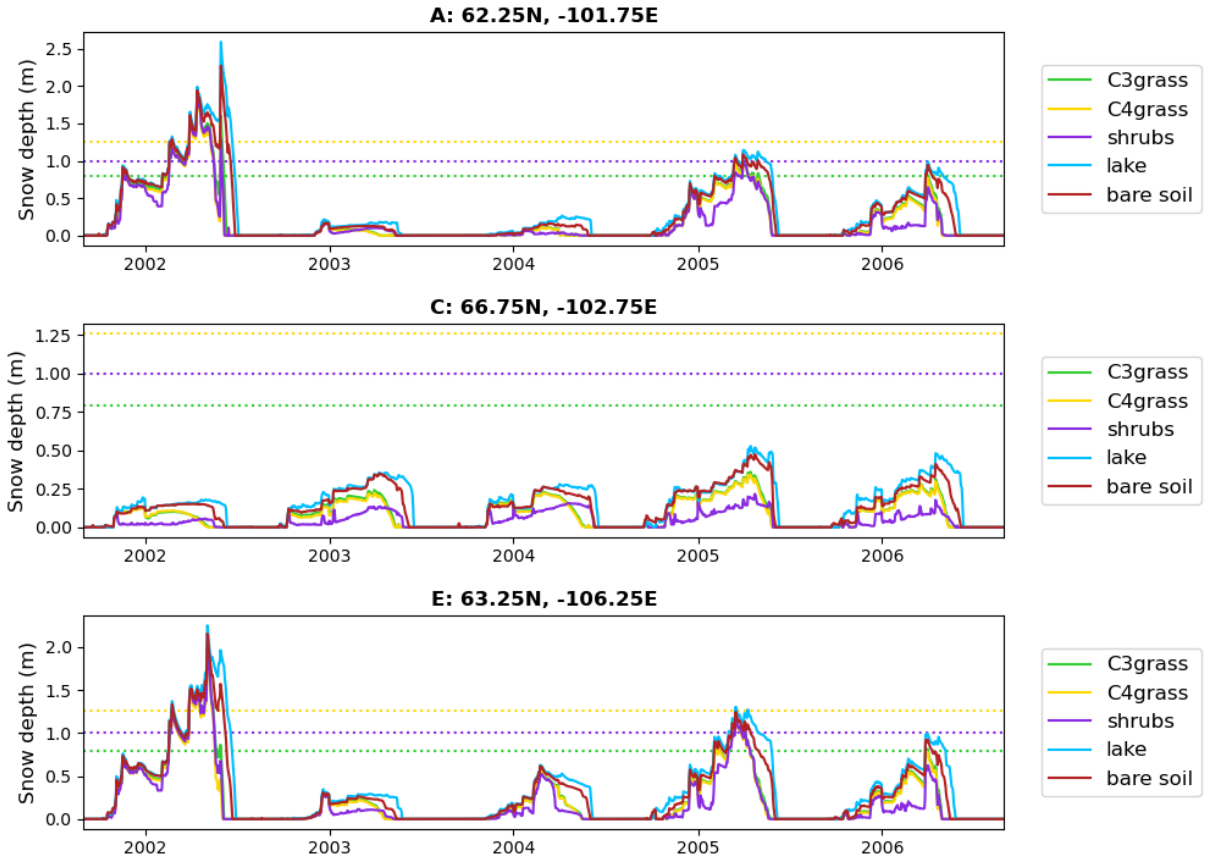

Figure 5.14: Snow depth on surface tiles in the control simulation for three vegetated gridboxes in North Eastern Canada. Dotted lines show the vegetation canopy heights of the different tiles.

to zero and the tile is considered to be completely snow covered. This formulation of the snow covered fraction is a more intuitive way of determining the impact of exposed vegetation on the albedo of snow covered tiles and is likely to perform better due to the capability for deep snow to completely cover the vegetation.

It is possible to recalculate the albedo for vegetated tiles using a different snow covered fraction by taking the minimum albedo for the gridbox to be the snow free albedo (figures 5.10 and 5.12 both show that modelled summertime albedos are constant values) and by using the albedo of the soil tile to indicate the snow covered albedo - the soil tile has a very low roughness length and so is close to completely snow covered during winter in the model and is thus predicting wintertime albedo reasonably well. Applying the snow covered fraction of $\frac{d}{h}$ then gives the albedos shown in dashed lines in figure 5.15.

This timeseries does not account for temporal feedbacks of changing the snow covered fraction as the calculations are performed on the model output rather than being built into the model. This means that impacts on snow melt timing cannot be seen. *Niu and Yang* (2007) found that the NCAR CLM model was very sensitive to changes in snow cover fraction with not just the

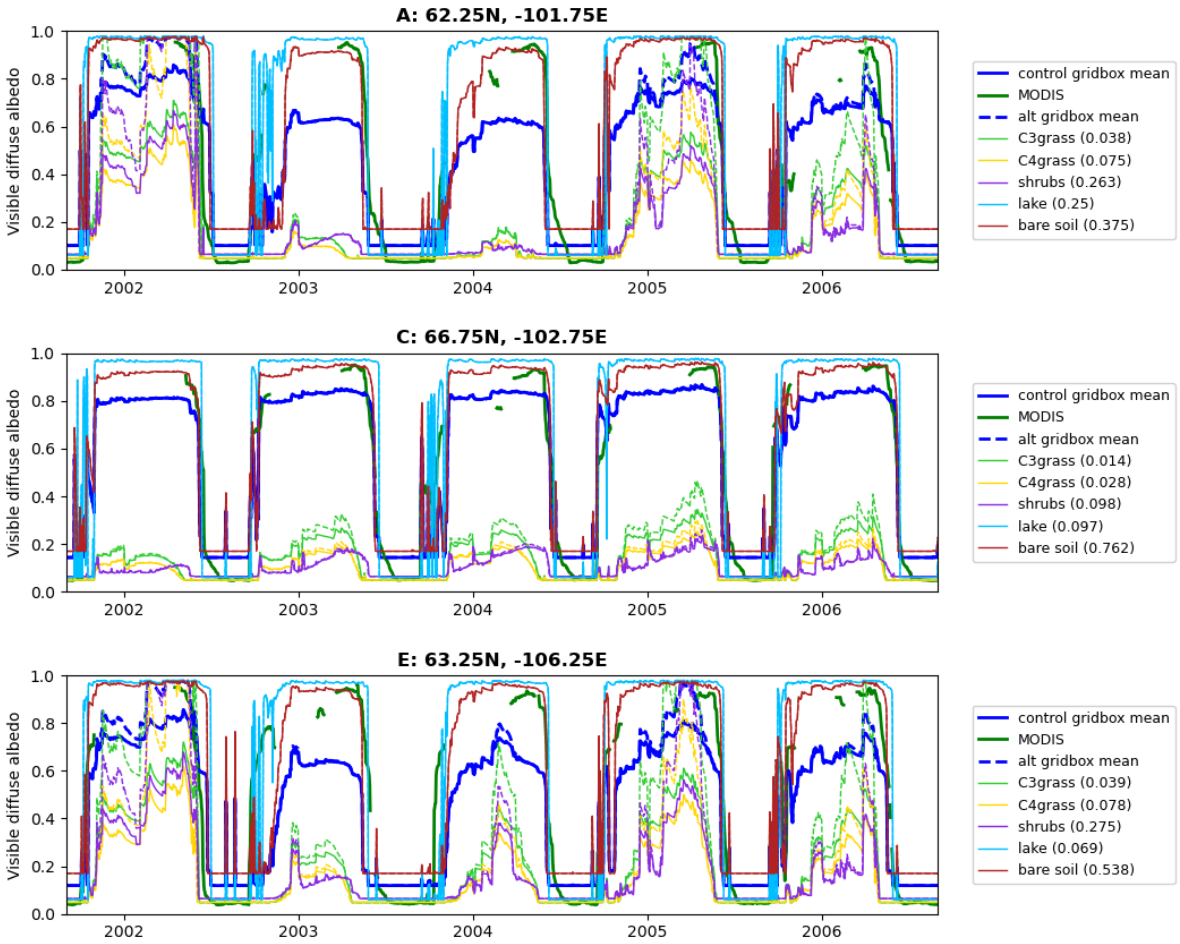

Figure 5.15: Timeseries of modelled visible diffuse albedo on surface tiles in the JULES control simulation, along with albedo adjusted to use new snow covered fraction (dashed lines) for three vegetated gridboxes. Gridbox mean albedo and MODIS satellite white sky albedo (dark green line) are also shown for comparison.

albedo being affected but also snow depth, surface temperature and net radiation. However, this offline approach should give a good indication of the impact that changing the formulation of snow covered fraction would have on peak wintertime albedo. In figure 5.15 the adjustment to snow covered fraction is seen to increase wintertime albedos although the impact is still too small in years with shallow snowpacks.

The other component affecting snow covered fraction is the canopy height (which is incorporated into the roughness length in equation 2.6). In these global JULES simulations a single value of canopy height was specified for each surface tile to apply across all gridboxes. The values given were 19.01m for broadleaf trees, 16.38m for needleleaf trees, 0.79m for C3 grasses, 1.26m for C4 grasses and 1.00m for shrubs. In reality however, vegetation height will vary from one part of the world to another and the harsh conditions of high latitude tundra locations causes plant growth to be stunted. As such the canopy heights used were not appropriate for this region

of Northern Canada. More appropriate canopy heights for this region might be 0.1m for C3 grasses, 0.2m for C4 grasses and 0.8m for shrubs [R. Essery, personal communication, 14th March 2023]. When these reduced canopy heights are used to re-calculate the adjusted snow covered fraction, the albedos produced are those shown by dashed lines in figure 5.16.

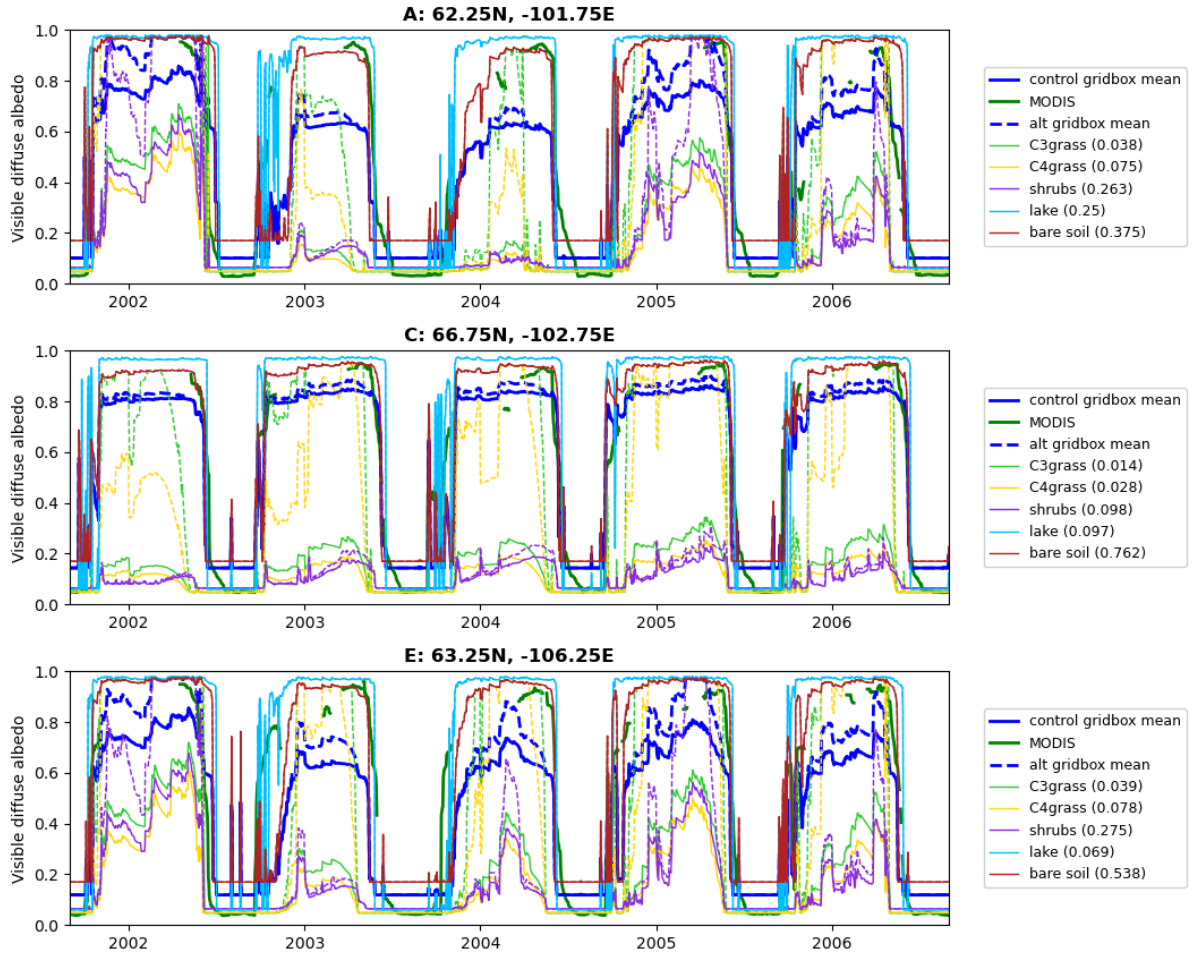

Figure 5.16: Timeseries of modelled visible diffuse albedo on surface tiles in the JULES control simulation, along with albedo adjusted to use new snow covered fraction and reduced canopy heights (dashed lines) for three vegetated gridboxes. Gridbox mean albedo and MODIS satellite white sky albedo (dark green line) are also shown for comparison.

With these adjusted canopy heights, even in years with very shallow snow, the albedo on grass tiles gets up to values close to or occasionally even slightly higher than the albedo values seen by MODIS. The shrub albedos are less affected as 0.8m high shrubs are still not completely obscured by snow. The fact that the gridbox mean albedos are still lower than the MODIS albedos in years with shallow snow suggests that it would be beneficial for the shrubs to be a little more snow covered. It could be that the 0.8m canopy height is still too high for shrubs in the region but other mechanisms may also be at play that are not represented in JULES - the shrub bending behaviour studied by *Ménard* (2010) is one possibility. Another factor could be

wind driven clumping of snow around shrubs.

5.7 Summary

The results presented in this chapter show that adding BC to snow in JULES improves albedo prediction in areas that mainly consisted of bare soil, such as the Canadian Shield region, and areas that experience very deep snowpacks, as was the case at Sapporo. It also offers considerable benefit in some gridboxes that had erroneously been modelled as being snow covered year round which are able to simulate summertime snow clearance once BC is added.

Adding BC to snow is intended to reduce snow albedo so inevitably it is only useful in areas where JULES overpredicts snow albedo to begin with. Comparison with the MODIS MCD43C satellite albedo product found that, in many regions, JULES simulations considerably underpredict wintertime albedo even prior to the addition of BC to the snowpack. Whilst the MODIS product is known to have some limitations, especially at high latitudes, the mean bias errors seen in the JULES control simulation are an order of magnitude greater than the MODIS biases reported in literature (see table 5.1). Furthermore, in situations where the MODIS product is weakest (high latitude regions and times when the backup inversion had to be used due to insufficient availability of reflectance measurements) the biases are generally found to be negative meaning that MODIS will tend to underpredict albedo in these circumstances rather than overpredict. It can therefore be concluded that in many cases JULES albedos are substantially underpredicted compared to reality.

Possible causes of this have been explored and it was found that only vegetated surface tiles were affected. Soil and lake tiles had peak wintertime albedos slightly higher than area mean MODIS values, as might be expected in a non-homogeneous gridbox. It was found that both the formulation of the snow covered fraction expression in JULES and the values selected for vegetation canopy heights contributed to the underprediction of wintertime albedo.

When JULES is used in operational UM forecasting, vegetation canopy heights are calculated separately for each gridbox based on an ancillary of LAIs derived from satellite measurements. This approach should improve snow albedo prediction compared to the standalone JULES simulations shown here but is still limited in some high latitude regions by poor satellite LAI retrievals, especially over Siberia. The approach in UM simulations still does not account for seasonal variations in canopy height so a representation of shrub (and perhaps also grass) bending under the weight of snow may still be of benefit.

It is suggested that improvements are made to JULES's representation of snow cover in vegetated areas. Once this has been achieved, it is expected that the BC on snow representation described in this thesis will prove to be of more widespread benefit.

Although the albedo product used in this chapter represents snow fairly well, the kernels used in the formulation of the BRDF were originally intended to represent vegetated surfaces rather than snow covered surfaces. Given snow is much more forward scattering than vegetated surfaces, it is thought that improvements can be made by developing a kernel specifically to represent snow covered surfaces; work is currently underway to develop such a kernal (*Jiao et al.*, 2019). As such, future versions of the MODIS MCD43 albedo products may offer improved accuracy for snow covered areas which would be of benefit for any future snow modelling validation work.

Chapter 6

Conclusions

The ability to predict the quantity and timing of seasonal snow melt allows contingency planners to prepare for severe weather events such as heavy rain, flooding, landslides and drought events, and also to manage water availability through the summer months. A gap within current seasonal snow modelling efforts is the representation of black carbon on snow. In particular, the Met Office's UM is a model that is used for a range of seasonal prediction purposes, as well as short term weather forecasting and long term climate prediction, but has not previously been capable of representing the impacts of BC on snowmelt timing because of a lack of capability to model the concentration of BC in snow within the land surface component of the UM ('JULES').

This thesis aimed to improve the representation of snow within the JULES by enabling the representation of snow darkening by black carbon. A new scheme has been presented to deposit BC onto snow and evolve its concentration in the snowpack over time so that albedo calculations can be adjusted to account for the presence of BC in the snow.

This scheme has been tested at a site in Sapporo, Japan, and its ability to simulate the concentration of BC in the surface layer of snow was investigated. It was found that there were two main elements to getting JULES to accurately simulate the near surface BC concentration. First, JULES needs to be provided with accurate BC deposition rates - an obvious enough statement but actually quite difficult for current chemistry and aerosol models to achieve. By comparing modelled deposition with observations of BC concentration in snow it was possible to establish that the CLASSIC chemistry and aerosol scheme used in this work underestimated deposition at Sapporo. Given its exceptionally long BC atmospheric residence times it is likely that the BC deposition rates predicted by CLASSIC will be inaccurate in other regions also. In order to get the correct cumulative BC deposition over the course of the snow season it was necessary to scale the CLASSIC predicted deposition values by a factor of 1.3, other locations may require different scaling factors.

The second aspect for accurately simulating BC concentration in snow was selecting the most

appropriate surface snow layer thickness. This is the depth of snow that the BC concentration is calculated over. It was found that a 1cm surface snow layer thickness gave BC concentration values that most closely matched the observations of BC near the surface of the snow at Sapporo. It is not clear how well this result would apply to other sites or the extent to which this finding depended on local snowfall, snow density and BC deposition rates. Unfortunately, it was not possible to explore the behaviour at other sites during the course of this work but it would be beneficial to do so. When running JULES with a 1cm thick top snow layer it is necessary to limit the model timestep to no more than 15 minutes in order to maintain model stability.

A remaining area of uncertainty in modelling the concentration of BC in surface snow is the meltwater scavenging efficiency. Using a value obtained from literature seems to allow for good prediction of BC concentration increases towards the end of the snow season but future refinement of this parameter as more observations become available may offer further slight improvements to snow albedo prediction.

Whilst it would be reassuring to see these results reproduced at a range of other locations, the results at Sapporo are sufficient to answer the first research question posed - **'Can a simple representation of BC evolution within the JULES snowpack simulate the real world near surface BC concentration?'**. The answer is yes, when JULES is provided with accurate BC deposition values and an appropriate selection of the top snow layer thickness parameter this relatively simple representation of BC snowpack evolution is capable of replicating the near surface concentration of BC in snow well over the course of the snow season, including the increases in surface BC concentration as the snowpack melts. There is however still some uncertainty surrounding whether the meltwater scavenging efficiency and top snow layer thickness parameters should be location dependant.

The experiments at Sapporo show that when observed BC concentration values are prescribed directly the albedo prediction towards the end of the snow season is greatly improved with the date of final snow clearance occurring only 4 days later than observed as opposed to 17 days in the standard JULES simulation. It is expected that other snow contaminants not represented here, such as dust, will also be contributing to snow darkening at this site and this will likely explain some of the remaining difference between modelled and observed date of final snow clearance. Prescribing deposition and calculating BC concentration within JULES leads to a similar improvement of modelled late season albedo and snow clearance.

Given the performance of the albedo simulations seen here, it is not thought that any further improvements to the formulation of the albedo response to BC on snow are required at this stage but it would be worthwhile to consider adding a representation of dust at some point.

Whilst including BC aids the prediction of albedo and snowmelt timing at Sapporo, this result is not replicated everywhere. Chapter 5 explored JULES's capability to predict Northern Hemisphere albedos during snow season compared to MODIS satellite data and revealed that ar-

eas with vegetated surfaces were already underpredicting snow albedo in JULES so therefore these areas do not benefit from the model developments presented here. Suggestions have been made as to other areas of the JULES snow scheme to improve in order to remove these low albedo biases and gain benefit from BC albedo adjustments: vegetation canopy heights and the formulation of the snow covered fraction are particular areas to focus on. The areas that did show improvement with the introduction of BC were mainly regions with large bare soil fractions, this included a large area of Northern Canada and the Canadian Arctic Archipelago. There was also a small number of gridboxes that experienced a dramatic improvement in the seasonality of snow cover when BC was introduced as it triggered summer time snow clearance when previously JULES had predicted year-round snow cover. So, in answer to the second research question, **'Does incorporating BC snow darkening into JULES simulations improve predictions of snow albedo and seasonal snowmelt timing?'**: not everywhere but some locations show considerable improvement and there is scope for other regions to benefit also if further improvements are made to the snow model in JULES.

The third research question, **'What are the subsequent radiative and hydrological impacts within JULES of including BC snow darkening?'**, was explored in chapter 4. It was shown that including BC in snow has wide ranging impacts within JULES including impacts on many aspects of the energy and water balance. BC causes a shift in snow melt, runoff and evaporation to earlier in the year. Whilst for most gridboxes the impacts are small, some gridboxes see snow cover duration reduced by weeks or even months. The region which saw the largest impacts was High Mountain Asia. The impacts on the energy balance reported here are generally smaller than found in other studies (such as those of *Flanner et al.* (2007); *Yasunari et al.* (2015) and *Lau et al.* (2018)) and it is thought that this is because the standalone land surface simulations reported in this thesis do not account for land-atmosphere feedback effects. It is expected that when JULES is coupled to the UM these feedback effects will amplify the impacts of BC on snow. For example, it is likely that in a coupled simulation the air temperature will increase along with springtime surface temperature increases, further exacerbating melt. A warmer atmosphere will also alter the phase of springtime precipitation and so what was prescribed as late season snowfall in these simulations may fall as rain in a coupled simulation, reducing springtime snowpack mass. Increases in springtime evapotranspiration will likely lead to increased precipitation, which may have positive or negative feedbacks on the snow albedo depending on precipitation phase and aerosol deposition conditions at the time. JULES does not currently represent the thermal impacts of rain on lying snow so extra precipitation falling as rain would not cause additional melting in JULES though it likely would in reality. It remains to be seen the extent to which these feedbacks will amplify the trends identified here but the coupled simulations referenced above typically report surface (or near surface) temperature increases an order of magnitude larger than those identified in these standalone JULES simulations when BC is introduced to snow.

6.1 Future work

As mentioned already, a weakness in this work is the lack of confidence in the BC deposition values generated by the CLASSIC aerosol scheme. Other aerosol schemes may perform better and should be considered for use in future work involving BC on snow. CLASSIC is now being superseded by the GLOMAP aerosol scheme for use in the UM so that presents an alternative option.

Any future attempts to model BC deposition for the purpose of prescribing BC deposition onto JULES snow should make sure to cover the period 2009–2013 so that additional tests of the BC on snow scheme in JULES can be performed at the site in Sodakylä, Finland, using BC concentration in snow observations reported by *Meinander et al.* (2020). This site will provide a very different environment to test JULES's response to BC on snow. During the course of this PhD it has proven difficult to acquire data from other sites where both BC concentration in snow, snow albedo and meteorological data to drive JULES have been available but it would be beneficial to test this scheme at any other sites where such data are available in order to explore how well the scavenging efficiency and top snow layer thickness values that were selected for use in this work apply in locations other than Sapporo. The snow modelling community would benefit from further efforts to observe the concentration of contaminants such as BC and dust in snow.

Chapter 4 did discuss a minority of modelled gridboxes that displayed some counter intuitive behaviour when BC is introduced to the snowpack such as increasing snow mass or a reduction in surface temperature. It has not yet been possible to identify the cause of this behaviour and it is important that further investigation is undertaken in order to ensure this behaviour is understood before this scheme is adopted more widely. A good starting point would be to examine soil and snow thermal behaviour at these gridboxes as one theory is that the unexpected reductions in surface temperature may relate to the insulating properties of the snowpack.

The configuration used in this work does not make use of the most up-to-date science options in JULES and so it would be beneficial to perform further tests of the performance of JULES's BC on snow representation using the embedded snow albedo scheme that is now being used operationally at the Met Office. Recent additions to the snow scheme of options for basal snow melting and thermal snow metamorphism should also be included in future tests. Another recent addition to JULES that would be of interest to test with BC on snow is the FLake representation of lakes. It is expected that the BC on snow scheme will perform similarly well on ice covered lakes as on bare soil but it has not been possible to gain a clear picture of the albedo performance on frozen lakes in this work due to the lake representation used not limiting snow cover on lakes to periods when the lakes are frozen.

The work in this thesis generated BC deposition in a UM simulation, processed the deposition fields offline and then fed those fields into a standalone JULES simulation. The long term aim

would be to build any necessary processing into JULES or the UM so that a fully coupled simulation could be performed that could account for land-atmosphere feedbacks. The other benefit of a fully coupled system is that it would ensure precipitation coincided with wet deposition - a feature that has not been possible to replicate in land surface simulations driven by precipitation observations or reanalyses. Based on these results, another priority for further development in the JULES snow scheme is improving snow-vegetation interactions such that snow covered fraction is more realistic in vegetated areas, particularly in high latitude locations where vegetation tends to be short and snow cover can be long-lived.

Once the issues with representing snow cover in vegetated areas have been addressed, it may be worth expanding the BC on snow scheme to include other snow darkening contaminants such as dust.

Future work to evaluate modelled snow albedos may be able to benefit from upcoming advances in the MODIS MCD43 products to improve performance in snow covered areas (*Ding et al.*, 2023; *Jiao et al.*, 2019).

6.2 Concluding remarks

The BC on snow scheme presented here is a relatively simple one. During the course of this PhD, state of the art snow-aerosol radiative schemes have progressed to include ever more detailed features such as the impact of non-spherical snow grain shapes and different BC-snow mixing structures (*He et al.*, 2018). However, it is not always the case that the most complex parametrization schemes produce the best results and the results here suggest that a simple representation can perform relatively well in predicting both the concentration of BC in snow and its impacts on albedo. Given the challenges in modelling the BC deposition to drive this BC on snow scheme, coupled with the fact that the impact of BC on snow is small in many places, these results suggest that a more complex representation is unlikely to be warranted in the short term except perhaps in regional modelling of more strongly affected areas such as High Mountain Asia. Efforts to further improve snow representation in JULES would be better spent improving BC deposition modelling, expanding this scheme to incorporate dust and improving the representation of snow cover in vegetated areas.

Data Availability

Model code used for the simulations in this thesis are available to researchers wishing to reproduce the results. Registration on the Met Office Science Reopository Service (MOSRS) is required. The workflow used to run each simulation was defined using a 'rose suite' that can also be found on MOSRS. The driving data used to force all the JULES simulations and the MODIS albedo data that was used to validate the JULES global simulations were taken from publicly available datasets. The locations of all of these resources are listed in table 6.1.

The data used for validating single site simulations at Sapporo was kindly supplied by Teruo Aoki and Masashi Niwano.

Table 6.1: Locations of data data and code used for the simulations in this thesis.

Simulation	**Locations of associated data**
UM CLASSIC simulation to generate black carbon deposition fields.	**Code:** UM10.3, `https://code.metoffice.gov.uk/trac/um/browser/main/trunk?rev=13189`, plus the following edits: `https://code.metoffice.gov.uk/trac/um/browser/main/branches/pkg/Config/vn10.3.1_GlobalAtmos7p0?rev=16352`, `https://code.metoffice.gov.uk/trac/um/browser/main/branches/dev/benjohnson/vn10.3_aer_rad_diag?rev=17408`, `https://code.metoffice.gov.uk/trac/um/browser/main/branches/dev/benjohnson/vn10.3_UKCA_RADAER_LUT_upgrade?rev=17527`, `https://code.metoffice.gov.uk/trac/um/browser/main/branches/dev/benjohnson/vn10.3_ignore_calendar?rev=25984` **Workflow:** u-af101, `https://code.metoffice.gov.uk/trac/roses-u/browser/a/f/1/0/1` **Emissions inventory ancillary data:** MACC/CityZEN (*Granier et al.*, 2011), downloadable from `https://eccad.sedoo.fr/` or `ftp://ftp-ipcc.fz-juelich.de/pub/emissions/`.

Simulation of snow at Sapporo with prescribed BC concentration.	**Code:** `https://code.metoffice.gov.uk/trac/jules/log/main/branches/dev/helenjohnson/r12869_snowBC_PrescNrSurfConc_1minTS` **Workflow:** u-bc541, `https://code.metoffice.gov.uk/trac/roses-u/browser/b/c/5/4/1` **Driving data:** collated by *Menard et al.* (2019) for ESM-SnowMIP, doi:10.1594/PANGAEA.897575 **Validation data:** Kindly supplied by Teruo Aoki and Masashi Niwano.
All other simulations at Sapporo. (Settings for the different experiments are defined in the optional configuration files of the rose suite.)	**Code:** `https://code.metoffice.gov.uk/trac/jules/log/main/branches/dev/helenjohnson/vn5.2_snowBC_take3` **Workflow:** u-ba775, `https://code.metoffice.gov.uk/trac/roses-u/browser/b/a/7/7/5` **Driving Data:** collated by *Menard et al.* (2019) for ESM-SnowMIP, doi:10.1594/PANGAEA.897575 **Validation data:** Kindly supplied by Teruo Aoki and Masashi Niwano.
Global JULES simulations in chapters 4 and 5.	**Code:** `https://code.metoffice.gov.uk/trac/jules/log/main/branches/dev/helenjohnson/vn7.0_snowBC` **Workflow for running spinup:** u-cz133, `https://code.metoffice.gov.uk/trac/roses-u/browser/c/z/1/3/3` **Workflow for control simulation:** u-db118, `https://code.metoffice.gov.uk/trac/roses-u/browser/d/b/1/1/8` **Workflow for simulation with BC applied:** u-db126, `https://code.metoffice.gov.uk/trac/roses-u/browser/d/b/1/2/6` **Driving data:** WFDEI (*Weedon et al.*, 2011), downloadable from `ftp://rfdata:forceDATA@ftp.iiasa.ac.at`. **Validation data:** MODIS MCD43C3, downloadable from `https://e4ftl01.cr.usgs.gov/MOTA/MCD43C3.061/` or via the interactive NASA Earthdata search tool at `https://search.earthdata.nasa.gov/search`.

Bibliography

Adam, J. C., E. A. Clark, D. P. Lettenmaier, and E. F. Wood, Correction of global precipitation products for orographic effects, *J. Clim.*, *19*, 15–38, doi:10.1175/JCLI3604.1, 2006.

Aoki, T., T. Aoki, M. Fukabori, A. Hachikubo, Y. Tachibana, and F. Nishio, Effects of snow physical parameters on spectral albedo and bidirectional reflectance of snow surface, *J. Geophys. Res.: Atmos.*, *105*(D8), 10,219–10,236, doi:10.1029/1999JD901122, 2000.

Aoki, T., K. Kuchiki, M. Niwano, Y. Kodama, M. Hosaka, and T. Tanaka, Physically based snow albedo model for calculating broadband albedos and the solar heating profile in snowpack for general circulation models, *J. Geophys. Res.: Atmos.*, *116*(D11), doi:10.1029/2010JD015507, 2011.

Bair, E., T. Stillinger, and J. Dozier, Snow Property Inversion From Remote Sensing (SPIReS): A generalized multispectral unmixing approach with examples from MODIS and Landsat 8 OLI, *IEEE Trans. Geosci. Remote Sens.*, *59*, doi:10.1109/TGRS.2020.3040328, 2021.

Baker, D., R. Skaggs, and D. Ruschy, Snow depth required to mask the underlying surface, *J. Appl. Meteorol. Climatol.*, *30*(3), 387–392, doi:10.1175/1520-0450(1991)030⟨0387:SDRTMT⟩2.0.CO;2, 1991.

Bartles, M., Where farmers' almanacs' weather predictions come from, *Sci. Am.*, 2023.

Bates, P., Inuit and scientific philosophies about planning, prediction, and uncertainty, *Arctic Anthropology*, *44*(2), 87–100, 2007.

Bellouin, N., J. Rae, A. Jones, C. Johnson, J. Haywood, and O. Boucher, Aerosol forcing in the climate model intercomparison project (CMIP5) simulations by HadGEM2-ES and the role of ammonium nitrate, *J. Geophys. Res.: Atmos.*, *116*, doi:10.1029/2011JD016074, 2011.

Best, M. J., et al., The Joint UK Land Environment Simulator (JULES), model description âĂŞ part 1: Energy and water fluxes, *Geosci. Model Dev.*, *4*(3), 677–699, doi:10.5194/gmd-4-677-2011, 2011.

Blanford, H. F., On the connexion of the himalaya snowfall with dry winds and seasons of drought in india, *Proc. R. Soc. London*, *37*, doi:10.1098/rspl.1884.0003, 1884.

Bond, T. C., and R. W. Bergstrom, Light absorption by carbonaceous particles: An investigative review, *Aerosol Sci. Technol.*, *40*, 27–67, doi:10.1080/02786820500421521, 2006.

Bond, T. C., et al., Bounding the role of black carbon in the climate system: A scientific assessment, *J. Geophys. Res.: Atmos.*, *118*(11), 5380–5552, doi:10.1002/jgrd.50171, 2013.

Bowling, L. C., et al., Simulation of high-latitude hydrological processes in the torneâĂŞkalix basin: Pilps phase 2(e): 1: Experiment description and summary intercomparisons, *Glob. Planet. Change*, *38*, 1–30, doi:10.1016/S0921-8181(03)00003-1, 2003.

Brun, E., Investigation on wet-snow metamorphism in respect of liquid-water content, *Ann. Glaciol.*, *13*, 22–26, doi:10.3189/S0260305500007576, 1989.

Brun, E., E. Martin, V. Simon, C. Gendre, and C. Coleou, An energy and mass model of snow cover suitable for operational avalance forecasting, *J. Glaciol.*, *35*(121), 333–342, doi:10.3189/S0022143000009254, 1989.

Cabanes, A., L. Legagneux, and F. Dominé, Rate of evolution of the specific surface area of surface snowlayers, *Environ. Sci. Technol.*, *37*, 661–666, doi:10.1021/es025880r, 2003.

Campbell, D. R., Early snowmelt projected to cause population declinein a subalpine plant, *PNAS*, *116*(26), 12,901–12,906, doi:10.1073/pnas.1820096116, 2019.

Chen, Y., X. Li, Y. Xing, S. Yan, D. Wu, T. Shi, J. Cui, X. Zhang, and X. Niu, Historical changes of black carbon in snow and its radiative forcing in CMIP6 models, *Atmosphere*, *13*(11), doi:10.3390/atmos13111774, 2022.

Chow, J., J. Watson, D. Crow, D. Lowenthal, and T. Merrifield, Comparison of IMPROVE and NIOSH carbon measurements, *Aerosol Sci. Technol.*, *34*, 23–34, doi:10.1080/02786820119073, 2001.

Clark, D. B., et al., The Joint UK Land Environment Simulator (JULES), model description âĂŞ part 2: Carbon fluxes and vegetation dynamics, *Geosci. Model Dev.*, *4*(3), 701–722, doi:10.5194/gmd-4-701-2011, 2011.

Conway, H., A. Gades, and C. F. Raymond, Albedo of dirty snow during conditions of melt, *Water Resour. Res.*, *32*(6), 1713–1718, doi:10.1029/96WR00712, 1996.

Ding, A., Z. Jiao, X. Zhang, Y. Dong, A. A. Kokhanovsky, J. Guo, and H. Jiang, A practical approach to improve the modis mcd43a products in snow-covered areas, *J. Remote Sens.*, *3*, doi:10.34133/remotesensing.0057, 2023.

Doherty, S. J., T. C. Grenfell, S. Forsström, D. L. Hegg, R. E. Brandt, and S. G. Warren, Observed vertical redistribution of black carbon and other insoluble light-absorbing particles in melting snow, *J. Geophys. Res.: Atmos.*, *118*(11), 5553–5569, doi:10.1002/jgrd.50235, 2013.

Doherty, S. J., C. Dang, D. A. Hegg, R. Zhang, and S. G. Warren, Black carbon and other light-absorbing particles in snow of central north america, *J. Geophys. Res.: Atmos.*, *119*(22), 12,807–12,831, doi:10.1002/2014JD022350, 2014.

Edwards, J., Towards implementation of the multilayer snow scheme in gl7.0 (draft 2.0), [unpublished documentation], 2014.

Edwards, J. M., J. Manners, J.-C. Thelen, W. J. Ingram, and P. G. Hill, *Unified Model Documentation Paper 023 The Radiation Code*, 2018.

Emerson, E. W., J. M. Katich, J. P. Schwarz, G. R. McMeeking, and D. K. Farmer, Direct measurements of dry and wet deposition of black carbon over a grassland, *J. Geophys. Res.: Atmos.*, *123*(21), 12,277–12,290, doi:10.1029/2018JD028954, 2018.

Essery, R., S. Morin, Y. Lejune, and C. B. Ménard, A comparison of 1701 snow models using observations from an alpine site, *Adv. Water Resour.*, *55*, 131–148, doi:10.1016/j.advwatres.2012.07.013, 2013.

Etchevers, P., et al., Validation of the energy budget of an alpine snowpack simulated by several snow models (snowmip project), *Ann. Glaciol.*, *38*, 150–158, doi:10.3189/172756404781814825, 2004.

Flanner, M. G., C. S. Zender, J. T. Randerson, and P. J. Rasch, Present-day climate forcing and response from black carbon in snow, *J. Geophys. Res.: Atmos.*, *112*(D11), doi:10.1029/2006JD008003, 2007.

Flanner, M. G., C. S. Zender, P. G. Hess, N. M. Mahowald, T. H. Painter, V. Ramanathan, and P. J. Rasch, Springtime warming and reduced snow cover from carbonaceous particles, *Atmos. Chem. Phys.*, *9*(7), 2481–2497, doi:10.5194/acp-9-2481-2009, 2009.

Flanner, M. G., X. Liu, C. Zhou, J. E. Penner, and C. Jiao, Enhanced solar energy absorption by internally-mixed black carbon in snow grains, *Atmos. Chem. Phys.*, *12*(10), 4699–4721, doi:10.5194/acp-12-4699-2012, 2012.

Flanner, M. G., et al., SNICAR-ADv3: a community tool for modeling spectral snow albedo, *Geosci. Model Dev.*, *14*(12), 7673–7704, doi:10.5194/gmd-14-7673-2021, 2021.

Forsström, S., et al., Elemental carbon measurements in European Arctic snow packs, *J. Geophys. Res.: Atmos.*, *118*, 13,614–13,627, doi:10.1002/2013JD019886, 2013.

Francon, L., et al., Assessing the effects of earlier snow melt-out on alpine shrub growth: The sooner the better?, *Ecological Indicators*, *115*, doi:10.1016/j.ecolind.2020.106455, 2020.

Ganey, G. O., M. G. Loso, A. B. Burgess, and R. J. Dial, The role of microbes in snowmelt and radiative forcing on an Alaskan icefield, *Nat. Geosci.*, *10*, 754–759, doi:10.1038/NGEO3027, 2017.

Gao, F., C. B. Schaaf, A. H. Strahler, A. Roesch, W. Luchadht, and R. Dickinson, MODIS bidirectional reflectance distribution function and albedo climate modeling grid products and the variability of albedo for major global vegetation types, *J. Geophys. Res.: Atmos.*, *110*, doi:10.1029/2004JD005190, 2005.

Gleason, K. E., J. R. McConnell, M. M. Arienzo, G. A. Sexstone, and S. Rahimi, Black carbon dominated dust in recent radiative forcing on Rocky Mountain snowpacks, *Env. Res. Lett.*, *17*(5), doi:10.1088/1748-9326/ac681b, 2022.

Granier, C., et al., Evolution of anthropogenic and biomass burning emissions of air pollutants at global and regional scales during the 1980–2010 period, *Climatic Change*, *109*(1), 163–190, doi:10.1007/s10584-011-0154-1, 2011.

Günther, D., T. Marke, R. Essery, and U. Strasser, Uncertainties in snowpack simulations–assessing the impact of model structure, parameter choice, and forcing data error on point-scale energy balance snow model performance, *Water Resour. Res.*, *55*, 2779–2880, doi:10.1029/2018WR023403, 2019.

Hallett, J., and B. J. Mason, The influence of temperature and supersaturation on the habit of ice crystals grown from the vapour, *Proc. R. Soc. London*, *247*, 440–453, doi:10.1002/2016JD025362, 1958.

Hancock, S., R. Baxter, J. Evans, and B. Huntley, Evaluating global snow water equivalent products for testing land surface models, *Remote Sens. Env.*, *128*, 107–117, doi:10.1016/j.rse.2012.10.004, 2013.

Hansen, J., and L. Nazarenko, Soot climate forcing via snow and ice albedos, *PNAS*, *101*, 423–428, doi:10.1073/pnas.2237157100, 2004.

Hao, D., et al., Improving snow albedo modeling in the E3SM land model (version 2.0) and assessing its impacts on snow and surface fluxes over the Tibetan Plateau, *Geosci. Model Dev.*, *16*(1), 75–94, doi:10.5194/gmd-16-75-2023, 2023.

Harder, S., S. Warren, R. Charlson, and D. Covert, Filtering of air through snow as a mechanism for aerosol deposition to the Antarctic ice sheet, *J. Geophys. Res.: Atmos.*, *101*, 18,533–18,881, doi:10.1029/96JD01174, 1996.

He, C., K.-N. Liou, Y. Takano, P. Yang, L. Qi, and F. Chen, Impact of grain shape and multiple black carbon internal mixing on snow albedo: Parameterization and radiative effect analysis, *J. Geophys. Res.: Atmos.*, *123*(2), 1253–1268, doi:10.1002/2017JD027752, 2018.

Jacobson, M. Z., Climate response of fossil fuel and biofuel soot, accounting for soot's feedback to snow and sea ice albedo and emissivity, *J. Geophys. Res.: Atmos.*, *109*, doi:10.1029/2004JD004945, 2004.

Jiao, C., et al., An AeroCom assessment of black carbon in arctic snow and sea ice, *Atmos. Chem. Phys.*, *14*(5), 2399–2417, doi:10.5194/acp-14-2399-2014, 2014.

Jiao, Z., et al., Development of a snow kernel to better model the anisotropic reflectance of pure snow in a kernel-driven BRDF model framework, *Remote Sens. Env.*, *221*, 198–209, doi:10.1016/j.rse.2018.11.001, 2019.

Jin, Y., C. B. Schaaf, F. Gao, X. Li, and A. H. Strahler, Consistency of MODIS surface bidirectional reflectance distribution function and albedo retrievals: 1. algorithm performance, *J. Geophys. Res.: Atmos.*, *108*(D5), doi:10.1029/2002JD002803, 2003a.

Jin, Y., C. B. Schaaf, C. E. Woodcock, F. Gao, X. Li, A. H. Strahler, W. Lucht, and S. Liang, Consistency of MODIS surface bidirectional reflectance distribution function and albedo retrievals: 2. validation, *J. Geophys. Res.: Atmos.*, *108*(D5), doi:10.1029/2002JD002804, 2003b.

Johannessen, M., T. Dale, E. T. Gjessing, A. Henriksen, and R. F. Wright, Acid precipitation in norway: the regional distribution of contaminants in snow and the chemical concentration processes during snowmelt, *Proc. Int. Assoc. Hydrol. Sci.*, (118), 116–120, 1977.

Kang, S., Y. Zhang, Y. Qian, and H. Wang, A review of black carbon in snow and ice and its impact on the cryosphere, *Earth-Sci. Rev.*, *210*, doi:10.1016/j.earscirev.2020.103346, 2020.

Keegan, K. M., M. R. Albert, J. R. McConnell, and I. Baker, Climate change and forest fires synergistically drive widespread melt events of the Greenland Ice Sheet, *PNAS*, *111*, 7964–7967, doi:10.1073/pnas.1405397111, 2014.

Krinner, G., et al., ESM-SnowMIP: assessing snow models and quantifying snow-related climate feedbacks, *Geosci. Model Dev.*, *11*, 5027–5049, doi:10.5194/gmd-11-5027-2018, 2018.

Kuchiki, K., T. Aoki, M. Niwano, S. Matoba, Y. Kodama, and K. Adachi, Elemental carbon, organic carbon, and dust concentrations in snow measured with thermal optical and gravimetric methods: Variations during the 2007-2013 winters at Sapporo, Japan, *J. Geophys. Res.: Atmos.*, *120*, 868–882, doi:10.1002/2014JD022144, 2015.

Lamarque, J.-F., et al., Historical (1850–2000) gridded anthropogenic and biomass burning emissions of reactive gases and aerosols: methodology and application, *Atmos. Chem. Phys.*, *10*(15), 7017–7039, doi:10.5194/acp-10-7017-2010, 2010.

Lau, W. K. M., M. K. K. Sang, R. D. Koster, and Y. T. J., Impacts of snow darkening by deposition of light-absorbing aerosols on hydroclimate of eurasia during boreal spring and summer, *J. Geophys. Res.: Atmos.*, *123*, 8441–8461, doi:10.1029/2018JD028557, 2018.

Lawrence-Mathers, A., Medieval origins of modern weather forecasting, *Weather*, *76*(5), 144–147, doi:10.1002/wea.3917, 2021.

Lazarcik, J., J. E. Dibb, A. C. Adolph, J. M. Amante, C. P. Wake, E. Scheuer, and M. R. Mineau, M. M. andAlbert, Major fraction of black carbon is flushed from the melting New Hampshire snowpack nearly as quickly as soluble impurities, *J. Geophys. Res.: Atmos.*, *122*(1), 537–553, doi:10.1002/2016JD025351, 2017.

Li, X., and A. H. Strahler, Geometric-optical bidirectional reflectance modeling of a conifer forest canopy, *IEEE Trans. Geosci. Remote Sens.*, *GE-24*(6), 906–919, doi:10.1109/TGRS.1986.289706, 1986.

Liang, S., A. H. Strahler, and C. Walthall, Retrieval of land surface albedo from satellite observations: A simulation study, *J. Appl. Meteorol. Clim.*, *38*, 712–725, doi:10.1175/1520-0450(1999)038⟨0712:ROLSAF⟩2.0.CO;2, 1999.

List, R. J., *Smithsonian Meteorological tables, sixth revised edition*, Smithsonian Institution Press, Washington D.C., reprinted in 1966, 1949.

Liu, A. Q., et al., The June 2013 Alberta catastrophic flooding event: Part1–climatological aspects and hydrometeorological features, *Hydrol. Processes*, *30*, doi:10.1002/hyp.10906, 2016.

Lucht, W., C. B. Schaaf, and A. H. Strahler, An algorithm for the retrieval of albedo from space using semiempirical BRDF models, *IEEE Trans. Geosci. Remote Sens.*, *38*(2), 977–998, doi:10.1109/36.841980, 2000.

Lund, M. T., B. H. Samset, R. B. Skeie, D. Watson-Parris, J. M. Katich, J. P. Schwarz, and B. Weinzierl, Short black carbon lifetime inferred from a global set of aircraft observations, *npj Clim. Atmos. Sci.*, *1*(31), doi:10.1038/s41612-018-0040-x, 2018.

Magono, C., T. Endoh, F. Ueno, S. Kubota, and M. Itasaka, Direct observations of aerosols attached to falling snow crystals, *Tellus*, *31*, 102–114, doi:10.1111/j.2153-3490.1979.tb00887.x, 1979.

Marshall, S. E., A physical parameterization of snow albedo for use in climate models, Ph.D. thesis, University of Colorado, 1989.

Meinander, O., A. Kontu, R. Kouznetsov, and M. Sofiev, Snow samples combined with long-range transport modeling to reveal the origin and temporal variability of black carbon in seasonal snow in Sodankylä (67°N), *Front. Earth Sci.*, *8*, doi:10.3389/feart.2020.00153, 2020.

Meinander, O., et al., Spectral albedo of seasonal snow during intensive melt period at Sodankylä, beyond the Arctic Circle, *Atmos. Chem. Phys.*, *13*, 3793–3810, doi:10.5194/acp-13-3793-2013, 2013.

Menard, C., et al., ESM-SnowMIP meteorological and evaluation datasets at ten reference sites (in situ and bias corrected reanalysis data), doi:10.1594/PANGAEA.897575, 2019.

Ménard, C. B., Modelling the effects of shrub-tundra on snow and runoff, Ph.D. thesis, University of Edinburgh, 2010.

Montanari, A., H. Nguyen, S. Rubinetti, S. Ceola, A. Rubino, and D. Zanchettin, Why the 2022 Po River drought is the worst in the past two centuries, *Sci. Adv.*, *9*, doi:10.1126/sciadv.adg8304, 2023.

Namazi, M., K. von Salzen, and J. N. S. Cole, Simulation of black carbon in snow and its climate impact in the Canadian Global Climate Model, *Atmos. Chem. Phys.*, *15*(18), 10,887–10,904, doi:10.5194/acp-15-10887-2015, 2015.

Niu, G., and Z.-L. Yang, An observation-based formulation of snow cover fraction and its evaluation over large North American river basins, *J. Geophys. Res.: Atmos.*, *112*(D21101), doi:10.1029/2007JD008674, 2007.

Niwano, M., T. Aoki, K. Kuchiki, M. Hosaka, and Y. Kodama, Snow metamorphism and albedo process (SMAP) model for climate studies: Model validation using meteorological and snow impurity data measured at Sapporo, Japan, *J. Geophys. Res.: Earth Surf*, *117*(F3), doi:10.1029/2011JF002239, 2012.

Niwano, M., T. Aoki, K. Kuchiki, M. Hosaka, Y. Kodama, S. Yamaguchi, H. Motoyoshi, and Y. Iwata, Evaluation of updated physical snowpack model SMAP, *Bull. Glaciol. Res.*, *32*, 65–78, doi:10.5331/bgr.32.65, 2014.

Niwano, M., et al., NHM–SMAP: spatially and temporally high-resolution nonhydrostatic atmospheric model coupled with detailed snow process model for Greenland Ice Sheet, *The Cryosphere*, *12*(2), 635–655, doi:10.5194/tc-12-635-2018, 2018.

Oaida, C. M., Y. Xue, M. G. Flanner, S. M. Skiles, F. De Sales, and T. H. Painter, Improving snow albedo processes in WRF/SSiB regional climate model to assess impact of dust and black carbon in snow on surface energy balance and hydrology over western u.s., *J. Geophys. Res.: Atmos.*, *120*(8), 3228–3248, doi:10.1002/2014JD022444, 2015.

O'Brien, H. W., and R. H. Munis, Red and near-infrared spectral reflectance of snow, *Tech. rep.*, Corps of Engineers, U.S. Army, Cold regions research and engineering laboratory, Hanover, New Hampshire, 1975.

of Engineers, U. S. A. C., Snow hydrology, *Tech. rep.*, North Pacific Division, Corps of Engineers, U.S. Army, 1956.

Oki, T., and Y. C. Sud, Design of total runoff integrating pathways (TRIP)–a global river channel network, *Earth Interact.*, *2*, 1–37, doi:10.1175/1087-3562(1998)002⟨0001:DOTRIP⟩2.3.CO;2, 1998.

Painter, T. H., A. C. Bryant, and S. M. Skiles, Radiative forcing by light absorbing impurities in snow from MODIS surface reflectance data, *Geophys. Res. Lett.*, *39*(17), doi:10.1029/2012GL052457, 2012.

Pedersen, C., J.-C. Gallet, J. Ström, S. Gerland, S. Hudson, S. Forsström, E. Isaksson, and T. Berntsen, In situ observations of black carbon in snow and the corresponding spectral surface albedo reduction, *J. Geophys. Res.: Atmos.*, *120*, 1476–1489, doi:10.1002/2014JD022407, 2015.

Peng, J., et al., Markedly enhanced absorption and direct radiative forcing of black carbon under polluted urban environments, *PNAS*, *113*(16), 4266–4271, doi:10.1073/pnas.1602310113, 2016.

Potter, C., Snowmelt timing impacts on growing season phenology in the northern range of Yellowstone National Park estimated from MODIS satellite data, *Landscape Ecol.*, *35*, 373–388, doi:10.1007/s10980-019-00951-3, 2020.

Privette, J. L., T. F. Eck, and D. W. Deering, Estimating spectral albedo and nadir reflectance through inversion of simple BRDF models with AVHRR/MODIS-like data, *J. Geophys. Res.: Atmos.*, *102*, 29,529–29,542, doi:10.1029/97JD01215, 1997.

Qian, Y., M. G. Flanner, L. R. Leung, and W. Wang, Sensitivity studies on the impacts of Tibetan Plateau snowpack pollution on the Asian hydrological cycle and monsoon climate, *Atmos. Chem. Phys.*, *11*(5), 1929–1948, doi:10.5194/acp-11-1929-2011, 2011.

Qian, Y., et al., Light-absorbing particles in snow and ice: Measurement and modeling of climatic and hydrological impact, *Adv. Atmos. Sci.*, *32*, 64–91, doi:10.1007/s00376-014-0010-0, 2015.

Reay, H. J., J. L. France, and M. D. King, Decreased albedo,e-folding depth and photolytic OH radical and NO_2 production with increasing black carbon content in arctic snow, *J. Geophys. Res.*, *117*(D00R20), doi:10.1029/2011JD016630, 2012.

Robinson, E. L., and D. B. Clark, Using gravity recovery and climate experiment data to derive corrections to precipitation data sets and improve modelled snow mass at high latitudes, *Hydrol. Earth Syst. Sci.*, *24*, 1763–1779, doi:10.5194/hess-24-1763-2020, 2020.

Rooney, G. G., and I. D. Jones, Coupling the 1-D lake model FLake to the community land-surface model JULES, *Boreal Env. Res.*, *15*(5), 501–512, 2010.

Ross, J., *The radiation regime and architecture of plant stands*, Dr. W. Junk, The Hague, Netherlands, 1981.

Roujean, J.-L., M. Leroy, and P.-Y. Deschamps, A bidirectional reflectance model of the earth's surface for the correction of remote sensing data, *J. Geophys. Res.: Atmos.*, *97*, 20,455–20,468, doi:10.1029/92JD01411, 1992.

Rutter, N., et al., Evaluation of forest snow processes models (SnowMIP2), *J. Geophys. Res.: Atmos.*, *114*, doi:10.1029/2008JD011063, 2009.

Samset, B. H., et al., Modelled black carbon radiative forcing and atmospheric lifetime in aerocom phase ii constrained by aircraft observations, *Atmos. Chem. Phys.*, *14*, doi:10.5194/acp-14-12465-2014, 2014.

Sang, J., M.-K. Kim, W. K. M. Lau, and K.-M. Kim, Possible impacts of snow darkening effects on the hydrological cycle over Western Eurasia and East Asia, *Atmosphere*, *10*(9), doi:10.3390/atmos10090500, 2019.

Sarangi, C., Y. Qian, K. Ritter, K. J. Bormann, Y. Liu, H. Wang, H. Wan, G. Lin, and T. H. Painter, Impact of light-absorbing particles on snow albedo darkening and associated radiative forcing over high-mountain Asia: high-resolution WRF-Chem modeling and new satellite observations, *Atmos. Chem. Phys.*, *19*(10), 7105 – 7128, doi:10.5194/acp-19-7105-2019, 2019.

Savoie, M. H., R. L. Armstrong, M. J. Brodzik, and J. R. Wang, Atmospheric corrections for improved satellite passive microwave snow cover retrievals over the Tibet Plateau, *Remote Sens. Env.*, *113*(12), 2661 – 2669, doi:10.1016/j.rse.2009.08.006, 2009.

Schneider, U., A. Becker, P. Finger, A. Meyer-Christoffer, M. Ziese, and B. Rudolf, GPCC's new land surface precipitation climatology based on quality-controlled in situ data and its role in quantifying the global water cycle, *Theor. Appl. Climatol.*, *115*, 15–40, doi:10.1007/s00704-013-0860-x, 2014.

Schwarz, J. P., R. S. Gao, A. E. Perring, J. R. Spackman, and D. W. Fahey, Black carbon aerosol size in snow, *Scientific Reports*, *3*(1356), doi:10.1038/srep01356, 2013.

Schwarz, J. P., et al., Measurement of the mixing state, mass, and optical size of individual black carbon particles in urban and biomass burning emissions, *Geophys. Res. Lett.*, *35*(13), doi:10.1029/2008GL033968, 2008.

Sinha, P. R., et al., Seasonal progression of the deposition of black carbon by snowfall at Ny-Å̈lesund, Spitsbergen, *J. Geophys. Res.: Atmos.*, *123*, 997–1016, doi:10.1002/2017JD028027, 2017.

Skeie, R. B., T. Berntsen, G. Myhre, J. Ström, S. Gerland, and J. A. Ogren, Black carbon in the atmosphere and snow, from pre-industrial times until present, *Atmos. Chem. Phys.*, *11*(14), 6809–6836, doi:10.5194/acp-11-6809-2011, 2011.

Skiles, S. M., and T. H. Painter, Toward understanding direct absorption and grain size feedbacks by dust radiative forcing in snow with coupled snow physical and radiative transfer modeling, *Water Resour. Res.*, *55*, 7362–7378, doi:10.1029/2018WR024573, 2019.

Slater, A. G., et al., The representation of snow in land surface schemes: Results from PILPS 2(d), *J. Hydrometeor.*, *2*, 7–25, doi:10.1175/1525-7541(2001)002⟨0007:TROSIL⟩2.0.CO;2, 2001.

Sommerfeld, R. A., and E. LaChapelle, The classification of snow metamorphism, *J. Glaciol.*, *9*(55), 3–18, doi:10.3189/S0022143000026757, 1970.

Sterle, K. M., J. R. McConnell, J. Dozier, R. Edwards, and M. G. Flanner, Retention and radiative forcing of black carbon in Eastern Sierra Nevada snow, *The Cryosphere*, *7*, 365–374, doi:10.5194/tc-7-365-2013, 2013.

Strahler, A. H., J.-P. Muller, W. Lucht, C. B. Schaaf, T. Tsang, F. Gao, X. Li, P. Lewis, and M. J. Barnsley, *MODIS BRDF/Albedo Product: Algorithm Theoretical Basis Document Version 5.0*, 1999.

Stroeve, J., J. E. Box, F. Gao, S. Liang, A. Nolin, and C. Schaaf, Accuracy assessment of the MODIS 16-day albedo product for snow: comparisons with Greenland in situ measurements, *Remote Sens. Env.*, *94*, 46–60, doi:10.1016/j.rse.2004.09.001, 2005.

Stroeve, J., J. E. Box, Z. Wang, C. Schaaf, and A. Barrett, Re-evaluation of MODIS MCD43 Greenland albedo accuracy and trends, *Remote Sens. Env.*, *138*, 199–214, doi:10.1016/j.rse.2013.07.023, 2013.

Svensson, J., Horizontal meter scale variability of elemental carbon in surface snow, Master's thesis, Stockholm University, 2011.

Tachibana, Y., M. Honda, H. Nishikawa, H. Kawase, H. Yamanaka, D. Hata, and Y. Kashino, High moisture confluence in Japan Sea polar air mass convergence zone captured by hourly radiosonde launches from a ship, *Sci. Rep.*, *12*, doi:10.1038/s41598-022-23371-x, 2022.

Taillandier, A., F. Domine, W. R. Simpson, M. Sturm, and T. A. Douglas, Rate of decrease of the specific surface area of dry snow: Isothermal and temperature gradient conditions, *J. Geophys. Res.: Earth Surf.*, *112*(F3), doi:10.1029/2006JF000514, f03003, 2007.

Takala, M., K. Luojus, J. Pulliainen, C. Derksen, J. Lemmetyinen, J.-P. Kärnä, J. Koskinen, and B. Bojkov, Estimating Northern Hemisphere snow water equivalent for climate research through assimilation of space-borne radiometer data and ground-based measurements, *Remote Sens. Env.*, *115*(12), 3517–3529, doi:10.1016/j.rse.2011.08.014, 2011.

Tarolli, P., J. Luo, E. Straffelini, Y.-A. Liou, K.-A. Nguyen, R. Laurenti, R. Masin, and V. D'Agostino, Saltwater intrusion and climate change impact on coastal agriculture, *PLOS Water*, *2*(4), 1–5, doi:10.1371/journal.pwat.0000121, 2023.

Tuzet, F., et al., A multi-layer physically-based snowpack model simulating direct and indirect radiative impacts of light-absorbing impurities in snow, *The Cryosphere*, *11*, 2633–2653, doi:10.5194/tc-11-2633-2017, 2017.

Tuzet, F., et al., Quantification of the radiative impact of light-absorbing particles during two contrasted snow seasons at Col du Lautaret (2058 m a.s.l., French Alps), *The Cryosphere*, *14*(12), 4553–4579, doi:10.5194/tc-14-4553-2020, 2020.

Urraca, R., C. Lanconelli, F. Cappucci, and N. Gobron, Comparison of long-term albedo products against spatially representative stations over snow, *Remote Sens.*, *14*(15), doi:10.3390/rs14153745, 2022.

Usha, K. H., V. S. Nair, and S. S. Babu, Deciphering the role of aerosol-induced snow albedo feedback on dust emission over the Tibetan Plateau, *J. Geophys. Res.: Atmos.*, *127*, doi:10.1029/2021JD036384, 2022.

van der Werf, G. R., J. T. Randerson, L. Giglio, G. J. Collatz, P. S. Kasibhatla, and A. F. Arellano Jr., Interannual variability in global biomass burning emissions from 1997 to 2004, *Atmos. Chem. and Phys.*, *6*(11), 3423–3441, doi:10.5194/acp-6-3423-2006, 2006.

Walden, V. P., S. G. Warren, and E. Tuttle, Atmospheric ice crystals over the Antarctic Plateau in winter, *J. Appl. Meteorol. Climatol.*, *42*, 1391–1405, doi:10.1175/1520-0450(2003)042⟨1391:AICOTA⟩2.0.CO;2, 2003.

Walters, D., et al., The Met Office Unified Model Global Atmosphere 7.0/7.1 and JULES Global Land 7.0 configurations, *Geosci. Model Dev.*, doi:10.5194/gmd-12-1909-2019, 2019.

Wang, Z., C. B. Schaaf, M. J. Chopping, A. H. Strahler, J. Wang, M. O. Román, A. V. Rocha, C. E. Woodcock, and Y. Shuai, Evaluation of moderate-resolution imaging spectroradiometer (MODIS) snow albedo product (MCD43A) over tundra, *Remote Sens. Env.*, *177*, 264–280, doi:10.1016/j.rse.2011.10.002, 2012.

Wang, Z., C. B. Schaaf, A. H. Strahler, M. J. Chopping, M. O. Román, Y. Shuai, C. E. Woodcock, and D. R. Fitzjarrald, Evaluation of MODIS albedo product (MCD43A) over grassland, agriculture and forest surface types during dormant and snow-covered periods, *Remote Sens. Env.*, *140*, 60–77, doi:10.1016/j.rse.2013.08.025, 2014.

Wang, Z., C. B. Schaaf, Q. Sun, Y. Shuai, and M. O. Román, Capturing rapid land surface dynamics with Collection V006 MODIS BRDF/NBAR/Albedo (MCD43) products, *Remote Sens. Env.*, *207*, 50–64, doi:10.1016/j.rse.2018.02.001, 2018.

Wanner, W., X. Li, and A. H. Strahler, On the derivation of kernels for kernel-driven models of bidirectional reflectance, *J. Geophys. Res.: Atmos.*, *100*, 21,007–21,089, doi:10.1029/95JD02371, 1995.

Warren, S. G., Optical properties of snow, *Rev. Geophys. Space Phys.*, *20*, 67–89, doi:10.1029/RG020i001p00067, 1982.

Warren, S. G., Can black carbon in snow be detected by remote sensing?, *J. Geophys. Res.: Atmos.*, *118*(2), 779–786, doi:10.1029/2012JD018476, 2013.

Warren, S. G., and W. J. Wiscombe, A model for the spectral albedo of snow. II: Snow containing atmospheric aerosols, *J. Atmos. Sci.*, *37*, 2734–2745, doi:10.1175/1520-0469(1980)037⟨2734:AMFTSA⟩2.0.CO;2, 1980.

Weedon, G. P., G. Balsamo, N. Bellouin, S. Gomes, M. J. Best, and P. Viterbo, The WFDEI meteorological forcing data set: WATCH Forcing Data methodology applied to ERA-Interim reanalysis data, *Water Resour. Res.*, *50*(9), 7505–7514, 2014.

Weedon, G. P., et al., Creation of the WATCH forcing data and its use to assess global and regional reference crop evaporation over land during the twentieth century, *J. Hydrometeor.*, *12*, 823–848, doi:10.1175/2011JHM1369.1, 2011.

Westerling, A. L., H. G. Hidalgo, D. R. Cayan, and T. W. Swetnam, Warming and earlier spring increase Western U.S. forest wildfire activity, *Science*, *313*, 940–943, doi:10.1126/science.1128834, 2006.

Wiscombe, W. J., and S. G. Warren, A model for the spectral albedo of snow. I: Pure snow, *J. Atmos. Sci.*, *37*, 2712–2733, doi:10.1175/1520-0469(1980)037⟨2712:AMFTSA⟩2.0.CO;2, 1980.

Yamamoto, S., K. Kawamura, and O. Seki, Long-range atmospheric transport of terrestrial biomarkers by the asian winter monsoon: Evidence from fresh snow from Sapporo, Northern Japan, *Atmos. Environ.*, *45*, 3553–3560, doi:10.1016/j.atmosenv.2011.03.071, 2011.

Yang, X., N. Wang, A. Chen, J. He, T. Hua, and Y. Qie, Changes in area and water volume of the Aral Sea in the arid Central Asia over the period of 1960âĂŞ2018 and their causes, *CATENA*, *191*, doi:10.1016/j.catena.2020.104566, 2020.

Yang, Z.-L., R. E. Dickinson, A. Robock, and K. Y. Vinnikov, Validation of the snow submodel of the Biosphere–Atmosphere Transfer Scheme with Russian snow cover and meteorological observational data, *Journal of Climate*, *10*(2), 353–373, doi:10.1175/1520-0442(1997)010⟨0353:VOTSSO⟩2.0.CO;2, 1997.

Yasunari, T. J., R. D. Koster, W. K. M. Lau, and K.-M. Kim, Impact of snow darkening via dust, black carbon, and organic carbon on boreal spring climate in the earth system, *J. Geophys. Res.: Atmos.*, *120*(11), 5485–5503, doi:10.1002/2014JD022977, 2015.

Yasunari, T. J., et al., The GOddard SnoW Impurity Module (GOSWIM) for the NASA GEOS-5 earth system model: Preliminary comparisons with observations in Sapporo, Japan, *Sci. Online Lett. on the Atmos.*, *10*, 50–56, doi:10.2151/sola.2014-011, 2014.

Yukimoto, S., et al., A new global climate model of the meteorological research institute: Mri-cgcm3 –model description and basic performance–, *J. Meteorol. Soc. Jpn., Ser. II*, *90A*, 23–64, doi:10.2151/jmsj.2012-A02, 2012.

Zampieri, M., E. Scoccimarro, S. Gualdi, and A. Navarra, Observed shift towards earlier spring discharge in the main alpine rivers, *Sci. Total Environ.*, *503-504*, 222–232, doi:10.1016/j.scitotenv.2014.06.036, 2015.

Zdunkowski, W. G., R. M. Welch, and G. Korb, An investigation of the structure of typical two-stream-methods for the calculation of solar fluxes and heating rates in clouds, *Contrib. Atmos. Phys.*, *53*(2), 147–167, 1980.

Appendix A

Science configuration settings used for simulations in this thesis

Below is a list of science configuration settings used for simulations shown in this thesis. Parameter descriptions are taken from the JULES user guide (`https://jules-lsm.github.io`):

Parameter	Description	Value
namelist:fire_switches		
l_fire	Switch to enable the fire module	.false.
namelist:jules_hydrology		
b_pdm	Shape factor for the pdf	0.40
dz_pdm	The depth of soil considered by PDM (m)	0.50
l_pdm	Switch for a PDM-type model of runoff production	.true.
l_spdmvar	Switch to use a linear function of topographic slope to calculate S0/Smax for PDM	.false.
l_top	Switch for a TOPMODEL-type model of runoff production	.false.
l_var_rainfrac		.false.
s_pdm	Minimum soil water content below which there is no surface runoff saturation excess production by PDM	0.0
namelist:jules_initial		
total_snow	Switch controlling simplified initialisation of snow variables	.true.
namelist:jules_nvegparm		
albsnc_nvg_io	Snow-covered albedo of non-vegetated tiles (Only used if l_snow_albedo = FALSE)	4.0e-1, 6.0e-2, 8.0e-1, 8.0e-1
albsnf_nvg_io	Snow-free albedo of non-vegetated tiles	1.8e-1, 6.0e-2, -1.0, 7.5e-1
catch_nvg_io	Capacity for water (kg m-2)	5.0e-1, 1.0e+3, 0.0, 0.0
ch_nvg_io	“Canopy” heat capacity of this surface type (J K-1 m-2)	2.80e+5, 4.18e+6, 0.00, 0.00
emis_nvg_io	Surface emissivity	9.70e-1, 9.85e-1, 9.00e-1, 9.90e-1

gs_nvg_io	Surface conductance (m s-1)	0.0, 0.0, 1.0e-2, 1.0e+6
infil_nvg_io	Infiltration enhancement factor	1.0e-1, 0.0, 5.0e-1, 0.0
vf_nvg_io	Fractional coverage of non-vegetation "canopy"	1.0, 1.0, 0.0, 0.0
z0_nvg_io	Roughness length of momentum (m)	1.0, 1.0e-4, 1.0e-3, 5.0e-4
z0hm_classic_nvg_io	(Only used in coupled simmulations with the CLASSIC chemistry and aerosol scheme)	1.0e-7, 2.5e-1, 2.0e-2, 2.0e-1
z0hm_nvg_io	Ratio of the roughness length for heat to the roughness length for momentum	1.0e-7, 2.5e-1, 2.0e-2, 2.0e-1
namelist:jules_pftparm		
a_wl_io	Allometric coefficient relating the target woody biomass to the leaf area index (kg carbon m-2)	0.65, 0.65, 0.005, 0.005, 0.10
a_ws_io	Woody biomass as a multiple of live stem biomass	10.00, 10.00, 1.00, 1.00, 10.00
albsnc_max_io	Snow-covered albedo for large leaf area index (only used if l_spec_albedo = FALSE)	1.5e-1, 1.5e-1, 6.0e-1, 6.0e-1, 4.0e-1
albsnc_min_io	Snow-covered albedo for zero leaf area index (only used if l_spec_albedo = FALSE)	3.0e-1, 3.0e-1, 8.0e-1, 8.0e-1, 8.0e-1
albsnf_max_io	Snow-free albedo for large LAI	1.0e-1, 1.0e-1, 2.0e-1, 2.0e-1, 2.0e-1
alnir_io	Leaf reflection coefficient for NIR	0.45, 0.35, 0.58, 0.58, 0.58
alpar_io	Leaf reflection coefficient for VIS (photosynthetically active radiation)	0.10, 0.07, 0.10, 0.10, 0.10
alpha_io	Quantum efficiency (mol CO2 per mol PAR photons)	0.08, 0.08, 0.08, 0.040, 0.08
b_wl_io	Allometric exponent relating the target woody biomass to the leaf area index	5*1.667
c3_io	Flag indicating whether PFT is C3 type: 0=Not C3 (i.e. C4), 1=C3	1, 1, 1, 0, 1
can_struct_a_io	Canopy structure factor (dimensionless)	5*1.0
canht_ft_io	The height of each PFT (m), also known as the canopy height	19.01, 16.38, 0.79, 1.26, 1.00
catch0_io	Minimum canopy capacity (kg m-2)	5*5.0e-1
dcatch_dlai_io	Rate of change of canopy capacity with LAI (kg m-2)	5*5.00000e-2
dgl_dm_io	Rate of change of leaf turnover rate with moisture availability	5*0.0
dgl_dt_io	Rate of change of leaf turnover rate with temperature (K-1)	9.0, 9.0, 0.0, 0.0, 9.0
dqcrit_io	Critical humidity deficit (kg H2O per kg air)	0.090, 0.060, 0.100, 0.075, 0.100
dz0v_dh_io	Rate of change of vegetation roughness length for momentum with height	5.0e-2, 5.0e-2, 1.0e-1, 1.0e-1, 1.0e-1
emis_pft_io	Surface emissivity	0.9800, 0.9900, 0.9800, 0.9800, 0.9800
eta_sl_io	Live stemwood coefficient (kg C/m/(m2 leaf))	5*0.01
f0_io	CI / CA for DQ = 0	0.875, 0.875, 0.900, 0.800, 0.900
fd_io	Scale factor for dark respiration	0.015, 0.015, 0.015, 0.025, 0.015

fsmc_mod_io	Switch for method of weighting the contribution that different soil layers make to the soil moisture availability factor fsmc	5*0 (Calculate fsmc in each soil layer and take a weighted average, using the fraction of roots in each layer as weights. Root distribution e-folding depth is given by rootd_ft_io)
fsmc_of_io	Moisture availability below which leaves are dropped	5*0.00
fsmc_p0_io		5*0.0
g_leaf_0_io	Minimum turnover rate for leaves (/360days)	5*0.25
glmin_io	Minimum leaf conductance for H2O (m s-1)	5*1.0e-6
infil_f_io	Infiltration enhancement factor	4.0, 4.0, 2.0, 2.0, 2.0
kext_io	Light extinction coefficient - used with BeerâĂŹs Law for light absorption through tile canopies	5*5.00000e-1
kn_io	Parameter for decay of nitrogen through the canopy, as a function of layers	5*0.78
kpar_io	PAR Extinction coefficient (m2 leaf / m2 ground)	5*0.50
lai_alb_lim_io	Minimum LAI permitted in calculation of the albedo in snow-free conditions	5*0.5
lai_io	The leaf area index (LAI) of each plant functional type	5.0, 4.0, 2.0, 4.0,1.0
neff_io	Scale factor relating V_{cmax} with leaf nitrogen concentration	0.8e-3, 0.8e-3, 0.8e-3, 0.4e-3, 0.8e-3
nl0_io	Top leaf nitrogen concentration (kg N/kg C)	0.040, 0.030, 0.060, 0.030, 0.030
nmass_io	Top leaf nitrogen content per unit mass (kgN kgLeaf-1)	0.0210, 0.0115, 0.0219, 0.0131, 0.0219
nr_nl_io	Ratio of root nitrogen concentration to leaf nitrogen concentration	5*1.00
ns_nl_io	Ratio of stem nitrogen concentration to leaf nitrogen concentration	0.10, 0.10, 1.00, 1.00, 0.10
omega_io	Leaf scattering coefficient for PAR	0.15, 0.15, 0.15, 0.17, 0.15
omnir_io	Leaf scattering coefficient for NIR	0.70, 0.45, 0.83, 0.83, 0.83
orient_io	Flag indicating leaf angle distribution: 0=Spherical, 1=Horizontal	5*0
q10_leaf_io	Q10 factor for plant respiration	5*2.00
r_grow_io	Growth respiration fraction	5*0.25
rootd_ft_io	Parameter determining the root depth (m)	3.0, 1.0, 5.0e-1, 5.0e-1, 5.0e-1
sigl_io	Specific density of leaf carbon (kg C/m2 leaf)	0.0375, 0.1000, 0.0250, 0.0500, 0.0500
tleaf_of_io	Temperature below which leaves are dropped (K)	273.15, 243.15, 258.15, 258.15, 243.15
tlow_io	Lower temperature for photosynthesis (deg C)	0.0, -5.0, 0.0, 13.0, 0.0
tupp_io	Upper temperature for photosynthesis (deg C)	36.0, 31.0, 36.0, 45.0, 36.0

z0hm_classic_pft_io	Ratio of the roughness length for heat to the roughness length for momentum for the CLASSIC aerosol scheme only	1.65, 1.65, 1.00e-1, 1.00e-1, 1.00e-1
z0hm_pft_io	Ratio of the roughness length for heat to the roughness length for momentum	1.65, 1.65, 1.00e-1, 1.00e-1, 1.000e-1
namelist:jules_prescribed		
n_datasets	The number of datasets that will be specified using instances of the JULES_PRESCRIBED_DATASET namelist	0
namelist:jules_radiation		
l_albedo_obs	Switch for using prognostic snow properties in model albedo.	.false.
l_cosz	Switch for calculation of solar zenith angle.	.true.
l_dolr_land_black	Switch to avoid using the surface emissivity in adjusting the OLR at land points. (For historical compatibility only)	.false.
l_embedded_snow	Switch to use embedded canopy model for calculation of snow albedo.	.false.
l_mask_snow_orog	Switch for orographic masking of snow.	.false.
l_sea_alb_var_chl		.false.
l_snow_albedo	Switch for using prognostic snow properties in model albedo.	.true.
l_spec_albedo	Switch for albedo model.	.true. (Use spectral albedo with visible and NIR components)
wght_alb	Weights to form the overall albedo from its components.	0
namelist:jules_rivers		
l_rivers	Switch for enabling river routing.	.false.
namelist:jules_snow		
cansnowpft	Flag indicating whether snow can be held under the canopy of each plant functional type	.false., .true., .false., .false., .false.
dzsnow	Prescribed thickness of each snow layer (m)	0.04, 0.12, 0.34
frac_snow_subl_melt	Switch for use of snow-cover fraction in the calculation of sublimation and melting	1 (on)
graupel_options	Switch for treatment of graupel in the snow scheme	0 (Include graupel as snowfall)
i_basal_melting_opt	Option to treat basal melting of the snow pack.	0 (basal melting is ommitted)
i_snow_cond_parm	Scheme used to calculate the conductivity of snow	0
l_et_metamorph	Switch to include the effect of thermal metamorphism on the snow density	.false.
l_snowdep_surf	Switch to use equivalent canopy snow depth for surface calculations on tiles with a snow canopy	.true.
nsmax	Maximum possible number of snow layers	3
namelist:jules_soil		

dzsoil_io	The soil layer depths (m), starting with the uppermost layer	0.10, 0.25, 0.65, 2.00
l_bedrock	Switch for using a thermal bedrock column beneath the soil column	.false.
l_dpsids_dsdz	Switch to calculate vertical gradient of soil suction with the assumption of linearity only for fractional saturation (consistent with the calculation of hydraulic conductivity).	.false.
l_holdwater	This switch fixes a problem in soil hydrology, whereby if a layer goes supersaturated during the implicit calulation, the excess water is pushed out of the soil column (l_holdwater = FALSE) instead of into an adjacent layer (l_holdwater = TRUE)	.false.
l_soil_sat_down	Switch for dealing with supersaturated soil layers.	.false. (Any excess is put into the layer above)
l_vg_soil	Switch for van Genuchten soil hydraulic model.	.true.
sm_levels	Number of soil layers.	4
soilhc_method	Option for soil thermal conductivity model	2
namelist:jules_soil_biogeochem		
const_ch4_cs	Scale factor for wetland CH4 emissions when soil carbon is taken as the substrate for ch4 emissions	7.41e-12
l_q10	Switch for use of Q10 approach when calculating soil respiration	.true.
l_soil_resp_lev2	Switch affecting the temperature and moisture used for soil respiration calculation	.false.
q10_ch4_cs	Q10 value for wetland CH4 emissions when soil carbon is taken as the substrate for ch4 emissions	3.7
soil_bgc_model	Choice for model of soil biogeochemistry	1
t0_ch4	Reference temperature for the Q10 function CH4 emission calculation	273.15
namelist:jules_surf_hgt		
zero_height	Switch used to simplify the initialisation of tile elevation	.true. (Set all tile elevations to zero)
namelist:jules_surface		
all_tiles	Perform calculations of tile properties on all tiles (except land ice) for all gridpoints even when the tile fraction is zero	0
cor_mo_iter	Corrections to Monin-Obukhov surface exchange calculation	3 (Limit Obukhov length in low winds)
formdrag	Switch for orographic form drag (only used in coupled simulations, should be set to zero in standalone)	0
i_modiscopt	Method of discretization in the surface layer	0

iscrntdiag	Switch controlling method for diagnosing screen temperature	0 (Use surface similarity theory)
isrfexcnvgust	Switch to include the effect of convective downdraughts on surface exchange (only used in coupled simulations, should be set to zero in standalone)	0
l_aggregate	Switch controlling number of tiles for each gridbox	.false. (A separate energy balance is calculated for each surface type)
l_anthrop_heat_src	Switch for inclusion of anthropogenic contribution to the surface heat flux from urban surface types	.true.
l_elev_land_ice	Switch allowing multiple ice tiles to exist in an ice gridbox, usually with each representing a different elevation band on in icesheet areas so that a sub-gridscale surface mass balance term (a strong function of altitude) can be derived for forcing icesheet/glacier models	.false.
l_epot_corr	Use correction to the calculation of potential evaporation	.true.
l_flake_model	Switch for using the freshwater lake model âĂŸFLakeâĂŹ on the lake/inland-water surface tile	.false.
l_land_ice_imp	Switch to control the use of implicit numerics to update land ice temperatures	.false.
l_urban2t	Switch for using the two-tile urban schemes (including MORUSES)	.false.
namelist:jules_surface_types		
ice	Index of the ice surface type	9
lake	Index of the lake surface type	7
nnvg	The number of non-plant surface types to be modelled	4
npft	The number of plant functional types to be modelled	5
soil	Index of the soil surface type	8
urban	Index of the urban surface type	6
namelist:jules_time		
l_360	Switch indicating use of 360 day years	.false.
l_leap	Switch indicating whether the calendar has leap years	.true.
timestep_len	Model timestep length in seconds	60
alloc_fast_io		0.6, 0.6, 1.0, 1.0, 0.8
alloc_med_io		0.3, 0.4, 0.0, 0.0, 0.2
alloc_slow_io		0.1, 0.0, 0.0, 0.0, 0.0
crop_io		0, 0, 1, 1, 0
dpm_rpm_ratio_io		0.25, 0.25, 0.67, 0.67, 0.33
g_area_io		0.005, 0.004, 0.25, 0.25, 0.05
g_grow_io		5*20.00
g_root_io		5*0.25
g_wood_io		0.01, 0.01, 0.20, 0.20, 0.05

lai_max_io		9.00, 9.00, 4.00, 4.00, 4.00
lai_min_io		3.00, 3.00, 1.00, 1.00, 1.00
retran_l_io		5*0.5
retran_r_io		5*0.2
namelist:jules_vegetation		
can_model	Choice of canopy model for vegetation	4 (Radiative canopy with heat capacity and a representation of snow beneath the canopy)
can_rad_mod	Switch for treatment of canopy radiation	4
fsmc_shape	Shape of soil moisture stress function on vegetation (fsmc)	0 (Piece-wise linear in vol. soil moisture)
ilayers	Number of layers for canopy radiation model	10
l_bvoc_emis	Switch to enable calculation of BVOC emissions	.false.
l_inferno	Switch that determines whether interactive fires (INFERNO) is used	.false.
l_irrig_dmd	Switch controlling the implementation of irrigation demand code	.false.
l_leaf_n_resp_fix	Switch for bug fix for leaf nitrogen content used in the calculation of plant maintenance respiration. The switch is included for backwards compatability with existing configurations	.false.
l_o3_damage	Switch for ozone damage	.false.
l_phenol	Switch for vegetation phenology model	.false.
l_scale_resp_pm	Scale whole plant maintanence respiration by the soil moisture stress factor, instead of only scaling leaf respiration	.false.
l_stem_resp_fix	Switch for bug fix for stem respiration to use balanced LAI to derive respiring stem mass. The switch is included for backwards compatability with existing configurations	.false.
l_trait_phys	Switch for using trait-based physiology	.false. (V_{cmax} is calculated based on parameters nl0 (kgN kgC-1) and neff)
l_trif_crop	Switch controlling the treatment of agricultural PFTs. Where agricultural PFTs are defined by the crop_io parameter	.false.
l_triffid	Switch for dynamic vegetation model (TRIFFID) except for competition	.false.
l_use_pft_psi	Switch for parameters in the soil moisture stress on vegetation function (fsmc)	.false. (Fsmc is calculated from sm_wilt and sm_crit in JULES_SOIL_PROPS and fsmc_p0_io)
l_vegcan_soilfx	Switch for enhancement to canopy model to allow for conduction in the soil below the vegetative canopy, reducing coupling between the soil and the canopy	.false.

l_vegdrag_pft	Switch for using vegetation canopy drag scheme on each PFT	5*.false.